

**NASA
Technical
Paper
3070**

April 1991

**Wall-Interference Assessment
and Corrections for Transonic
NACA 0012 Airfoil Data From
Various Wind Tunnels**

**Lawrence L. Green
and Perry A. Newman**



**NASA
Technical
Paper
3070**

1991

**Wall-Interference Assessment
and Corrections for Transonic
NACA 0012 Airfoil Data From
Various Wind Tunnels**

Lawrence L. Green
and Perry A. Newman
*Langley Research Center
Hampton, Virginia*



National Aeronautics and
Space Administration
Office of Management
Scientific and Technical
Information Division

Summary

A nonlinear, four-wall, post-test wall-interference assessment/correction (WIAC) code has been developed for transonic airfoil data from solid-wall wind tunnels with flexibly adaptive top and bottom walls. The WIAC code has been applied over a broad range of test conditions to four sets of NACA 0012 airfoil data from two different adaptive-wall wind tunnels. The data include many test points for fully adapted walls as well as numerous partially adapted and unadapted test points, which together represent many different model/tunnel configurations and possible wall-interference effects.

Small corrections to the measured Mach numbers and angles of attack are obtained from the WIAC code even for the fully adapted data. Larger corrections to the Mach number and angle of attack are generally obtained for partially adapted and unadapted data. The corrections are applied to determine new free-air flow conditions that should be associated with the measured data; the new Mach number is also used to renormalize the measured pressure coefficient data for comparisons with other corrected or interference-free data. For most of the cases investigated, the corrections improve the correlation among the various sets of airfoil data and simultaneously improve the correlation of the data with calculations from a two-dimensional, free-air Navier-Stokes code. For several cases, however, three-dimensional effects, possibly due to flow separation on the airfoil or the tunnel walls, undermine the success of the correction scheme and can lead to poorer correlation among data sets.

The WIAC corrections for fully adapted data from two differently sized models in the same adaptive-wall tunnel are somewhat different in magnitude, but the corrections generally improve the correlation between the data sets. This demonstrates the effectiveness of the sidewall boundary-layer approximation used in the corrections, which includes the model aspect ratio. The WIAC corrections for fully adapted data from two similar-sized models in two different adaptive-wall tunnels are shown to be quite small. This shows the effectiveness of the adaptive-wall tunnels in reducing wall interference for properly sized models. The WIAC corrections for airfoil data taken in test sections with fully adapted walls are shown to be significantly smaller than those for comparable airfoil data from test sections with straight, slotted walls. This indicates, as expected, a lesser degree of wall interference in the adaptive-wall tunnels relative to the slotted-wall tunnels. Despite the successes shown in correcting a broad range of data, application of the WIAC code to these data has

been somewhat more difficult and time-consuming than initially expected from similar previous experience with WIAC applications to slotted-wall data. This is apparently due to a sensitivity within the correction code to the details of the pressure distributions for the high blockage-ratio tests considered in the adaptive-wall tunnel.

Introduction

Wind-tunnel wall interference for two-dimensional-airfoil data arises from a variety of sources. First, the top and bottom tunnel walls confine the vertical flow and may induce blockage, flow-angularity, blockage-gradient, and streamline-curvature interferences as described classically in references 1 and 2. Second, the boundary layers on all four tunnel walls interact with the model pressure field to influence the blockage interference and add three-dimensionality to the flow. Third, shock waves spanning the test section in transonic flow may interact with the tunnel sidewall boundary layer to induce flow separation in the model/sidewall junction region independent of any top and bottom wall interaction. Fourth, turbulence, noise, and temperature fluctuations within the wind-tunnel circuit may cause premature flow transition or the separation of model or tunnel-wall boundary layers.

All these factors adversely affect airfoil data measured in wind tunnels and point to the need for a reliable and robust means to eliminate and/or correct wind-tunnel interference. Certainly, ventilated- and adaptive-wall experimental test sections significantly reduce some aspects of transonic wall interference compared with that encountered with solid, fixed-geometry wind-tunnel walls. Simultaneously, many useful computational schemes have been developed to assess and correct some aspects of wall interference in wind-tunnel data. It should not be expected, however, that all wind-tunnel wall interference can be removed from airfoil data solely through the use of ventilated- or adaptive-wall test sections, or solely through the use of wall-interference correction schemes. Instead, the combined use of ventilated- or adaptive-wall test sections and wall-interference assessment/correction (WIAC) schemes may be the most practical route for obtaining airfoil data that are nearly free of interference.

Such a combined experimental/computational effort toward obtaining interference-free transonic airfoil data appeared in reference 3, which described the nonlinear, two-wall, post-test WIAC program TWINTAN (applicable to airfoil data from wind tunnels with ventilated top and bottom walls) and which utilized measured airfoil and wind-tunnel data in the construction of its boundary conditions. In

references 4, 5, and 6, this scheme was improved to account for four-wall interference by including a simple model for the tunnel sidewall boundary layer (SWBL) based on reference 7. The improved program, called TWINTN4, was applied to a limited amount of data from the Langley 0.3-Meter Transonic Cryogenic Tunnel/slotted-wall test section (0.3-m TCT/SWTS), and comparisons were made with free-air calculations from the GRUMFOIL aerodynamic analysis code described in reference 8. The TWINTN4 program was then incorporated within a semiautomatic procedure described in reference 9, which included data preprocessing, the TWINTN4 WIAC program, a collection of corrected data into a data base, and comparisons with the GRUMFOIL code. This WIAC procedure was then applied to a much larger sampling of 0.3-m TCT/SWTS data in reference 10, which showed that the WIAC corrections significantly improved the correlation of the various sets of lift-curve data.

The TWINTN4 program of the WIAC procedure was modified in reference 11 to include an improved sidewall boundary-layer model based upon reference 12, which includes the model aspect-ratio effect; the improved program was applied to selected data from the 0.3-m TCT/SWTS for two different-sized models. It was shown in reference 11 that the model aspect ratio played an important role in correlating the drag-rise data for the different-sized models, but that the quality of the corrections available from the TWINTN4 code quantifiably deteriorates as the lift coefficient is increased in transonic flow. The program was further modified in reference 13 to account for wall interference within a tunnel having flexibly adaptable top and bottom walls; the modified program, called TWNTN4A, was applied to limited data from both simulated and real adaptive and ventilated walls for an NACA 0012 airfoil. The TWNTN4A program was applied in reference 14 to a very large sampling of NACA 0012 data over a broad range of test conditions and possible wall-interference effects; comparisons were made in reference 14 with the free-air calculations for flow around an NACA 0012 airfoil computed using the finite-volume, multi-grid Navier-Stokes solver described in reference 15.

Using the data of references 13 and 14, the present paper is intended to show clearly the following four points pertinent to airfoil data from adaptive-wall wind tunnels: (1) the effectiveness of fully adapted walls in eliminating most wall-interference effects compared with partially adapted or unadapted walls, (2) the effectiveness of fully adapted walls in eliminating most wall-interference effects compared with typical transonic slotted-wall tunnels, (3) the importance of TWNTN4A WIAC corrections for all

airfoil data, even data from fully adapted tunnels, and (4) the effectiveness of the TWNTN4A WIAC code in eliminating different kinds and severities of wall interference. The TWNTN4A WIAC program is used to correlate airfoil data from up to seven different sources of various quality levels across a broad range of test conditions for different model sizes and from different tunnel types and sizes. The TWNTN4A WIAC program is also applied to a reasonable amount of data with certain wall-interference effects peculiar to an adaptive-wall tunnel.

Symbols and Abbreviations

AWTS	adaptive-wall test section
BC	boundary condition
B-S SWBL	Barnwell-Sewall SWBL approximation
b	model span or test section width
b/c	model aspect ratio
C_p	pressure coefficient
c	model chord
c_d	drag coefficient
c_l	lift coefficient
$c_{l\alpha}$	lift-curve slope
c_n	normal-force coefficient
EDM	empirically correlated Davis-Moore correction
H	tunnel-empty SWBL shape factor at model location
h/c	ratio of tunnel half-height to model chord
k_2	Murthy aspect-ratio factor defined by equation (4)
ΔM	Mach number correction
M_T	tunnel Mach number
M_∞	free-air Mach number
MSWBL	Murthy SWBL approximation
N-S	Navier-Stokes
q	magnitude of total velocity
Re_c	Reynolds number based on model chord
RMS	root mean square
S	SWBL coefficient defined by equation (3)

SWBL	sidewall boundary layer
SWTS	slotted-wall test section
TCT	transonic cryogenic tunnel
TPT	transonic pressure tunnel
TSDE	transonic small-disturbance equation
u, U	components of total velocity in x -direction (see eqs. (5) and (2), respectively)
v	component of total velocity in y -direction
WIAC	wall-interference assessment/correction
x	streamwise direction of TSDE
y	normal (vertical) direction in TSDE
α	angle of attack
$\Delta\alpha$	angle-of-attack correction
α_T	tunnel angle of attack
γ	ratio of specific heats
δ^*	tunnel-empty SWBL displacement thickness
θ	flow angle with respect to x -direction
θ_W	tunnel wall inclination with respect to x -direction
Λ	coefficient in TSDE defined by equation (2)
ϕ	dimensionless disturbance velocity potential
2-D, 3-D	two- and three-dimensional, respectively

WIAC Procedure

Overview

The TWNTN4A program is a nonlinear, four-wall, post-test WIAC code applicable to transonic airfoil data obtained in wind tunnels where the top and bottom walls can be slotted, porous, or shaped to reduce interference. The program solves several boundary-value problems subject to the two-dimensional (2-D) transonic small-disturbance equation (TSDE) but with differing boundary conditions

imposed: measured wind-tunnel data for the in-tunnel solution, and unbounded flow and source/doublet distributions for two different free-air solutions. The WIAC code includes two options to account for the influences of the sidewall boundary layer in the in-tunnel solution.

The lift and drag coefficients are constraints within this procedure; values of the lift and drag coefficients are changed only because of renormalization effects. The Mach number and angle-of-attack corrections, ΔM and $\Delta\alpha$, respectively, that result from the TWNTN4A WIAC code are added to the experimental values to obtain the "interference-free" conditions for the measured airfoil data. Of course, for the corrections to be considered valid, all calculated solutions must be sufficiently well-converged and several measures of correctability must be below specified tolerances, as discussed later. Under these circumstances, data from different-sized models and different tunnel configurations should collapse to a common curve, or a family of curves, at the corrected flow conditions. Not all airfoil data will be correctable by this means alone; the interference may be too large or not adequately modeled (i.e., boundary-layer separation, vortex interactions, and extreme Mach number or downwash gradients through the test section).

It is important to realize that the TWNTN4A WIAC program represents a significant improvement over classical wind-tunnel correction methods such as those summarized in reference 1. Classical correction methods generally give reasonable trends for subcritical flows at low-to-moderate lift coefficient (c_l) levels, but these methods tend to fail if the flow is transonic or at high c_l . Also, most classical methods are linear and use linear homogeneous boundary conditions (such as ref. 2, for example), whereas the TWNTN4A program solves for nonlinear transonic effects and includes a higher order term to enhance the transonic modeling. Classical correction methods may rely on empirical correlations and cannot correct for angle-of-attack (α) biases that are due to misalignment of the airfoil and tunnel reference lines; on the other hand, measured data are used in both the exterior and interior boundary conditions of the TWNTN4A program. Classical correction methods do not account for sidewall boundary-layer (SWBL) effects, whereas the TWNTN4A program has two options to approximately account for some influence of the test section flow-field interaction between sidewall boundary layer and model pressure. Some essentially classical correction methods use measured data in the boundary conditions of linear-flow solvers; such a method was used during the acquisition of some of the data shown herein to determine the magnitude of residual corrections as wall adaptation

proceeded. These correction methods, however, do not accurately represent the nonlinear behaviors of the tunnel flow field and viscous interactions within the test section.

Wind-Tunnel Data

The TWNTN4A WIAC code for transonic, adaptive-wall airfoil tunnels requires as input the following two data arrays: (1) the coordinates of the pressure taps and the corresponding values of pressure coefficient C_p along the two bounding outer surfaces (generally the upper and lower walls of the test section) extending fore and aft of the model, and (2) the coordinates of the pressure taps and the corresponding values of C_p on the model upper and lower surfaces. The WIAC code also requires as input the values of M_T , α_T , c_l , c_d , R_c , and the tunnel-empty SWBL parameters δ^* and H at the model location. Also required as inputs are measurements of the vertical (upwash) velocity component along the forward face of the test section near the upper and lower bounding surfaces; in practice, these velocity components are rarely measured, which complicates the correction process by introducing a global iteration to deduce these velocity components and establish the proper computational inflow boundary condition.

Corrections using TWINTN4 for a limited amount of data taken on a 6-in-chord NACA 0012 airfoil in the 8-in-wide by 24-in-high 0.3-m TCT/SWTS ($h/c = 2.0$) have been previously reported in reference 10; the entire uncorrected data set has been published in references 16 and 17. Two NACA 0012 airfoils with chords of 6.5 and 13 in. have since been tested in the 0.3-m TCT with its nominally 13- by 13-in. adaptive-wall test section. (These unpublished data were provided by E. J. Ray, R. E. Mineck, S. W. D. Wolf, W. G. Johnson, Jr., and A. S. Hill, all of the Langley Research Center.) Timeliness and ease of access to these data, plus the experience gained through prior application of the WIAC code to the slotted-wall data for this airfoil, led to the NACA 0012 airfoil being selected for this study of transonic wall-interference assessment and corrections.

In the 0.3-m TCT/AWTS, the top and bottom walls are deformable using motor-driven jacks under the control of one (refs. 18 and 19) of several possible adaptation strategies. The straight, solid sidewalls include turntables that rotate the model, in this case, about the 50-percent-chord location. The 6.5-in-chord NACA 0012 model installed in the 13- by 13-in. 0.3-m TCT/AWTS has $h/c = 1.0$ with a model aspect ratio (b/c) of 2.0. The 13-in-chord NACA 0012 model in the same facility has $h/c = 0.5$ with

a model aspect ratio of 1.0. The data presented in this paper include cases with both free transition and transition fixed at 5 percent of the model chord; the data are shown, however, with different symbols for free and fixed transition.

The models were instrumented in the streamwise direction with pressure taps on both the upper and lower surfaces. In addition, the upper surface of each model was instrumented with three spanwise rows of pressure taps. The top and bottom walls of the test section contained a streamwise row of pressure taps along the centerline of each wall. For the small-chord model (6.5-in.), these pressure taps extended from 4.3 chords ahead of the model to 5.1 chords behind it. For the large-chord model (13-in.), pressure taps extended from 1.9 chords ahead of the model to 2.3 chords behind it. Figure 1 shows a streamwise vertical plane through the test section appropriate to the large-chord model ($h/c \approx 0.5$) with walls adapted at $M_T \approx 0.5$ and $\alpha_T \approx 4^\circ$.

The TWNTN4A program was also applied to a limited amount of NACA 0012 data reported in reference 20 from the ONERA/CERT T2 adaptive-wall tunnel in Toulouse, France. The 15.75-in-wide by 15-in-high wind tunnel was instrumented with pressure taps on the centerline of the top and bottom walls that extended 4.7 chords ahead of the model and 2.4 chords behind the model. The 5.9-in-chord model was instrumented with a row of pressure taps in the streamwise direction along the model centerline; no report was given, however, of any spanwise rows of pressure taps on the model. All data from the ONERA/CERT T2 test were with transition fixed at 5 percent of the model chord. The ONERA/CERT T2 model had $h/c = 1.27$ with a model aspect ratio of 2.7.

The data taken in the 0.3-m TCT are written on a file that must be preprocessed (ref. 9) in order to select and format the proper inputs for the TWNTN4A WIAC code. The preprocessor plots the model and wall pressure coefficient data, as well as the spanwise drag-rake measurements. Some examples of these preprocessor plots are shown in this report to allow for qualitative assessments of the 2-D character of the tunnel flow field as no flow-visualization techniques were employed in any of these tests. Although these preprocessor plots are useful, specific features of the flow field, such as separation bubbles on the model or tunnel walls, cannot be detected with this limited amount of data. Data from the ONERA/CERT T2 test were manually digitized from the tables and charts of reference 20 and put into proper format for input to the WIAC code.

The TWNTN4A WIAC Code

In the TWNTN4A WIAC code, the 2-D transonic small-disturbance equation is solved for three distinct sets of boundary conditions. A simplified description of the solution methodology follows, but more complete details are given in reference 5. The first boundary-value problem is an inverse one using the measured wind-tunnel data (mentioned earlier) as boundary conditions; it attempts to numerically model the in-tunnel flow field. If no normal velocity components have been measured at the upstream face of the test section, they are approximated from the wall shape and used in the inflow boundary condition. This first solution results in the determination of an equivalent inviscid body, as sensed by the tunnel flow field, consisting of the actual model geometry and integrated effects of the model and wall boundary layers and their interaction with shocks.

The second solution is actually a sequence of converging boundary-value problems to determine the free-air flow field around the equivalent inviscid body. During this process, the free-stream boundary conditions are incrementally changed in an attempt to minimize the root-mean-square (RMS) difference between the velocity distribution computed with the free-air model and the velocity distribution deduced from the pressure coefficient data measured with the tunnel model.

The third solution is required in order to determine the "classical-type" wall-induced perturbation velocity field. The solution for the tunnel flow perturbation due to the model uses the corrected free-air boundary conditions determined from the second (previous) solution and an airfoil boundary condition that matches the in-tunnel doublet strength and vorticity distributions. This third solution is then subtracted from the in-tunnel solution (the first solution) to determine the wall-induced perturbation velocity field in regions of interest, such as along the coordinate line containing the model slit.

The computed, equivalent, inviscid-body camber line may distort during this process to accommodate the removal of the wall-induced perturbation. If no normal velocity components have been measured at the upstream face of the test section, it is assumed that the camber line of the equivalent inviscid body should align over the forward part of the airfoil with that of the actual model geometry. This, in turn, may require subsequent correction passes using updated normal velocity components in the TWNTN4A inflow boundary condition to align the computed body shape as well as possible with the model geometry. The three solutions are then repeated, comprising a

globally iterative (multiple-pass) correction scheme, as discussed in references 9-11, 13, and 14.

As described in reference 5, a dimensionless disturbance velocity potential ϕ is used to allow for different far-field velocities. The 2-D, transonic small-disturbance equation is written in the form

$$\Lambda \phi_{xx} + \phi_{yy} = 0 \quad (1)$$

where

$$\Lambda = 1 - M_\infty^2 - (\gamma + 1) M_\infty^2 \frac{U_R}{U_\infty} \phi_x \left(1 + \frac{U_R}{2U_\infty} \phi_x \right) + S \quad (2)$$

The quantity U_R is the velocity at M_T , whereas U_∞ is the velocity at M_∞ . It should be noted that the classical TSDE includes only the first three terms of equation (2); the resulting ϕ_x^2 term is included to enhance the TSDE modeling of the sonic condition. The last term in equation (2) is introduced to model the effect of the sidewall boundary layer. This term, called the SWBL influence coefficient, includes three options when defined as

$$S = \frac{2\delta^*}{b} \left(2 + \frac{1}{H} - M_T^2 \right) \left[\frac{k_2}{\sinh(k_2)} \right] \quad (3)$$

where b is the model span and δ^* and H are the tunnel-empty sidewall boundary-layer (SWBL) displacement thickness and shape factor, respectively. The Murthy SWBL aspect-ratio factor k_2 for the approximation model (ref. 12) is

$$k_2 = \frac{\pi(1 - M_T^2)b}{c} \quad (4)$$

where c is the model chord. Murthy obtained the form of S (see eq. (3)) by considering the subsonic flow past a wavy sidewall. In equation (4) the wavy sidewall wavelength has been set to c (the model chord) in k_2 , which approximates the SWBL response to the model pressure field at the model. Note that if k_2 is set to zero (i.e., $b/c = 0$ or $M_T = 1$), the ratio of $k_2/\sinh(k_2)$ is unity and S is the Barnwell-Sewall sidewall factor as given in reference 7. Also, if δ^* is taken to be zero, the sidewall term drops out and only a two-wall (top and bottom) correction is applied. For four-wall corrections, the sidewall approximations can be applied either sequentially (2-D/2-D) or unified (3-D/2-D). (See ref. 10.) For results in the present paper, the unified procedure has been used. Only corrected results using the Murthy sidewall boundary-layer (MSWBL) approximation will be shown in this paper, based on conclusions detailed in references 11 and 14 which show

the Murthy approximation to be superior to the Barnwell-Sewall or two-wall approximations.

The grid for all three processes is generally stretched Cartesian, although the airfoil boundary condition is applied in a region of uniform streamwise spacing. Outer boundary conditions are applied on rectangular contours surrounding the airfoil slit. Placement of the outer boundary conditions and the information used to construct the outer boundary conditions are different for each of the three small-disturbance solutions previously discussed. Figure 2 shows a schematic diagram of the TWNTN4A grid, but only the upper half-plane is shown.

For the in-tunnel solution with shaped, solid walls, the effective outer boundary condition is

$$u = q(C_p) \cos \theta \quad (5)$$

where u is the x -component of velocity (also equal to $1 + \phi_x$), q is the total velocity determined from the measured pressure coefficient, and θ is the flow angle. It is assumed herein that the flows on the top and bottom test section walls are attached and that $\theta \approx \theta_W$. The TWNTN4A WIAC program spline fits the input ordinates of the top and bottom tunnel walls and then interpolates at streamwise grid points. The wall tangent angles are found and used in equation (5) to modify Kemp's original in-tunnel wall boundary conditions (ref. 5). Since the wall adaptation process may result in the top and bottom walls being unequally spaced above and below the airfoil, the TWNTN4A program searches for the grid locations in the normal direction that most closely approximate average upper and lower wall positions. A Dirichlet boundary condition is applied along straight lines at these locations; it is obtained by integrating the x -derivative of the disturbance potential given by

$$\phi_x = q(C_p) \cos \theta_W - 1 \quad (6)$$

The upstream boundary condition for the in-tunnel solution is a fourth-degree polynomial for ϕ in terms of the normal coordinate y . It is uniquely determined with the five conditions: (a) $\phi = 0$ at the upstream lower wall, (b) and (c) $\phi_y = v$ at the upstream top and bottom walls, respectively, as an input quantity assumed to be measured in the wind tunnel, and (d) and (e) ϕ_{yy} at the upstream top and bottom walls, respectively, as determined from the governing equation (1) by expressing ϕ_{xx} in terms of streamwise differences in the measured upstream wall pressure coefficients. As no measurements of v were made at the inflow face of the test sections for the data considered to date, it was found in refer-

ences 9-11, 13, and 14 that several global iterations or passes through the correction code were required using sequentially updated values of v at the inflow corners.

These successive passes, in general, improve the overall agreement between the actual tunnel flow and the TWNTN4A-computed tunnel flow by better matching some average value of v along the inflow face of the computational tunnel domain. Changes to these inflow corner values of v are made using a flow-alignment criterion over the forward part of the airfoil and assuming that the magnitude of the velocity component v at a point upstream of the airfoil is linearly related to the lift coefficient (valid for low-lift cases). For the high-lift cases, or those cases with transonic flows where shock waves lie on the forward part of the airfoil and distort the equivalent body, these updated normal velocity components may be extrapolated from lower lift data on the same polar plot. More discussion of this iteration process is given in references 10, 11, 13, and 14.

The downstream boundary condition for the in-tunnel solution is the same as that described in reference 5. The reference and far-field Mach numbers are set to the measured tunnel Mach number for the in-tunnel solution; therefore, $U_R = U_\infty = U_T$, which simplifies equation (2). The airfoil boundary condition for the in-tunnel solution uses measured wind-tunnel data as described in reference 5. An effective inviscid body is deduced from the in-tunnel solution that includes the real airfoil geometry plus integrated effects of the model boundary layers, wall boundary layers between the top and bottom walls, and any shock interaction with the boundary layers.

The effective inviscid body is then used in a free-air search (constrained optimization as described in ref. 5) in which the free-stream Mach number and angle of attack are varied until the computed velocity distribution at the body surface best fits the distribution deduced from the measured C_p data. Note that this measured C_p must be re-reduced (i.e., shifted and renormalized) using the WIAC-computed free-stream Mach number and static and dynamic pressures. The RMS error in this matching is taken as a measure of the data correctability. The Mach number and angle-of-attack corrections that result from this free-air search are added to the measured conditions, and then the results are taken to be the corrected flow conditions for the re-reduced (shifted and renormalized) airfoil data.

WIAC Validation

For the TWNTN4A corrections to be assumed valid, several criteria must be met. First, all calculated results must be sufficiently well-converged.

Second, the accuracy of the in-tunnel flow field modeling must be such that the global properties are well-represented. Third, several measures of goodness for the data correctability must be within specified tolerances.

With respect to the convergence, both the in-tunnel and the free-air search solutions must be considered. Input parameters set the convergence criterion to be met. At each grid point, the change in the disturbance potential per iteration was less than 0.5×10^{-5} for the present results. In addition, for the free-air solution, the change in free-stream velocity per iteration was specified to be less than 0.1×10^{-3} . Using a vertical-line over-relaxation scheme to solve equation (1), most of the in-tunnel solutions converge in under 100 iterations, but some cases require 200 or 300 iterations to converge. Generally, cases that are not correctable either will not converge the in-tunnel solution at all or they may take many hundreds of iterations to converge. The free-air search generally takes anywhere from 300 to 700 iterations to converge, although some cases take more than 2000 iterations to converge. Stopping the calculations before they reach convergence is generally found to give questionable corrections. It should be noted that no attempt was made to optimize the WIAC code execution; significant improvements in code performance beyond that stated may be possible.

With respect to the accuracy of the in-tunnel solution, it is not possible to resolve fine details of the flow field. Certainly, by current computational standards for fluid dynamics, the WIAC resolution of the flow field is very coarse. Typically, the transonic small-disturbance equation is solved on a free-air grid having 73×44 points; fewer points are generally used to model the in-tunnel flow field depending on where the wall and inflow/outflow boundaries occur with respect to the airfoil.

The RMS difference between the free-air surface velocities (at the corrected Mach number and angle of attack) and the surface velocities deduced from the measured pressure coefficient distribution, re-reduced at the corrected free-stream conditions, is taken as one measure of the goodness for data correctability. Another criterion could be used that would place less emphasis on the rapid gradients at the leading and trailing edges and near shocks. Nevertheless, some quantifiable parameter consistently produced by the WIAC code for a wide variety of cases is most useful in assessing the converged corrections. Typically, this measure of goodness would be better for low-lift cases and becomes poorer as the lift levels increase as shown in reference 11. However, no quantitative upper threshold has been established to clearly distinguish valid corrections from invalid

corrections. A second measure of goodness for the data correctability is the flow-alignment criterion at the airfoil, as mentioned earlier. This criterion is used in adjusting the upstream in-tunnel boundary condition, as discussed previously. This correlation generally holds for low lift coefficients and cases for which no shock is found on the forward part of the airfoil.

There are two further expectations of valid corrections. The first of these is that data sets from different model/tunnel configurations, but at the same nominal tunnel Mach number, angle of attack, and Reynolds number, should collapse (when corrected) to a common curve or family of curves. The second is similar to the first: that corrected data should agree with interference-free data at the same flow conditions. Thus, corrected or interference-free data for the same airfoil should have the same lift coefficient versus angle-of-attack behavior and the same drag divergence behavior, independent of whether the data were measured in a straight solid-wall tunnel, a slotted-wall tunnel, an adaptive-wall tunnel, in free air, or were calculated numerically. That is, there is only one interference-free flow field for a given airfoil at a given Mach number, angle of attack, and Reynolds number, assuming that the flow is steady and not separated. The WIAC correction is considered valid if it eliminates different kinds and different severities of wall interference. The problem for transonic flow comes in finding "interference-free" data to compare with the WIAC-produced corrections, since both numerical and experimental techniques involve, to some degree, different kinds of boundary interference.

For the data presented in this paper, comparisons are made with the Swanson/Turkel 2-D Navier-Stokes code described in reference 15; this code is taken to represent the state-of-the-art in interference-free viscous numerical solutions for the airfoil problem. Previous comparisons in references 6 and 10 were made with the GRUMFOIL code (ref. 8); that program uses a conservative full-potential solver for the inviscid calculations that has been shown by Salas and Gumbert (ref. 21) to admit nonphysical solutions when shocks are present in the flow field.

A similar problem occurs in all conservative full-potential programs including the flow solver used in references 13 and 14 to simulate the inviscid, 2-D airfoil data and its "interference-free" reference data. Even the TWNTN4A WIAC code itself uses the conservative formulation for the transonic small-disturbance equation which may exhibit similar behavior. Usage has been restricted to low transonic Mach numbers and lift levels where some errors may exist, but where the magnitude of this problem is not

severe. The results from the WIAC code appear to be reasonable corrections well into the transonic flow regime. To the authors' knowledge, these nonphysical solutions have not occurred in the TWNTN4A program, which uses the measured pressure coefficient data as boundary conditions for the in-tunnel solution and then the derived equivalent inviscid shape as a boundary condition in the free-air search. Use of such physical boundary data should restrict the shock location and strength to reasonable values in the potential solution. Some of these points are illustrated in the lift-curve results for the NACA 0012 airfoil at $M_T \approx 0.80$ presented in reference 10.

Other comparisons are made with airfoil data from the 0.3-m TCT/SWTS and WIAC corrections to these data from reference 10. The data of Harris (ref. 22) from the Langley 8-Foot Transonic Pressure Tunnel (8-ft TPT) are also used in comparisons with the 0.3-m TCT adaptive-wall data. TWNTN4A WIAC corrections could not be made to these 8-ft TPT data since wall pressure signatures were not available. However, estimates of classical blockage corrections to these data (based on refs. 1, 2, and 23) and to those due to sidewall effects are discussed when the data are presented.

Results and Discussion

Presentation Format

The uncorrected and TWNTN4A WIAC-corrected airfoil data and results will be presented in two types of plots. Plots of drag coefficient versus Mach number (drag curves) for a given nominal chord Reynolds number and lift coefficient will be shown to describe Mach number corrections. Plots of lift coefficient versus angle of attack (lift curves) for a given nominal tunnel Mach number and chord Reynolds number will be shown to describe angle-of-attack corrections. Table I presents a symbol key for these figures in which the shape of each symbol distinguishes the test data by its ratio of tunnel half-height to chord (h/c). Also, the shading of each symbol distinguishes the number of global correction passes applied to the data. Recall that each pass consists of three distinct TSDE solutions; as part of each pass, upwash velocity components of the inflow boundary condition are iteratively approximated, which serves to align the effective inviscid body with the actual model geometry. The lift and drag coefficients are constrained to the measured values during this correction process, except for effects due to renormalization at the corrected Mach number; the constraint on drag, however, is not strongly enforceable in the TSDE approximation.

Shown first in this paper are data from models of two different sizes in the same adaptive-wall tunnel at chord Reynolds numbers of 9×10^6 and 15×10^6 ; several of these figures include special data obtained to allow for the study of specific kinds of wall interference peculiar to an adaptive-wall tunnel. Following this are data from two different adaptive-wall tunnels at a chord Reynolds number of 3×10^6 . Comparisons are then made between data from adaptive- and slotted-wall tunnels at a chord Reynolds number of 9×10^6 . It should be kept in mind, however, that although the chord Reynolds number has been matched for these results, the unit Reynolds number, which influences the growth of the wall boundary layers, is different between the various data sets. Also, the model aspect ratios that influence the streamwise gradients within the tunnel are different between the various data sets. These differences result in different SWBL behavior and in different wall-interference characteristics between the various data sets.

AWTS Data for Different Model Sizes

The data and corrections presented in this section illustrate the effects of model size and include a wide variety of unadapted and partially and fully adapted points for both the 6.5- and 13-in-chord models in the 0.3-m TCT/AWTS. The data at a chord Reynolds number of 9×10^6 are the most extensive sets available and include both free and fixed (5 percent chord) transition points. The Murthy sidewall boundary-layer (MSWBL) approximation has been used for all TWNTN4A results shown here.

Two conventions, based on conclusions drawn from reference 13, have been followed in correcting this large amount of data. First, all data on the 13-in-chord model have received three correction passes; this is generally the minimum number of passes required to adequately correct at least the lifting cases in this data set because of the large disturbances present in the flow field. Second, most of the data for the 6.5-in-chord model have received only two correction passes. Some lifting data on the 6.5-in-chord model previously shown in reference 13, however, have received as many as three correction passes, whereas other data points (both lifting and nonlifting) from the same reference were deemed to be corrected after only one correction pass.

$R_c \approx 9 \times 10^6$. Uncorrected, fully adapted, zero-lift drag curves at $R_c \approx 9 \times 10^6$ are compared in figure 3(a) with Navier-Stokes free-air results. The experimental drag coefficients are in reasonable agreement with each other up to a Mach number of 0.7, but all are above the Navier-Stokes curve. The large-model data (circle symbols) are generally higher than the rest up to a Mach number of 0.74

(the highest Mach number for the large-model data); for Mach numbers above 0.70, there is considerable spread in the data, especially in the free-transition data. In figure 3(a) the best agreement overall with the Navier-Stokes curve is found in the first test entry of the small model (square symbols) which, though at a slightly higher drag level than the Navier-Stokes calculation, closely follows the theoretical curve even into the drag rise.

WIAC corrections to this fully adapted data with the MSWBL approximation are shown in figure 3(b). At first glance it would appear that the correlation of the WIAC-corrected data in figure 3(b) is worse than that of the uncorrected data shown in figure 3(a). It is important to realize, however, that the WIAC corrections in this figure primarily change the Mach number associated with a particular data point and that changes to the drag coefficient occur only because of a renormalization of the data. Thus, it is expected that the corrections will act to improve the correlation of the drag-rise Mach number of the various data sets without significantly improving the correlation of the different levels of drag associated with the various data sets. Within these expectations there is considerable improvement in figure 3(b) to the large-model data (circle symbols), both in agreement with the rest of the experimental data and in agreement with the Navier-Stokes curve, through application of Mach number corrections up to about 0.025.

The first-entry data of the small model (square symbols) are also in better agreement with the Navier-Stokes curve; Mach number corrections in this case are much smaller than those of the large model, indicating that this data set has much less wall interference than the large-model data set. (See fig. 3(b).) Also, notice that for a range of M_T from approximately 0.60 to 0.70 the data points have been somewhat rearranged along a family of lines parallel to the theoretical drag curve. Some of the second-entry data for the small model (diamond symbols) in this figure are also in better correlation with the other data; however, some points of this data set have received corrections that are too large, or even in the wrong direction. Generally, such points are at or above the drag-rise Mach number where strong shock waves and their interaction with the tunnel SWBL are present.

One such free-transition, second-entry point for the 6.5-in-chord model (diamond symbol marked with an arrow) has received a particularly large Mach number correction (and, surprisingly, for this nominally zero-lift case, a large α -correction as well) that throws it out of the line with the rest of the points. The point is still badly corrected even after two cor-

rection passes, and it may be uncorrectable because of three-dimensional effects and possible separation within the test section. Preprocessor plots for this point are shown in figure 4. The spanwise drag coefficient distribution from the wake-rake survey and the pressure coefficient distribution of the spanwise model (oblique view) are seen in figure 4(a). A large spanwise variation in the wake-rake drag coefficient is observed, although the spanwise pressure coefficient distribution varies only slightly.

The streamwise pressure coefficient distributions for the model and wall are shown in figure 4(b). The airfoil is shown in its proper streamwise position relative to the wall pressure coefficient; note, however, that the vertical scales of the two pressure coefficient plots are different. Noticeably different minimum wall pressure coefficients are observed for the upper and lower walls and model surfaces; moreover, the wall C_p curves are shifted considerably away from the expected upstream asymptotic value of zero, possibly because of massive flow separation within the test section. The sonic pressure coefficient for this case is about -0.5 ; thus the forward sonic point occurs near the leading edge in a region where the SWBL may be thinning. The spanwise variation in the wake-rake drag coefficient and the downward shift of the wall pressure coefficients from the asymptotic value of zero are common to those second-entry, free-transition points with $M_T \geq 0.76$. The example shown in figure 4(b) has the largest downward shift in the wall C_p curves; however, its spanwise variation is not the worst of those points. The observed three-dimensional effect and the possible separation within the test section are not properly accounted for within the WIAC code, which assumes 2-D flow. No flow visualization, however, is available in the 0.3-m TCT/AWTS to determine if separation regions are present.

To be more specific, the Murthy SWBL approximation used in these calculations is based upon a subsonic wavy-wall problem; the approximation cannot properly model the 3-D supercritical flow that exists when the forward sonic point occurs where the SWBL is thinning (near the model leading edge), such as at high Mach numbers and high lift coefficient. Unfortunately, an analogous sonic wavy-wall approximation is probably not practical and would be of little use anyway. Those cases where the forward sonic point is located in a region where the SWBL is thinning result in correspondingly strong aft shocks downstream, which will generally cause the SWBL to separate and introduce even more 3-D effects into the flow field. In these cases, it is expected that only a full 3-D viscous solution will improve the

modeling of the tunnel flow field sufficiently and lead to an improved correction.

A variety of special, uncorrected zero-lift drag data are shown in figure 5(a). These data points were obtained by operating the 0.3-m TCT/AWTS in unusual ways to allow for the study of specific kinds of wall-interference effects peculiar to an adaptive-wall tunnel. The unusual operations, discussed in more detail in references 13 and 14, included the following: (1) adaptation sequences (the walls being iteratively adjusted from nominally straight contours with data taken at each wall shaping step) to compare results for unadapted, partially and fully adapted walls, (2) runs in which some wall jacks were made inoperative at the entrance and exit of the test section to simulate tunnel truncation effects, and (3) runs in which the centerline of the tunnel was artificially rotated up 0.5° in the adaptation software to simulate an error in the angle of attack measured in the test section. The data points of figure 5(a) include three adaptation sequences for the large model (circle symbols, $M_T \approx 0.60, 0.65$, and 0.70) and one adaptation sequence for the small model (square symbols, $M_T \approx 0.60$). These sequences are characterized by a group of like data points at the same nominal Mach number, for which the drag coefficient varies significantly due to the changing wall-interference effects during the iterative wall shaping.

Also included in figure 5(a) are: (1) a group of fixed-transition, small-model data points (flagged diamond symbols) for which the walls were kept in a nominally straight position as the Mach number was varied from 0.6 to 0.74; (2) several free-transition, small-model data points (unflagged diamond symbols at $M_T \approx 0.7$ and 0.76) with simulated tunnel truncation effects, which exhibit a small variation in the drag coefficient at these Mach numbers; and (3) three free-transition, small-model data points (unflagged diamond symbols, one at $M_T \approx 0.7$ and two at $M_T \approx 0.76$) with simulated angle-of-attack errors with a drag coefficient of approximately the mean value in each of these groups. The WIAC corrections to these unadapted or partially adapted zero-lift drag data are shown in figure 5(b). The various sets of drag data are all made to correlate much better with each other and with the Navier-Stokes curve through the application of Mach number corrections as large as 0.1 for the large-model data, and as much as 0.05 for the small-model data.

Uncorrected, fully adapted lift-curve data over a range of angles of attack at $M_T \approx 0.6$ and $R_c \approx 9 \times 10^6$ are shown in figure 6(a). The data sets are in reasonably good agreement with each other and with the Navier-Stokes results, although the first-entry data for the small model (square sym-

bols) appear to have a slightly lower lift-curve slope c_{l_α} than the other data sets. The α corrections shown in figure 6(b) are generally small but range up to 0.35° for the small model at $\alpha \approx 4^\circ$. The corrected data lie mostly on a line with nearly the same slope as, but shifted to the left of, the Navier-Stokes calculations. WIAC corrections for the highest α data shown in figure 6(a) did not converge and the point is not shown in figure 6(b).

The special, uncorrected data shown in figure 6(c) for the same Mach number and Reynolds number include three adaptation sequences (both circles and squares at $\alpha \approx 2^\circ$, and squares only at $\alpha \approx 0^\circ$), with each displaying some variation in c_l at the same nominal angle of attack because of changes in the wall-interference effects during the iterative wall shaping. WIAC corrections to these data are shown in figure 6(d). Most of the variation in lift coefficient at $\alpha \approx 0^\circ$ and 2° has been corrected into a variation along a family of curves with the same slope as the Navier-Stokes lift curve, but shifted slightly to the left of the theoretical curve. The overall agreement among the data sets and with the Navier-Stokes curve is better than that of the uncorrected data shown in figure 6(c); however correlations for the small-model data are better than those for the large-model data. The largest α correction is about 0.5° for one large-model point. It is interesting to note that the Mach number corrections shown in figure 5(b) for the large-model points at nominally zero lift improve the correlation, whereas the α corrections to the same data shown in figure 6(d) do not improve, and possibly worsen, the correlation.

Lift-curve data are shown in figure 7 for $M_T \approx 0.65$ and $R_c \approx 9 \times 10^6$. The uncorrected, fully adapted data in figure 7(a) are all in good agreement with each other and with the Navier-Stokes results, although the small-model data (diamonds) appear to have a slightly lower lift-curve slope than the Navier-Stokes data. WIAC corrections to these data shown in figure 7(b) do not correlate as well as the uncorrected data because the large-model points (circles), indicated with arrows, have not met the body-alignment criterion even after three correction passes. However, the lift-curve slope of the small-model data points is in better agreement with the Navier-Stokes curve despite those points being shifted to the left of the Navier-Stokes curve.

The uncorrected data shown in figure 7(c) include a large- and small-model adaptation sequence (circles and squares, respectively) at $\alpha \approx 2^\circ$ and also one (circles) at $\alpha \approx 0^\circ$. Corrections to the data are shown in figure 7(d). The correlation is considerably better between the large- and small-model data (circles and squares), except for one point (indicated with an

arrow) that has received a Mach number correction of about 0.1. The large Mach number correction may indicate a large separation region within the tunnel. It is again noted that the Mach number corrections shown in figures 3(b) and 5(b) for the large-model data points at nominally zero lift improve the correlation, whereas the α corrections to the same data shown in figures 7(b) and 7(d) worsen the correlation. It is possible that a separation region in the tunnel, when considered part of the effective inviscid body as in TWNTN4A, may produce a correctable increase in the blockage while altering the effective body cambering that undermines the α corrections. No visualization techniques were employed in the 0.3-m TCT/AWTS that could validate or dispel any speculation about flow separation within the tunnel.

Uncorrected, fully adapted lift-curve data at $M_T \approx 0.7$ and $R_c \approx 9 \times 10^6$ are shown in figure 8(a). There is reasonably good correlation among the different data sets, although most of the small-model data (squares and diamonds) appear to have a slightly lower lift-curve slope than the Navier-Stokes curve. Corrections to the data from the TWNTN4A WIAC program are shown in figure 8(b). Most of the data in the range of angle of attack from -2° to 2° lie on one or more lines with slopes nearly the same as the Navier-Stokes curve, but shifted to the left of that curve. In this instance, the first-entry small-model data point (square) and the large-model data point (circle), indicated with arrows, have not met the body-alignment criterion.

A wide variety of unadapted and partially adapted data for the same nominal Mach number and Reynolds number are shown in figure 8(c). The data include large- and small-model adaptation sequences (circles at $\alpha \approx 1^\circ$ and 2° and squares at $\alpha \approx 2^\circ$ and 4° , respectively), points with simulated truncation effects (clustered diamonds on the Navier-Stokes curve), and points for which the test section centerline was rotated up (diamonds above the Navier-Stokes curve) in the adaptation software. WIAC corrections to the data are shown in figure 8(d). The corrected small-model data (squares and diamonds) correlate better with each other along a line with nearly the same slope as the Navier-Stokes curve, but once again shifted to the left of it. The large-model data (circles) have received α corrections as large as 0.8° , and these points do not correlate well with the other data or with the Navier-Stokes curve. Most of the large-model data points shown in figure 8(d), however, failed to meet the body-alignment criterion, and corrections for two of these points, which did not converge, are not shown in figure 8(d).

It is important to note, however, that several of the data points shown in figures 8(b) and 8(d) have

corrected Mach numbers significantly higher than 0.70. The Navier-Stokes results are shown in figures 8(b) and 8(d) at the nominal tunnel Mach number, whereas the corrected data should properly be compared with free-air results at the corrected Mach numbers for each test data point. The spread of the individual corrected Mach numbers (from 0.692 to 0.760 in this case) was much broader than the spread of uncorrected Mach numbers (from 0.697 to 0.711, also for this case) over the range of angle of attack at the same nominal Reynolds number. Additionally, the range of corrected Mach numbers was typically skewed to higher mean values than the nominal uncorrected free-air Mach number. In order to more fairly assess the corrections in this case, the data from figures 8(b) and 8(d) are repeated in figures 8(e) and 8(f), respectively, with an additional Navier-Stokes curve at a Mach number of 0.76 added to the plots. The large-model corrected data are seen to correlate better with the Navier-Stokes curve at a Mach number of 0.76 than at 0.70, whereas the small-model data correlate better with the lower Mach number curve, at least for low lift.

Lift-curve data at $M_T \approx 0.72$ and $R_c \approx 9 \times 10^6$ are shown in figure 9. Uncorrected, fully adapted data are shown in figure 9(a) that agree quite well with the Navier-Stokes results. The corrected results in figure 9(b) seem to have a lift-curve slope that is too large, although there are not enough data points to see a trend for either model. Two unadapted data points shown in figure 9(c) are made to correlate better (fig. 9(d)) with the Navier-Stokes curve through the WIAC corrections, although the corrected Mach numbers of these points are significantly higher than the measured value.

Uncorrected, fully adapted lift-curve data at $M_T \approx 0.74$ and $R_c \approx 9 \times 10^6$ are shown in figure 10(a) that correlate well with each other and with the theoretical curve. Corrections to the data in figure 10(b) have slightly more scatter at $\alpha \approx 0^\circ$ than the uncorrected data, whereas there is a slight improvement in correlation with the Navier-Stokes results at $\alpha \approx 2^\circ$. Two unadapted, uncorrected data points at the same Mach number and Reynolds number are shown in figure 10(c). The WIAC correction for only one of these data points is shown in figure 10(d); the correction for the point at $\alpha_T \approx 2^\circ$ did not converge and it is not shown in the figure. The corrected Mach number of the data point shown in figure 10(d) is significantly higher than the nominal tunnel Mach number.

Uncorrected lift-curve data for one adaptation sequence of the small model at $M_T \approx 0.75$ and $R_c \approx 9 \times 10^6$ are shown in figure 11(a). Corrections to the data with the MSWBL

approximation are shown in figure 11(b). Agreement with the Navier-Stokes curve is not as good as with the uncorrected data; however, most of these data points have corrected Mach numbers somewhat above 0.75, but not as high, relatively, as those in the preceding corrected figures.

Uncorrected, fully adapted lift-curve data at $M_T \approx 0.76$ and $R_c \approx 9 \times 10^6$ over a range of angle of attack are shown in figure 12(a). The two small-model data sets agree well with each other and with the Navier-Stokes curve. Corrections to these data are shown in figure 12(b); correlation of the two data sets with each other and with the theoretical curve is not as good as the uncorrected data. The corrected data for the first entry (squares) lie on a line with nearly the same slope as the Navier-Stokes results, but shifted to the left of it; corrected data from the second entry have a slightly larger lift-curve slope than the other data. Figure 12(c) shows many unadapted or partially adapted, uncorrected data, including several data points with simulated test section truncation and with the tunnel centerline artificially rotated up 0.5° . Corrections to the data are shown in figure 12(d). The correlation among the data sets and with the Navier-Stokes results is somewhat improved at low lift levels; however, the points at $\alpha \approx 2^\circ$ do not correlate as well as the uncorrected data.

Two uncorrected, fully adapted lift-curve data points at $M_T \approx 0.8$ are shown in figure 13(a). The corrected data shown in figure 13(b) correlate better with the Navier-Stokes curve than the uncorrected data. The uncorrected lift-curve data from one small-model adaptation sequence at $M_T \approx 0.8$ and $R_c \approx 9 \times 10^6$ are shown in figure 13(c). WIAC corrections to the data are shown in figure 13(d). Correlation with the Navier-Stokes data is improved, although there is again a fairly large spread in the corrected Mach numbers.

Uncorrected, fully adapted drag-curve data for large- and small-chord models interpolated from figures 6(a), 7(a), 8(a), and 12(a) at a lift coefficient of 0.2 are shown in figure 14(a). The large-chord model, as observed previously, has higher drag levels than the small-chord model, but it is impossible to determine its drag-divergence Mach number since no drag data with a lift coefficient greater than zero were obtained above $M_T \approx 0.7$ for the large-chord model. The corrected, interpolated drag curve taken from figures 6(b), 7(b), 8(b), and 12(b) at a lift coefficient of 0.2 are shown in figure 14(b). It is clear that two corrected data sets (circles and squares) correlate better with each other than with the uncorrected data, but the third data set shows little improvement. The limited corrected data appear to

correlate slightly better with the Navier-Stokes drag rise than do the uncorrected data.

It is interesting that a significant improvement in the correlation of these interpolated drag curves (circles and squares) is observed when improvement in lift-curve correlations for these fully adapted data was not always clearly observed. It was hoped that with the larger amount of transonic data (including unadapted and partially adapted data) given in this report (compared with that in ref. 13), the improvement in drag-rise correlation at lift could be even more easily seen. However, the spreads in corrected Mach numbers for these diverse data, which were greater than the spreads in the uncorrected Mach numbers, made drag-rise interpolation rather uncertain, and the resulting curves showed no better correlation than those presented in figure 14(b). Additional drag-rise curves at lift are shown in references 13 and 14.

In general, small angle-of-attack and Mach number corrections were calculated with the TWNTN4A WIAC code for the fully adapted data with $R_c \approx 9 \times 10^6$, indicating that little wall interference is present in the fully adapted data. As expected, larger corrections were calculated for the many partially adapted and unadapted data points that were included here to study different kinds and severities of wall interference. The corrections shown in the preceding figures were typically larger for the large-chord model. Large-model data generally required at least three global correction passes. Small-model data were generally easier to correct, and usually two passes were sufficient. The shape of the drag curves and the point of drag divergence were made to correlate better through application of the WIAC corrections; the level of drag measured in the tunnel was relatively unchanged through the corrections.

Agreement among the various lift-curve slopes was generally improved with corrections. Most of the 0.3-m TCT/AWTS data, however, were corrected slightly to the left of the Navier-Stokes results. The effects of free or fixed transition on the WIAC corrections are not clear in these examples. The corrections tended to improve correlation among the various sets of data and simultaneously improve correlation with the Navier-Stokes free-air calculations, unless severe three-dimensional effects or possible flow separation were present in the uncorrected data. The 3-D effects, however, are not properly modeled by the Murthy SWBL approximation in supercritical flow, thus resulting in corrections that are either too large or, perhaps, even in the wrong direction.

A surprising number of points, however, especially for the large model, either did not converge or did not meet the body-alignment criterion

after several global correction passes. This behavior was neither encountered as much in the slotted-wall data previously reported in reference 9 for which the wall pressure signatures were much milder nor in the smoothly varying simulated, inviscid, adaptive-wall data presented in references 13 and 14. The behavior suggests that the TWNTN4A WIAC program is very sensitive to the details (including randomness due to viscous effects and instrument imperfections) of the pressure distributions used in the boundary conditions. Despite this sensitivity, the WIAC code seems capable of detecting and correcting even small amounts of the different kinds or severities of wall interference, or, on the other hand, of giving some indication that it is not correctable.

$R_c \approx 15 \times 10^6$. The following figures show data from the large- and small-chord NACA 0012 model tests of the 0.3-m TCT/AWTS at a chord Reynolds number of 15×10^6 . The figures include almost every data point available for the 6.5- and 13-in. models at this Reynolds number. The data again include a variety of wall-interference conditions with several points having partially adapted or unadapted test sections; the data also include a mix of free and fixed transition points.

Uncorrected, fully adapted drag-curve data at zero lift are shown in figure 15(a). There is more disagreement among these data sets at the lower Mach numbers than among the comparable data sets at $R_c \approx 9 \times 10^6$ shown in figure 3(a). One large-model data point (indicated by an arrow) is obviously out of line with the rest of the data, probably due to tunnel choking. Corrections to these fully adapted data shown in figure 15(b) generally improve the correlation among the various data sets up to a Mach number of about 0.78; the corrections primarily change the Mach number associated with particular points, which tends to make them lie along curves that parallel the Navier-Stokes curve. Although the corrected points shown in figure 15(b) are all converged and have met the body-alignment criterion, three small-model data points and the large-model point previously noted have received large Mach number corrections in the wrong direction. These points are indicated in figure 15(b) by arrows and exhibit a noticeable spanwise variation in the pressure coefficient and wake-rake drag survey.

Preprocessor plots for the large-model data point are shown in figure 16. Considerable spanwise variation in the wake-rake drag coefficient is observed in figure 16(a); the spanwise variation in the measured drag is typical of all the data points that have been badly corrected. In figure 16(b) note the large disturbances impressed upon the walls and the extent

to which these disturbances propagate upstream in the test section. These strong disturbances may violate the assumptions in the WIAC code and the assumptions of linear flow exterior to the walls that are inherent in the adaptation scheme (refs. 18 and 19) used to shape the walls. Moreover, the computed equivalent inviscid body shapes resulting from the TWNTN4A code for these poorly corrected cases are two to three times the actual thickness of the models.

These extremely thick, effective inviscid bodies may indicate substantial viscous interaction and/or massive flow separation since the model and wall boundary layers must be considered as part of the effective inviscid body shape within this approximation. Once again, the forward sonic point occurs in a region where the SWBL is probably thinning, and the Murthy SWBL approximation cannot properly model the resulting supercritical 3-D flow. None of these effects is properly accounted for within the correction code. Data from one adaptation sequence for the small model are shown in figure 17(a). Corrections to these data shown in figure 17(b) significantly improve the correlation by spreading the points along a curve parallel to the Navier-Stokes curve.

Uncorrected, fully adapted lift-curve data at $M_T \approx 0.6$ and $R_c \approx 15 \times 10^6$ are shown in figure 18(a). Some disagreement is observed between the three data sets. The data appear to have a slightly lower lift-curve slope than the Navier-Stokes solution. WIAC corrections to the data are shown in figure 18(b). The corrected data agree better with each other and appear to have the same slope as the Navier-Stokes curve in the angle-of-attack range from -2° to 2° , although displaced somewhat to the left of the Navier-Stokes curve. Corrections for the highest angle-of-attack cases for the small model did not converge and are not shown in the figure. The correction for one small-model point, indicated by an arrow, did not meet the body-alignment criterion.

Uncorrected, fully adapted lift-curve data at $M_T \approx 0.7$ and $R_c \approx 15 \times 10^6$ are shown in figure 19(a). The data are in good agreement with each other and with the Navier-Stokes results. Corrections to these data are shown in figure 19(b); the data have, in general, been moved from one side of the Navier-Stokes curve to the other side of it with a resulting slight increase in the lift-curve slope. It is difficult to conclude that the corrections have improved the correlation. The partially adapted data shown in figure 19(c) include several adaptation sequences for the small model. The corrected data shown in figure 19(d) correlate better with each other and with the Navier-Stokes data up to stall. Corrections for three small-model data points, indicated by arrows, failed to meet the body-alignment criterion.

Uncorrected, fully adapted lift-curve data at $M_T \approx 0.76$ and $R_c \approx 15 \times 10^6$ over a range of angle of attack are shown in figure 20(a); noticeable disagreement is observed among the small-model data at angles of attack of 1° and 2° . Corrections to the data shown in figure 20(b) display an improved correlation in lift-curve slope, although the corrected data points are displaced to the left of the Navier-Stokes curve.

For the data presented at this Reynolds number of 15×10^6 , the WIAC code again appears to generally improve the correlation in lift-curve slope among the various data sets (except for those data points as noted), although the corrected experimental data were generally displaced to the left of the Navier-Stokes data. Corrections also generally improved the correlation among the various drag data sets. Several data points corrected at this Reynolds number failed to meet the body-alignment criterion, as noted previously with the data at a chord Reynolds number of 9×10^6 .

It should be noted from the preceding examples that the large-chord-model test envelope was significantly smaller than that of the small-chord model because of two effects. First, limitations on wall displacement and curvature (wall safety criteria) prohibited testing at high angles of attack. Second, another limitation was imposed then by an earlier onset of choked flow conditions within the test section for high Mach numbers at zero lift. The data shown herein include almost every point available for the 13-in-chord model, and also most of those points available from both tunnel entries of the 6.5-in-chord model. Considerably more discussion about the limitations of the large-chord test envelope and their impact on this study is given in reference 14.

AWTS Data From Different Tunnels

The following figures show data for the small-chord NACA 0012 model test from the 0.3-m TCT/AWTS and data for a similar-sized model in the ONERA/CERT T2 AWTS at a nominal chord Reynolds number of 3×10^6 . The data shown include almost every data point available for the two models at this Reynolds number. Only fully adapted data are shown.

The uncorrected zero-lift drag divergence at a nominal chord Reynolds number of 3×10^6 for the ONERA/CERT T2 data and the fixed-transition 6.5-in-chord model data from the 0.3-m TCT/AWTS are shown in figure 21(a). Three distinct data sets are shown in figure 21; these include normal fixed-transition drag data obtained with a wake rake (flagged triangles, squares, and the diamond), some free-transition drag data obtained with a wake rake

from the 0.3-m TCT/AWTS (unflagged squares), and some fixed-transition drag data obtained from the ONERA/CERT T2 tunnel obtained by pressure integration (flagged, inverted triangles). Navier-Stokes results with the transition fixed are shown as the solid line for comparison purposes. The WIAC corrections to these data with the MSWBL approximation are shown in figure 21(b). As expected, the fixed-transition wake-rake data agree best with the Navier-Stokes results, but the drag-rise data point of all the corrected curves is aligned well despite the noticeable differences in the levels of the various drag curves. Sample preprocessor plots for highest Mach number data (marked with an arrow) from the 0.3-m TCT are shown in figure 22. The data again display a large spanwise variation in the drag coefficient that is not accounted for in the WIAC code and that results in rather poor correlation at the highest Mach numbers.

Uncorrected, fully adapted lift-curve data at $M_T \approx 0.6$ and $R_c \approx 3 \times 10^6$ are shown in figure 23(a). Some disagreement is observed between the two data sets, but overall the agreement is very good. The data appear to have a slightly lower lift-curve slope than that of the Navier-Stokes solution. The WIAC corrections to these data are shown in figure 23(b). The corrected data appear to have the same slope as the Navier-Stokes curve, but the 0.3-m TCT data are displaced slightly to the left of the curve and the ONERA/CERT T2 data fall nearly on the Navier-Stokes curve.

The uncorrected, fully adapted lift-curve data at $M_T \approx 0.7$ and $R_c \approx 3 \times 10^6$ are shown in figure 24(a). Agreement is good between the data sets, although the $c_{l\alpha}$ again appears to be slightly less than that of the Navier-Stokes curve. Corrections to the adaptive-wall data with the MSWBL approximation are shown in figure 24(b). The corrected ONERA/CERT T2 data again lie almost on top of the Navier-Stokes curve, whereas the 0.3-m TCT data are corrected to slightly left of the Navier-Stokes curve with possibly a slightly higher lift-curve slope.

The uncorrected, fully adapted lift-curve data at $M_T \approx 0.75$ and $R_c \approx 3 \times 10^6$ over a range of angle of attack are shown in figure 25(a). Corrections to the data are shown in figure 25(b). Both sets of data have the same lift-curve slope as the Navier-Stokes curve, but the 0.3-m TCT data are again displaced to the left.

The Mach number and angle-of-attack corrections for $R_c \approx 3 \times 10^6$ were small in all cases, indicating that little wall interference was present in these fully adapted cases. Since the ONERA/CERT T2 tunnel is similar to, but slightly larger than, the

0.3-m TCT ($h/c \approx 1.27$ compared with 1.0; $b/c \approx 2.7$ compared with 2.0), it was expected that corrections would be about the same size as, or less than, those of the 0.3-m TCT/AWTS that were already shown to be small. Angle-of-attack corrections, though small, generally tended to improve the lift-curve-slope correlation among the data sets. The displacement of the corrected 0.3-m TCT data was not observed with the ONERA/CERT T2 data and may indicate some angle-of-attack bias in the 0.3-m TCT/AWTS, such as a misalignment between the tunnel and the model zero-angle reference lines.

AWTS and SWTS Data

The figures discussed in this section repeat selected fully adapted data and WIAC corrections from the large- and small-chord NACA 0012 model tests of the 0.3-m TCT/AWTS at a chord Reynolds number of 9×10^6 taken from figures 3–14. Adaptive-wall data are compared with slotted-wall data from two different sources. Uncorrected and corrected adaptive-wall data are first compared with slotted-wall data from the 0.3-m TCT/SWTS for which WIAC corrections by Gumbert and Newman were presented in reference 10 using an earlier version (TWINTN4) of the present TWNTN4A WIAC program. The present TWNTN4A program includes all the previous capability and can be used to correct data from fixed-geometry, solid- or slotted-wall tunnels or from adaptable tunnels with variable porosity or flexible walls. Empirical corrections to these slotted-wall data also shown in reference 10 are likewise compared with the adaptive-wall data to aid in the analysis of upcoming figures. The adaptive-wall data are then compared with earlier slotted-wall data from the 8-ft TPT tunnel that were reported and empirically corrected by Harris in reference 22. No WIAC corrections for these slotted-wall data were possible because of the lack of wall pressure coefficient data, but useful comparisons are made with adaptive-wall data by building upon the analysis of the 0.3-m TCT/SWTS data.

Figure 26(a) shows a comparison of uncorrected lift curves for slotted-wall and fully adapted NACA 0012 data from the 0.3-m TCT. Data for $M_T \approx 0.7$ and $R_c \approx 9 \times 10^6$ are shown. The adaptive-wall data are for only the first entry of the small-chord model; the slotted-wall data are for a 6-in-chord model in the 8-in-wide by 24-in-high test section at the same nominal tunnel conditions. It is clear that the uncorrected slotted-wall data have a different $c_{l\alpha}$ than the adaptive-wall or Navier-Stokes data. Also, the slotted-wall data have a zero-lift coefficient at an angle of attack of about 0.3° . TWINTN4 corrections (fig. 26(b)) to the slotted-wall data have

a lift-curve slope much nearer to the TWNTN4A-corrected adaptive-wall data and the Navier-Stokes solution. TWINTN4 corrections also remove the zero shift from the slotted-wall data. The overall correlation among the data sets is dramatically improved over the uncorrected data.

The empirically correlated Davis-Moore corrections (fig. 26(c)) to the 0.3-m TCT slotted-wall data are shown in order to aid in the analysis of upcoming figures with slotted-wall data from the 8-ft TPT. It is important to notice that the empirically correlated Davis-Moore corrections have nearly the same $c_{l\alpha}$ as the TWINTN4-corrected slotted-wall data, but they do not remove the zero shift in the data. The following three factors, taken together about this comparison, give clear evidence that the fully adapted data have significantly less wall interference than the slotted-wall data: (1) the uncorrected data indicate that corrections for the slotted-wall data should be much larger than those for the adaptive-wall data to improve the correlation of the three data sets, (2) the size of corrections applied to the slotted-wall data are much larger than those applied to the fully adapted wall data, and (3) the correlation of the three data sets after corrections are applied is improved.

Comparisons similar to those of figure 26 are shown in figure 27 at a nominal tunnel Mach number of 0.76. In figure 27(a) it is easily seen that the uncorrected adaptive-wall data and the uncorrected slotted-wall data do not correlate well either with each other or with the Navier-Stokes curve. The TWNTN4A-corrected adaptive-wall data (fig. 27(b)) correlate very well with the TWINTN4-corrected slotted-wall data, but both disagree somewhat with the Navier-Stokes results. The Navier-Stokes results tend to lie between the uncorrected adaptive-wall data and the corrected data sets. The empirically correlated Davis-Moore corrections (fig. 27(c)) in this case lie below the Navier-Stokes curve, similar to the uncorrected adaptive-wall data, but with a small zero-lift shift.

Figure 28(a) shows the uncorrected drag divergence at lift ($c_l = 0.2$) for large and small models with walls fully adapted (i.e., fig. 14(a)) with the 6-in-chord-model slotted-wall data superimposed. These uncorrected slotted-wall data appear to agree well with the Navier-Stokes results. The drag divergence of the small model from the adaptive-wall tunnel may also agree as well, but it is difficult to see this clearly with the limited amount of data. Data for the 13-in-chord model in the adaptive-wall test section have higher drag levels than the 6.5-in-chord-model data, the 6-in-chord slotted-wall data, and the Navier-Stokes results. The TWINTN4- and TWNTN4A-corrected drag divergence for the same

three tests is shown in figure 28(b). It is clear that the WIAC corrections make all the data correlate well with each other and agree better with the Navier-Stokes results. The slotted-wall data in figures 26, 27, and 28 were corrected (ref. 10) using the B-S SWBL approximation, whereas the adaptive-wall data were corrected using the MSWBL approximation. References 11 and 14 demonstrate that this difference may have a noticeable effect on the drag-curve corrections (with MSWBL being the better of the two options for improving drag correlations), but the difference should have almost no effect on lift-curve corrections.

A comparison of fully adapted wall, small-model lift-curve data with data from the 8-ft TPT seen in figures 29 and 30 shows the same format as that in figures 26 and 27. In figure 29(a) a comparison is made at $M_T \approx 0.7$ with uncorrected slotted-wall data from the 8-ft TPT as reported in reference 22. Noticeable disagreement in the lift-curve slope is observed in this figure among the sets of data. TWNTN4A corrections are not possible for this set of slotted-wall data because of the lack of measured wall pressure signatures. The empirically correlated, Davis-Moore angle-of-attack correction for slotted-wall test sections assumes (among other things) constant openness-ratio slots of infinite length. Slot shapes in the 8-ft TPT vary a good bit over their finite length so that several (perhaps) meaningful averages can be obtained. Both the original Davis-Moore correction (ref. 2) and the empirically correlated, Davis-Moore angle-of-attack correction (ref. 23) require a value for the geometric openness ratio of the slotted wall. For the data of reference 22, the 25-in-chord airfoil was placed in the 8-ft TPT test section so that several average openness ratios and their corresponding empirically correlated, Davis-Moore angle-of-attack corrections were as given in chart A. The empirically correlated Davis-Moore results from the 8-ft TPT for the largest and smallest angle-of-attack corrections are shown in figure 29(b). These data agree reasonably well with Navier-Stokes calculations and TWNTN4A-corrected adaptive-wall data.

Chart A

Region of slot width averaged	Openness ratio	$\Delta\alpha$ (from ref. 22)
Over 25-in. chord	0.051	$-1.55c_n$
Effective test section length	0.062	$-1.67c_n$
Total slot length	0.085	$-1.82c_n$

In figure 30(a) uncorrected lift-curve results similar to those in figure 29(a) are shown for a nominal

tunnel Mach number of 0.76. Once again there is a noticeable difference in $c_{l\alpha}$ in these data sets. Good correlation is shown in figure 30(b) among the empirically correlated, Davis-Moore-corrected slotted-wall data, the TWNTN4A-corrected adaptive-wall data, and the Navier-Stokes data.

In figures 26, 27, 29, and 30 it is important to notice that the uncorrected, fully adapted data receive much smaller α corrections than either set of uncorrected slotted-wall data. It is worth recalling that the slotted-wall tunnels have h/c ratios of 2.0 (0.3-m TCT/SWTS) and 1.7 (8-ft TPT); the adaptive-wall tunnel, by contrast, has an h/c ratio of 1.0 for these comparisons. Simulated, inviscid 2-D results from references 13 and 14 for straight solid-wall tunnels show the opposite effect of h/c on the corrections. This clearly demonstrates that the adaptive-wall tunnel can eliminate most of the wall interference present in typical transonic slotted-wall test sections.

In figure 31(a) uncorrected drag-divergence results are shown for the data interpolated at a lift coefficient of 0.2. Agreement between the uncorrected 8-ft TPT data and the Navier-Stokes data is quite good. Uncorrected 0.3-m TCT/AWTS data are taken from figure 14(a) and do not agree as well with the 8-ft TPT data or with the Navier-Stokes results. The disagreement between the small-model data from the 0.3-m TCT/AWTS and the 8-ft TPT data is not very great and both sets of data appear to have nearly the same drag-rise point. Corrections to adaptive-wall data from figure 14(b) for this case clearly improve the correlation among all data sets as shown in figure 31(b). TWNTN4A corrections are not possible for the 8-ft TPT data because of the lack of measured wall pressure distributions; however, we estimate that Mach number corrections to these data from the TWNTN4A procedure would be small, as shown in the following discussion.

The range of openness ratios discussed above in regard to the angle-of-attack corrections (figure 29(b)) also gives rise to an uncertainty in the classical-model solid-blockage correction for Mach number. All openness ratios quoted in chart A give test sections more closed than that for minimum (2-D) blockage according to the classical theory outlined in references 1, 2, and 23. The solid-blockage correction of the classical 2-D model for Mach number varies from 0.003 to 0.001 with openness ratio at $M_T = 0.7$, whereas at $M_T = 0.82$ it varies from 0.007 to 0.002. These are compensated by the sidewall boundary-layer Mach number correction that is of opposite sign. The maximum Mach number changes for the Barnwell-Sewall and Murthy sidewall approximations can be estimated from the known displacement thickness and model

aspect ratio for the slotted-wall data. These maximum Mach number changes are -0.008 for the Barnwell-Sewall approximation and -0.0002 or less for the Murthy sidewall approximation. Since the magnitudes of sidewall Mach number corrections were about the same size as the solid-blockage corrections, but of opposite sign and somewhat uncertain anyway, we did not assign any Mach number corrections to the 8-ft TPT slotted-wall data.

The NACA 0012 slotted-wall data for the 8-ft TPT given in reference 22 discussed above were also investigated by McCroskey (ref. 24) and found to be among the best transonic data available for this airfoil if suitable angle-of-attack corrections, such as the empirically correlated Davis-Moore correction, were applied. McCroskey also found that these data would require only very small, if any, Mach number corrections and that the data set was a probable candidate for the best overall set of NACA 0012 data. This finding is consistent with the higher aspect ratio of the model compared with those ratios in the adaptive-wall test section and with the resultant reduced SWBL effect. The agreement between the small-chord data from the 0.3-m TCT/AWTS and the Harris data shown in figure 31 supports the above conclusion of reference 24. McCroskey also looked at the limited amount of data presented in reference 13 and found it (the TWNTN4A-corrected NACA 0012 data of the 0.3-m TCT/AWTS) to be among the best data sets available for this airfoil for the Mach number range tested.

Concluding Remarks

This application of the wall-interference assessment/correction (WIAC) modified code TWNTN4A to a large amount of transonic wind-tunnel data, including a broad range of model/tunnel configurations and possible wall-interference effects for the NACA 0012 airfoil, has led to the formulation of several conclusions. With respect to corrected data from the Langley 0.3-Meter Transonic Cryogenic Tunnel (0.3-m TCT) having an adaptive-wall test section (AWTS), good correlations were shown in lift and drag curves at low-to-moderate lift coefficients for unadapted and partially to fully adapted walls over a wide range of Reynolds numbers at transonic Mach numbers using the Murthy sidewall boundary-layer approximation for the four-wall correction in the TWNTN4A WIAC code. As expected, corrections for the fully adapted data were much smaller than for the partially adapted or unadapted data; this indicates that the fully adapted data have very little wall interference, although the corrections for fully adapted data do tend to improve the data correlations. Smaller, more easily obtained corrections were

found for larger ratios of tunnel half-height to model chord (h/c), as evidenced by the large-chord model frequently requiring three or more correction passes, although two were generally sufficient for the small-chord model. Only two correction passes were required in previous research for all slotted-wall cases.

The considerable number of data points that either did not converge or for which the body-alignment criterion was not met indicates that the TWNTN4A WIAC program is sensitive to the details of the pressure distributions used in formulating the boundary conditions. Hence, the correction procedure was found to be more difficult and time-consuming to apply for some adaptive-wall cases compared with the slotted-wall cases. In almost every case the 0.3-m TCT data were corrected to the left of the Navier-Stokes curves. In some cases, this may be partly due to the corrected Mach numbers being significantly higher than the Mach number used for the Navier-Stokes calculations. The Navier-Stokes calculations are shown at the nominal tunnel Mach numbers, whereas the corrected data should properly be compared with curves at higher Mach numbers with greater slopes. In other cases, the discrepancy between the WIAC results and the Navier-Stokes calculations may be due to several factors including problems with the Navier-Stokes solution, an inability of the WIAC sidewall boundary-layer approximation to correctly model three-dimensional supercritical flows, or an angle-of-attack bias within the 0.3-m TCT/AWTS facility due to misalignment of the tunnel and model reference lines. Certainly, improvements made in any of these factors may influence the data correlations presented. The difficulty in correcting some of the data, particularly for the large-chord model, indicates that some flow-visualization techniques should be available to determine if separation regions exist within the test section.

Data from the ONERA/CERT T2 adaptive-wall tunnel were found to correct easily and correlated well with the Navier-Stokes data and with a limited amount of 0.3-m TCT/AWTS small-chord data. Corrections were very small in all the cases investigated in this study. A comparison of these corrected data with those of the small model from the 0.3-m TCT/AWTS supported a possible angle-of-attack bias in the latter facility.

It was also found that the uncorrected, fully adapted lift-curve data from the 0.3-m TCT were much better than the uncorrected slotted-wall data in correlating with the Navier-Stokes free-air data. TWNTN4A-corrected adaptive-wall data and TWINTN4-corrected slotted-wall data correlated much better with each other and with the Navier-Stokes calculations in the limited number of

comparisons shown. Comparisons between 0.3-m TCT/AWTS data and slotted-wall data from the Langley 8-Foot Transonic Pressure Tunnel (8-ft TPT) were similar to the previous comparisons in that the uncorrected adaptive-wall data correlated much better with the Navier-Stokes data than did the uncorrected slotted-wall data. TWNTN4A-corrected, adaptive-wall lift-curve data and empirically corrected, slotted-wall lift-curve data from the 8-ft TPT correlated reasonably well also. Correlation in the drag-curve data between the corrected adaptive-wall data and the 8-ft TPT data was very good despite some noticeable differences in the drag levels.








NASA Langley Research Center
Hampton, VA 23665-5225
February 5, 1991

References









1. Pindzola, M.; and Lo, C. F.: *Boundary Interference at Subsonic Speeds in Wind Tunnels With Ventilated Walls*. AEDC-TR-69-47, U.S. Air Force, May 1969. (Available from DTIC as AD 687 440.)
2. Davis, Don D., Jr.; and Moore, Dewey: *Analytical Study of Blockage- and Lift-Interference Corrections for Slotted Tunnels Obtained by the Substitution of an Equivalent Homogeneous Boundary for the Discrete Slots*. NACA RM L53E07b, 1953.
3. Kemp, William B., Jr.: *TWINTAN: A Program for Transonic Wall Interference Assessment in Two-Dimensional Wind Tunnels*. NASA TM-81819, 1980.
4. Kemp, William B., Jr.; and Adcock, Jerry B.: Combined Four-Wall Interference Assessment in Two-Dimensional Airfoil Tests. *AIAA J.*, vol. 21, no. 10, Oct. 1983, pp. 1353-1359.
5. Kemp, William B., Jr.: *TWINTN4: A Program for Transonic Four-Wall Interference Assessment in Two-Dimensional Wind Tunnels*. NASA CR-3777, 1984.
6. Gumbert, Clyde R.; Newman, Perry A.; Kemp, William B., Jr.; and Adcock, Jerry B.: Adaptation of a Four-Wall Interference Assessment/Correction Procedure for Airfoil Tests in the 0.3-m TCT. *Wind Tunnel Wall Interference Assessment/Correction—1983*, Perry A. Newman and Richard W. Barnwell, eds., NASA CP-2319, 1984, pp. 393-411.
7. Barnwell, Richard W.; and Sewall, William G.: Similarity Rules for Effects of Sidewall Boundary Layer in Two-Dimensional Wind Tunnels. *Wall Interference in Wind Tunnels*, AGARD-CP-335, Sept. 1982, pp. 3-1-3-10.
8. Melnik, R. E.; Mead, H. R.; and Jameson, A.: A Multi-Grid Method for the Computation of Viscid/Inviscid Interactions on Airfoils. AIAA-83-0234, Jan. 1983.
9. Gumbert, Clyde R.: *User Manual for 0.3-M TCT Wall-Interference Assessment/Correction Procedure: 8- by 24-Inch Airfoil Test Section*. NASA TM-87582, 1985.
10. Gumbert, Clyde R.; and Newman, Perry A.: Validation of a Wall Interference Assessment/Correction Procedure for Airfoil Tests in the Langley 0.3-m Transonic Cryogenic Tunnel. AIAA-84-2151, Aug. 1984.
11. Gumbert, Clyde R.: *Wall Interference Assessment/Correction of Data From Tests of a CAST 10-2/DOA 2 Airfoil in the Langley 0.3-m Transonic Cryogenic Tunnel*. M.S. Thesis, George Washington Univ., May 1988.
12. Murthy, A. V.: *Effects of Aspect Ratio on Sidewall Boundary-Layer Influence in Two-Dimensional Airfoil Testing*. NASA CR-4008, 1986.
13. Green, Lawrence L.; and Newman, Perry A.: Transonic Wall Interference Assessment and Corrections for Airfoil Data From the 0.3-Meter TCT Adaptive Wall Test Section. AIAA-87-1431, June 1987.
14. Green, Lawrence Lee Richard: *Wall Interference Assessment and Corrections for Transonic Adaptive Wall Airfoil Data*. M.S. Thesis, George Washington Univ., Apr. 1988.
15. Swanson, R. C.; and Turkel, Eli: A Multistage Time-Stepping Scheme for the Navier-Stokes Equations. AIAA-85-0035, Jan. 1985.
16. Ladson, Charles L.; Hill, Acquilla S.; and Johnson, William G., Jr.: *Pressure Distributions From High Reynolds Number Transonic Tests of an NACA 0012 Airfoil in the Langley 0.3-Meter Transonic Cryogenic Tunnel*. NASA TM-100526, 1987.
17. Ladson, Charles L.; and Hill, Acquilla S.: *High Reynolds Number Transonic Tests of an NACA 0012 Airfoil in the Langley 0.3-Meter Transonic Cryogenic Tunnel*. NASA TM-100527, 1987.
18. Judd, M.; Wolf, S. W. D.; and Goodyer, M. J.: *Analytical Work in Support of the Design and Operation of Two Dimensional Self Streamlining Test Sections*. NASA CR-145019, 1976.
19. Goodyer, M. J.; and Wolf, S. W. D.: The Development of a Self-Streamlining Flexible Walled Transonic Test Section. *A Collection of Technical Papers—AIAA 11th Aerodynamic Testing Conference*, Mar. 1980, pp. 325-335. (Available as AIAA-80-0440.)
20. Archambaud, J. P.; Seraudie, A.; and Gobert, J. L.: *Rapport d'Essais sur le Profil NACA 0012 de 150 mm de Corde en Presence de Parois Adaptables a la Soufflerie T2 de l'ONERA/CERT*. Rapp. Tech. OA 22/3075 AND, O.N.E.R.A., Juillet 1981.
21. Salas, M. D.; and Gumbert, Clyde R.: *Breakdown of the Conservative Potential Equation*. NASA TP-2539, 1986.
22. Harris, Charles D.: *Two-Dimensional Aerodynamic Characteristics of the NACA 0012 Airfoil in the Langley 8-Foot Transonic Pressure Tunnel*. NASA TM-81927, 1981.
23. Barnwell, Richard W.: *Design and Performance Evaluation of Slotted Walls for Two-Dimensional Wind Tunnels*. NASA TM-78648, 1978.
24. McCroskey, W. J.: A Critical Assessment of Wind Tunnel Results for the NACA 0012 Airfoil. *Aerodynamic Data Accuracy and Quality: Requirements and Capabilities in Wind Tunnel Testing*, AGARD-CP-429, July 1988, pp. 1-1-1-21.

Table I. Key to Data Symbols Used in Figures

(a) Data symbols depicting ratio of tunnel half-height to chord (h/c)

Data symbol	h/c	Data source
	0.5	Adaptive wall; test 208 in 0.3-m TCT
	1.0	Adaptive wall; test 201 in 0.3-m TCT
	1.0	Adaptive wall; test 209 in 0.3-m TCT
	1.27	Adaptive wall; ONERA/CERT tunnel (ref. 20)
	1.7	Slotted wall; 8-ft TPT (ref. 22)
	2.0	Slotted wall; test 119 in 0.3-m TCT (ref. 10)
	∞	Free air; Navier-Stokes code (ref. 15)

(b) Definition of data symbols

Data symbol	Visual description	Definition
	Open	Uncorrected data
	Right filled	First pass; WIAC-corrected
	Left filled	Second pass; WIAC-corrected
	Filled	Third pass; WIAC-corrected
	Diagonally filled	Empirically corrected
	Flagged	Fixed transition (5 percent)
	Solid line	Free-air calculation
	Arrow	Special features

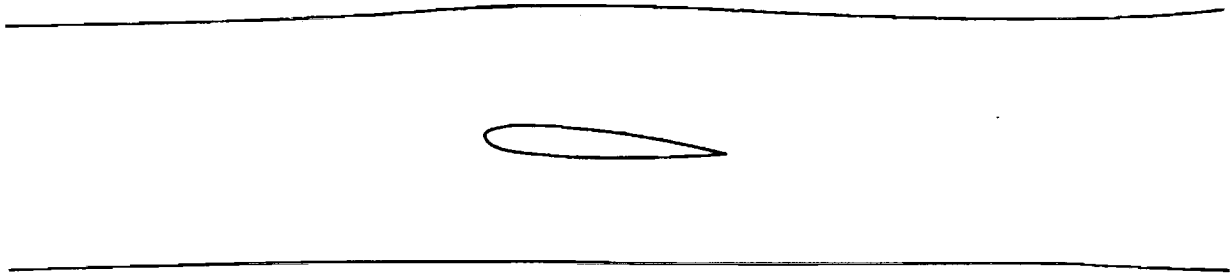


Figure 1. Streamwise section view of NACA 0012 airfoil in the Langley 0.3-m TCT with walls adapted for $h/c \approx 0.5$, $M_T \approx 0.5$, and $\alpha_T \approx 4^\circ$.

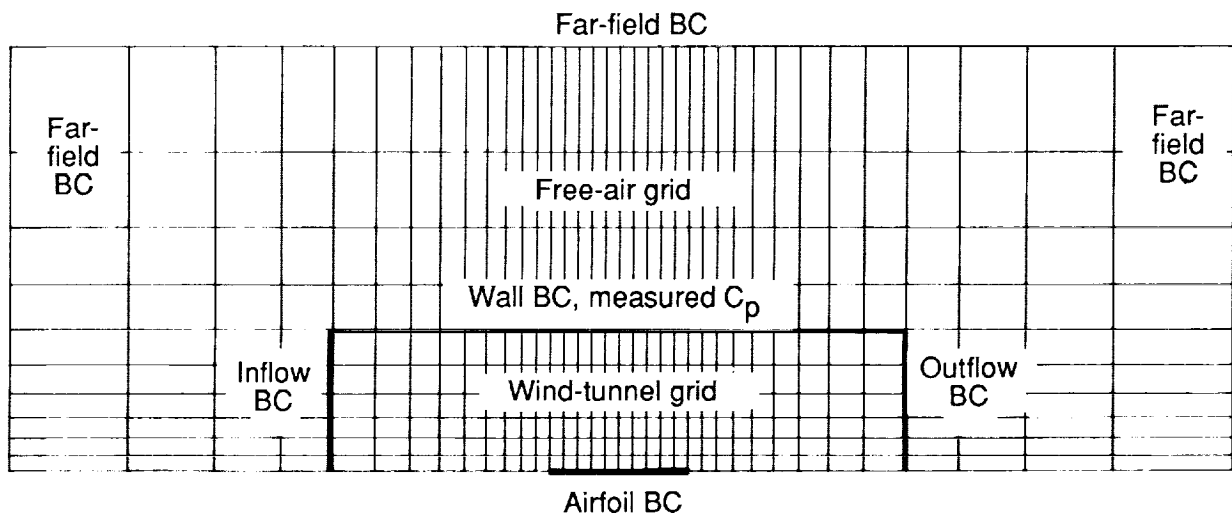
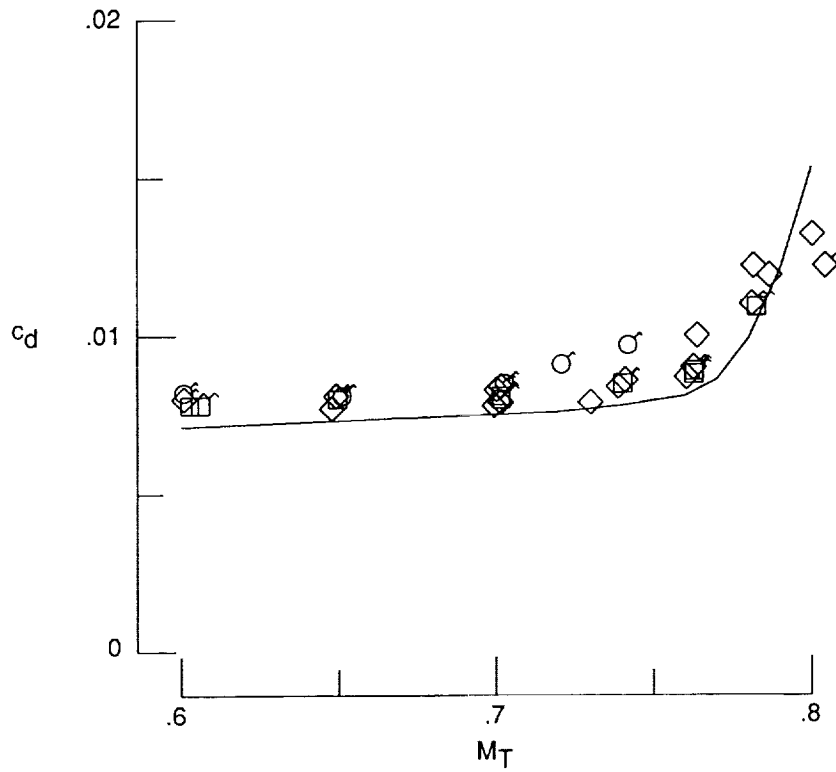
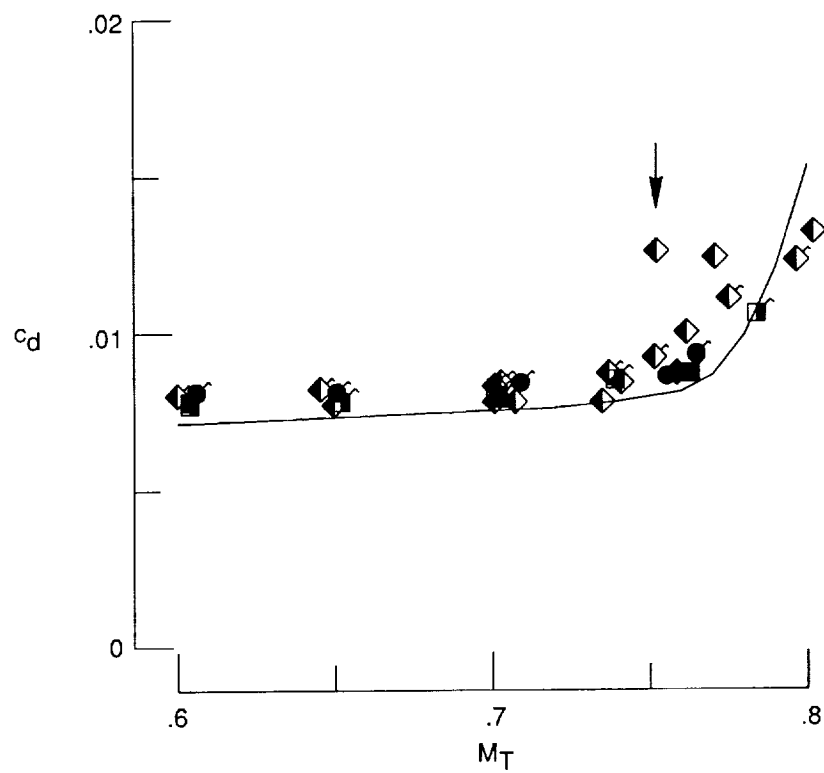


Figure 2. Schematic diagram of TWNTN4A computational grid (upper half-plane only).

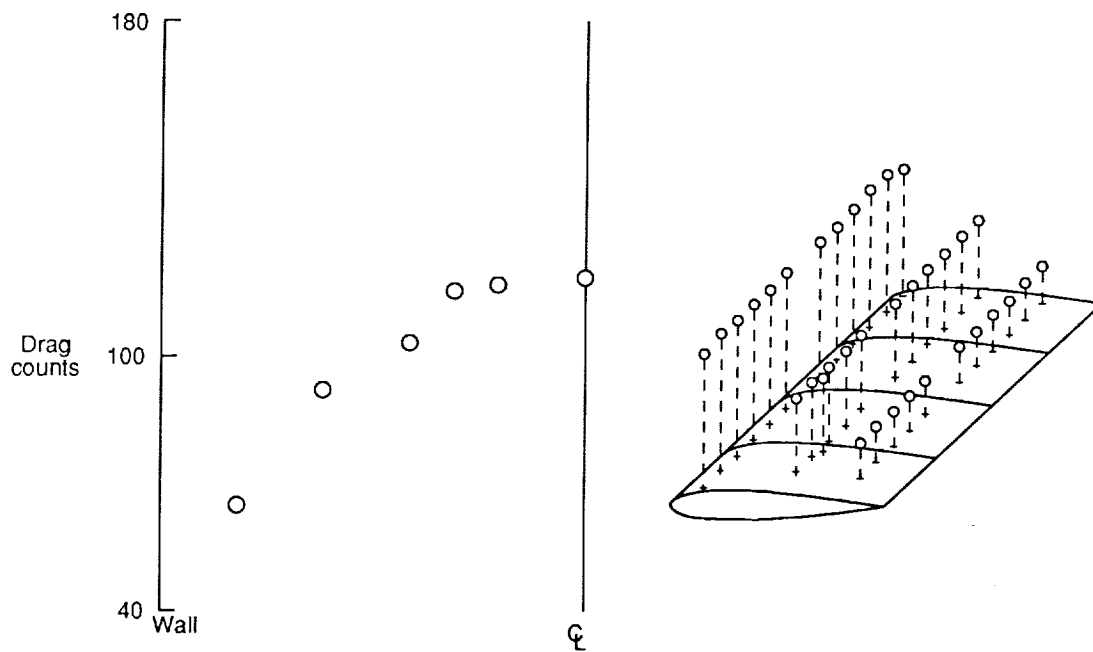


(a) Uncorrected, fully adapted data.

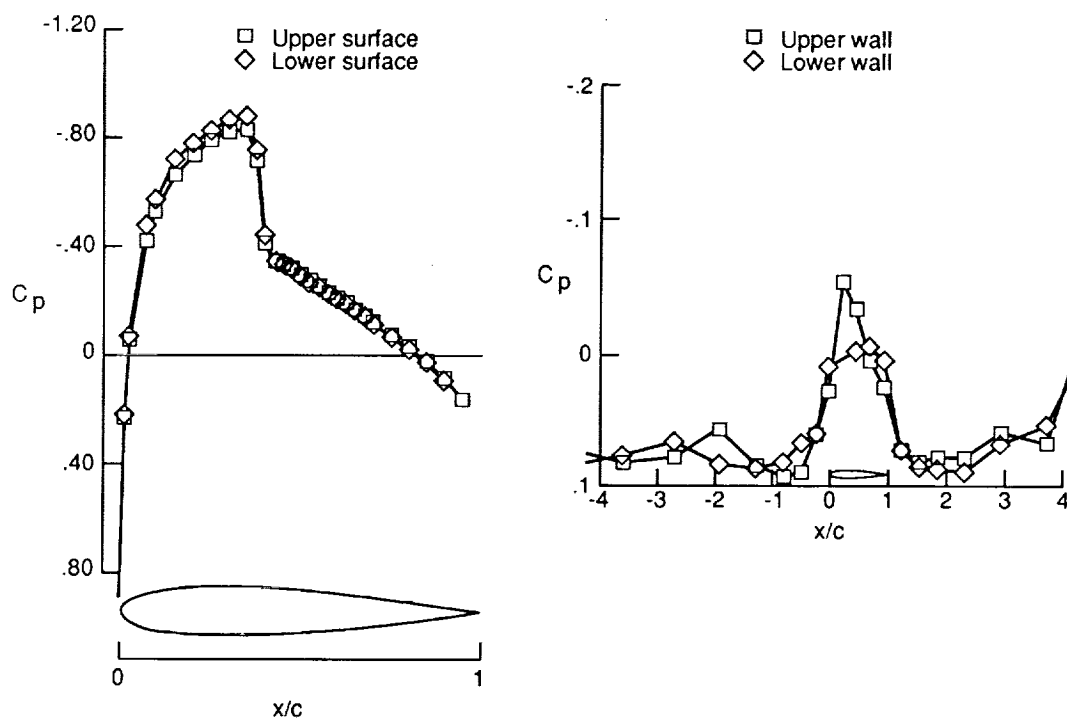


(b) TWNTN4A-corrected, fully adapted data.

Figure 3. Drag curves for NACA 0012 airfoil at $R_c \approx 9 \times 10^6$ and $c_l \approx 0$. See table I for symbol key.

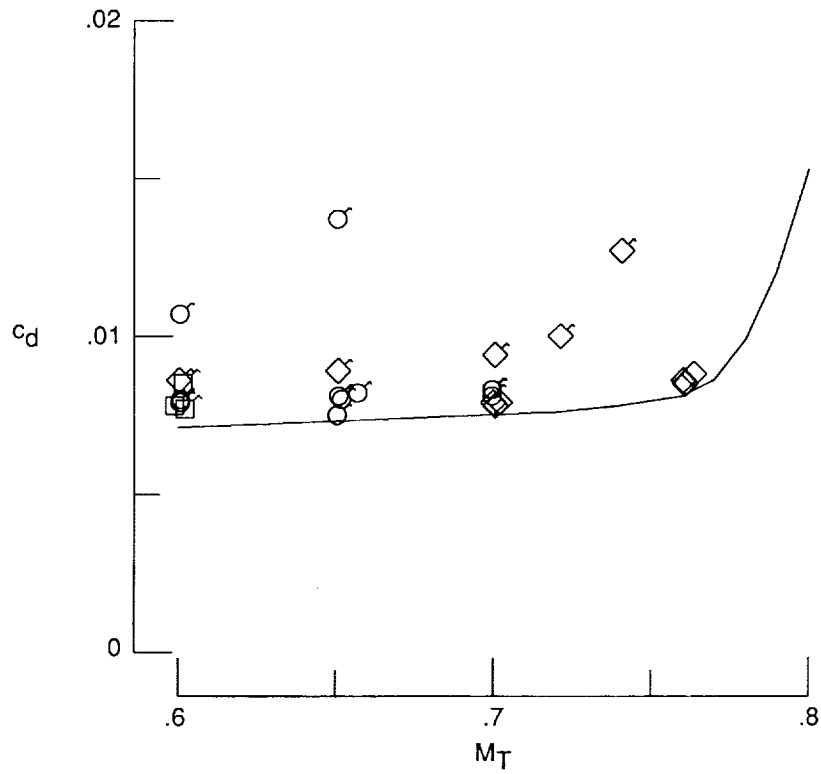


(a) Spanwise drag-rake survey and model pressure coefficient distribution.

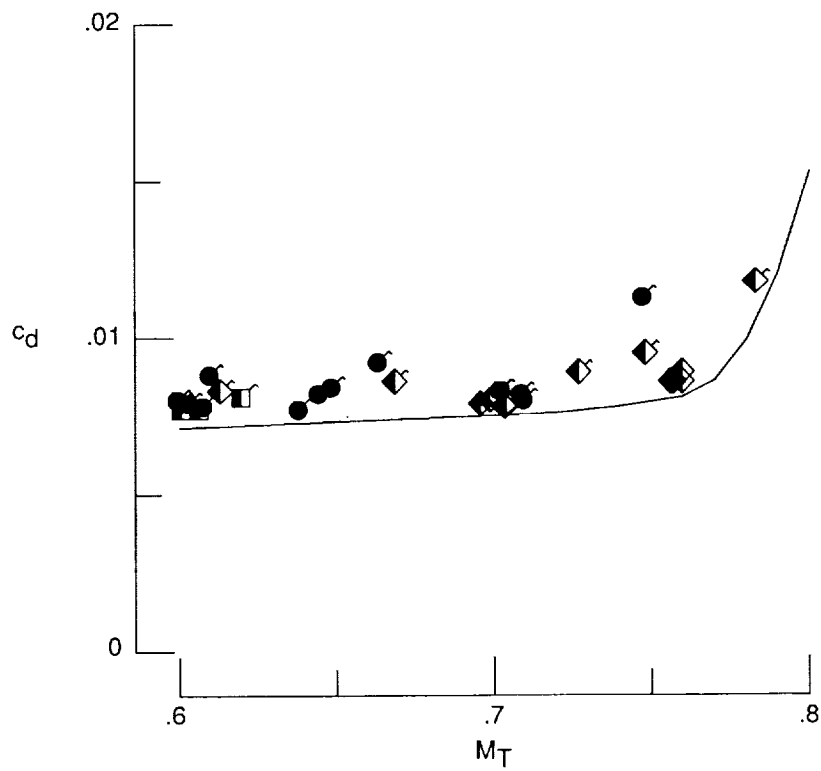


(b) Model and wall pressure coefficient distributions.

Figure 4. Preprocessor plots for NACA 0012 airfoil at $R_c \approx 9 \times 10^6$, $M_T \approx 0.79$, and $\alpha_T \approx 0^\circ$.

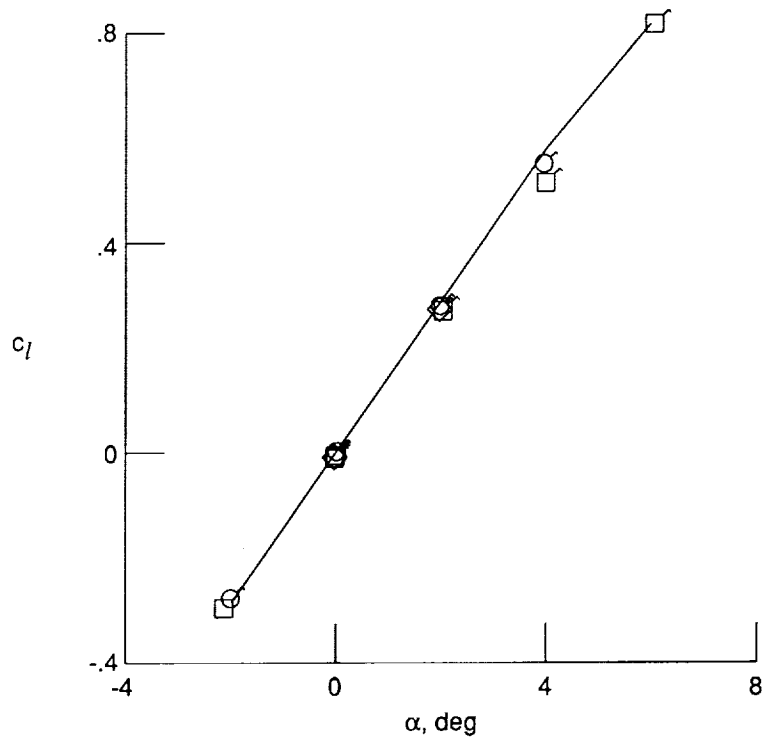


(a) Uncorrected, unadapted, or partially adapted data.

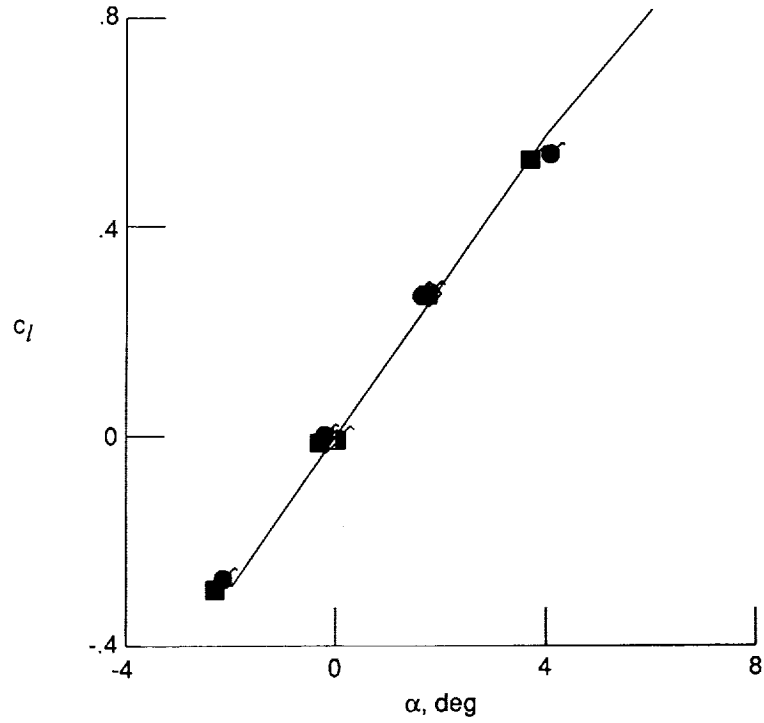


(b) TWNTN4A-corrected, unadapted, or partially adapted data.

Figure 5. Drag curves for NACA 0012 airfoil at $R_c \approx 9 \times 10^6$ and $c_l \approx 0$. See table I for symbol key.

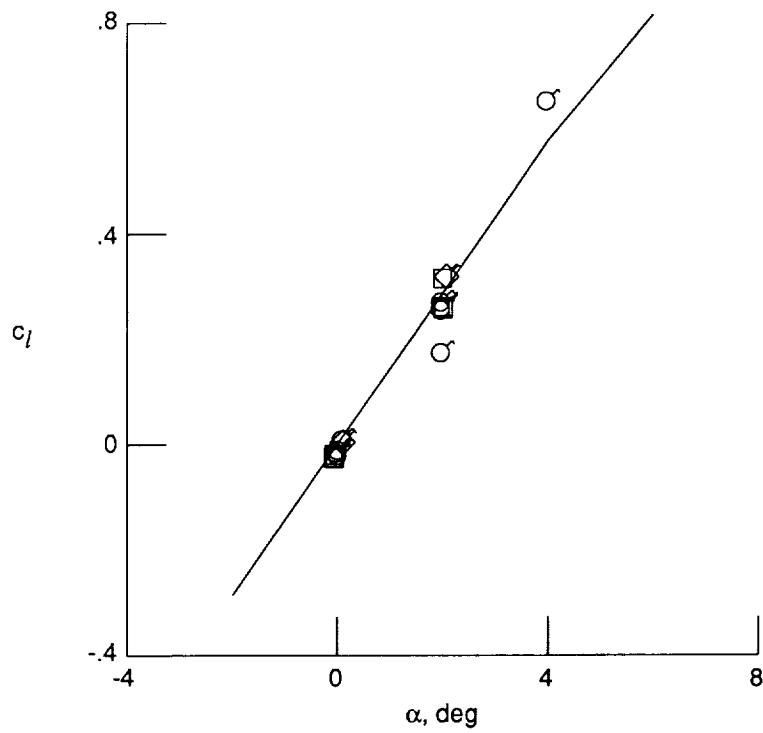


(a) Uncorrected, fully adapted data.

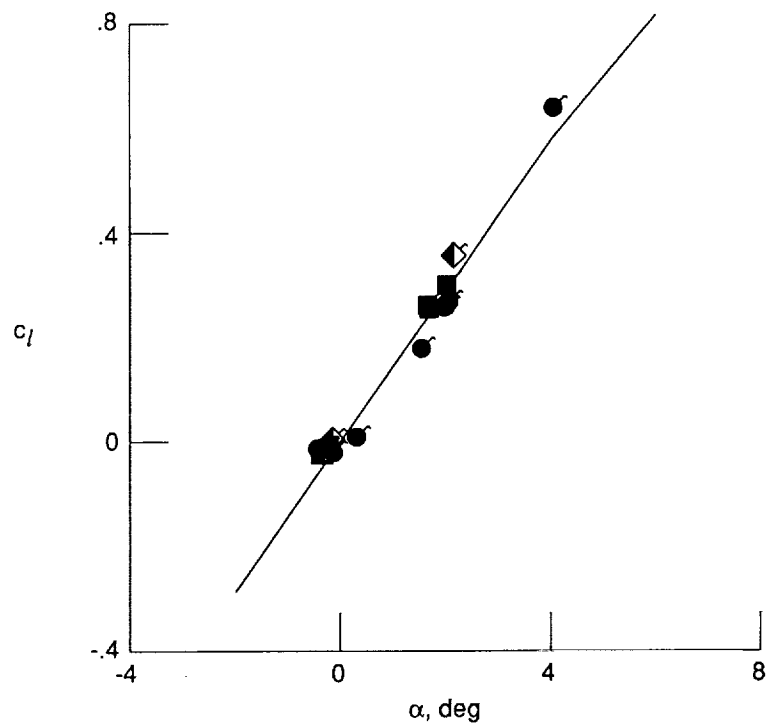


(b) TWNTN4A-corrected, fully adapted data.

Figure 6. Lift-curve data for NACA 0012 airfoil at $R_c \approx 9 \times 10^6$ and $M_T \approx 0.6$. See table I for symbol key.

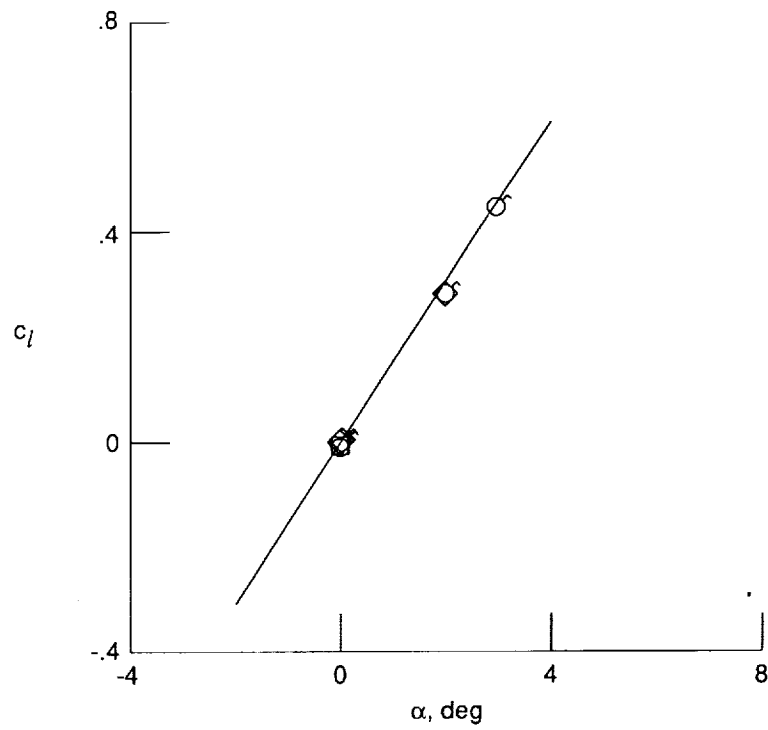


(c) Uncorrected, unadapted, or partially adapted data.

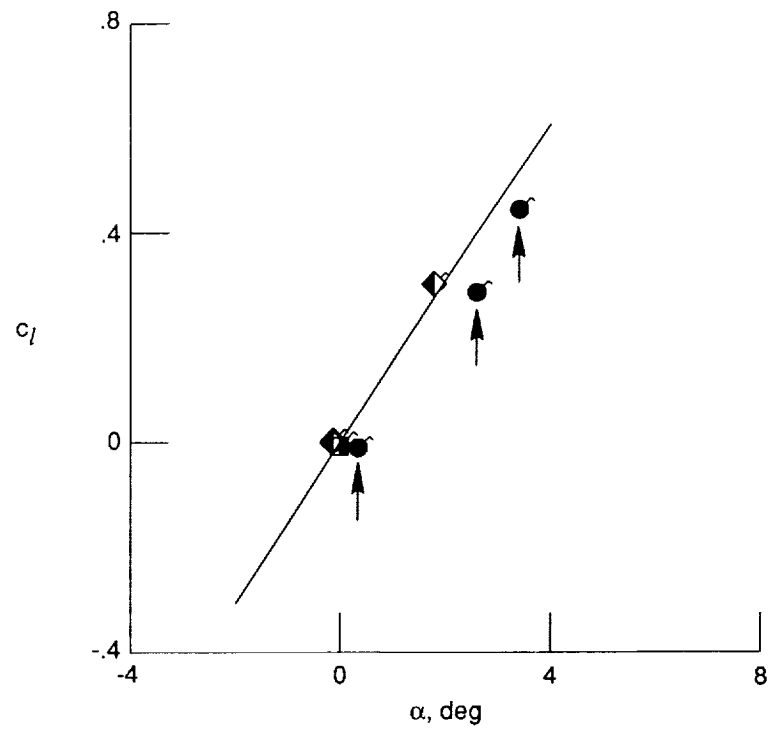


(d) TWNTN4A-corrected, unadapted, or partially adapted data.

Figure 6. Concluded.

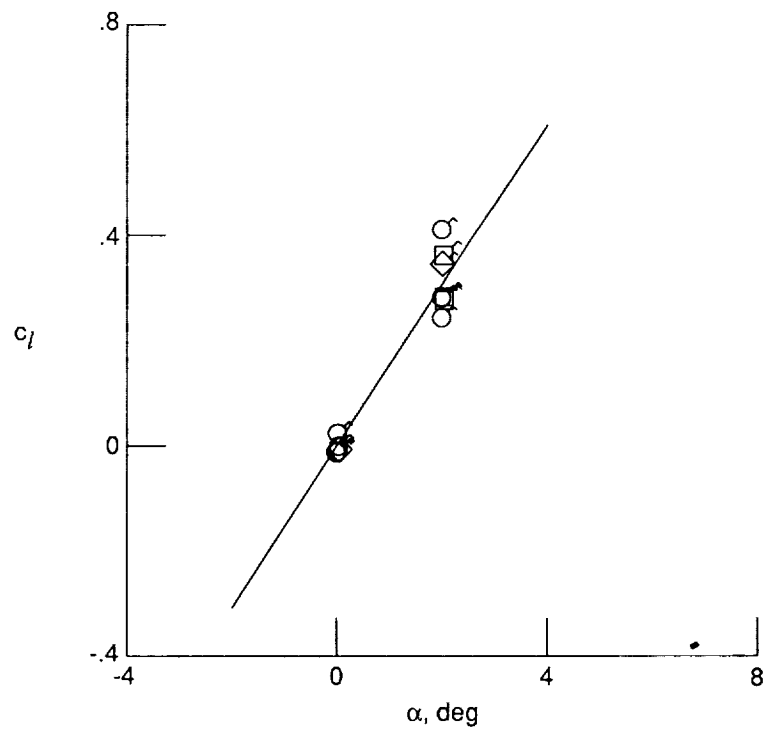


(a) Uncorrected, fully adapted data.

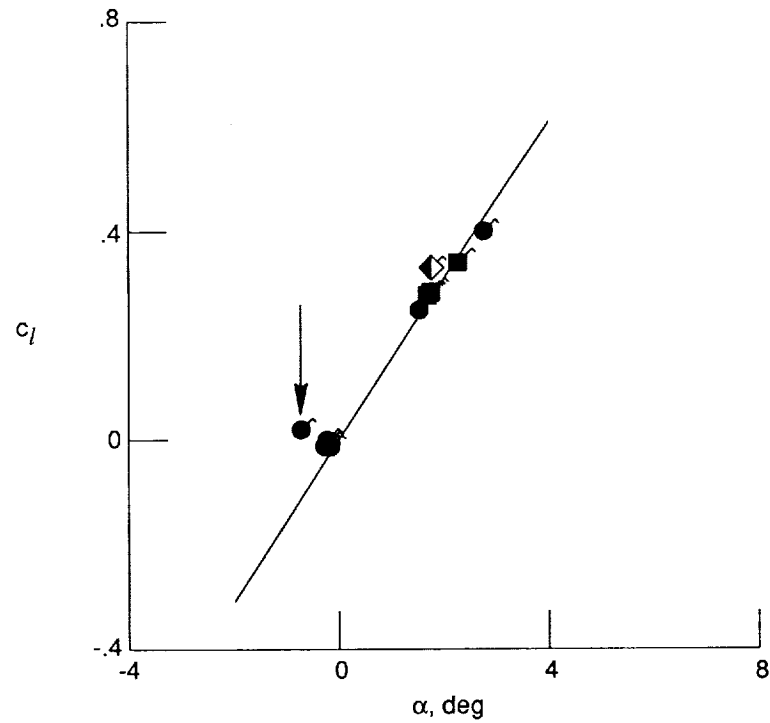


(b) TWNTN4A-corrected, fully adapted data.

Figure 7. Lift-curve data for NACA 0012 airfoil at $R_c \approx 9 \times 10^6$ and $M_T \approx 0.65$. See table I for symbol key.

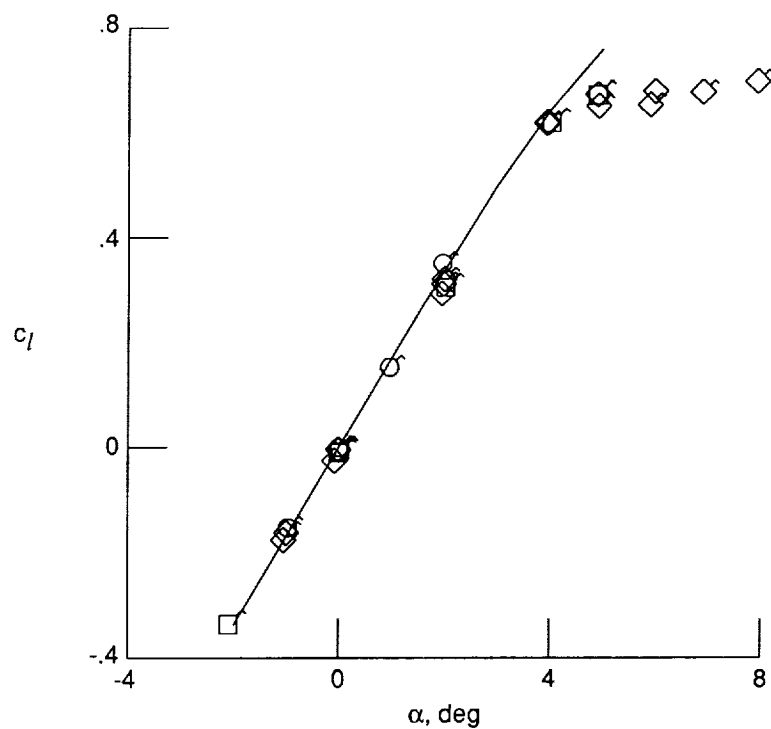


(c) Uncorrected, unadapted, or partially adapted data.

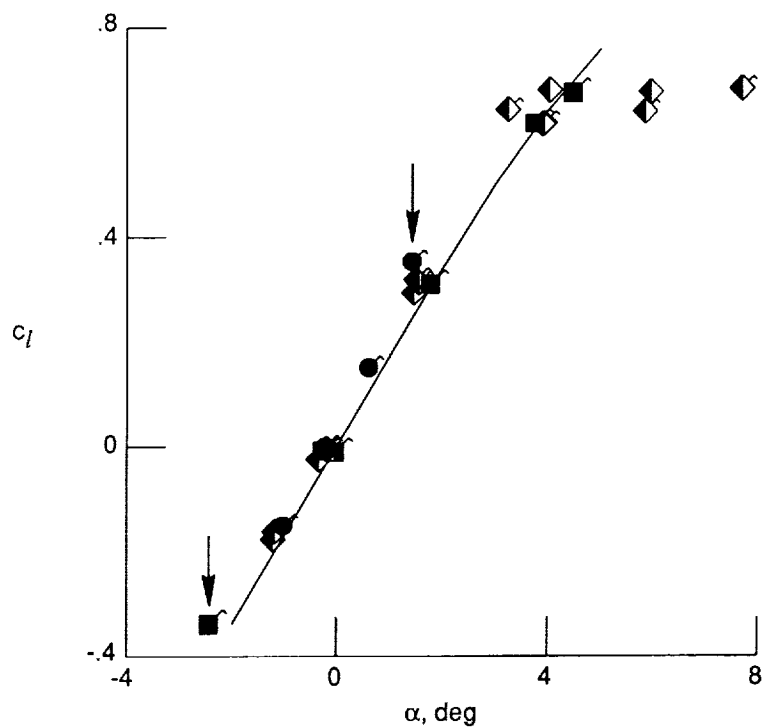


(d) TWNTN4A-corrected, unadapted, or partially adapted data.

Figure 7. Concluded.

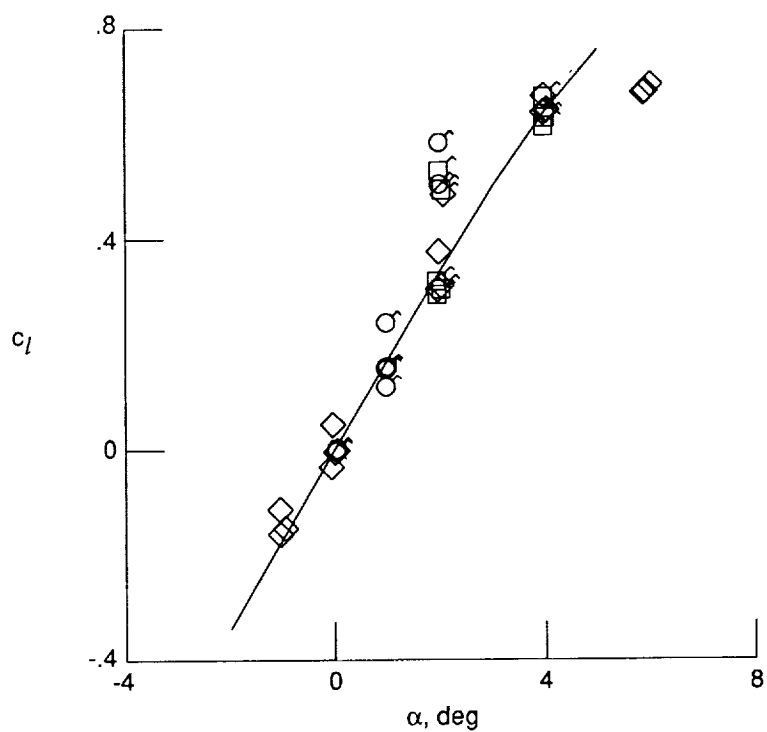


(a) Uncorrected, fully adapted data.

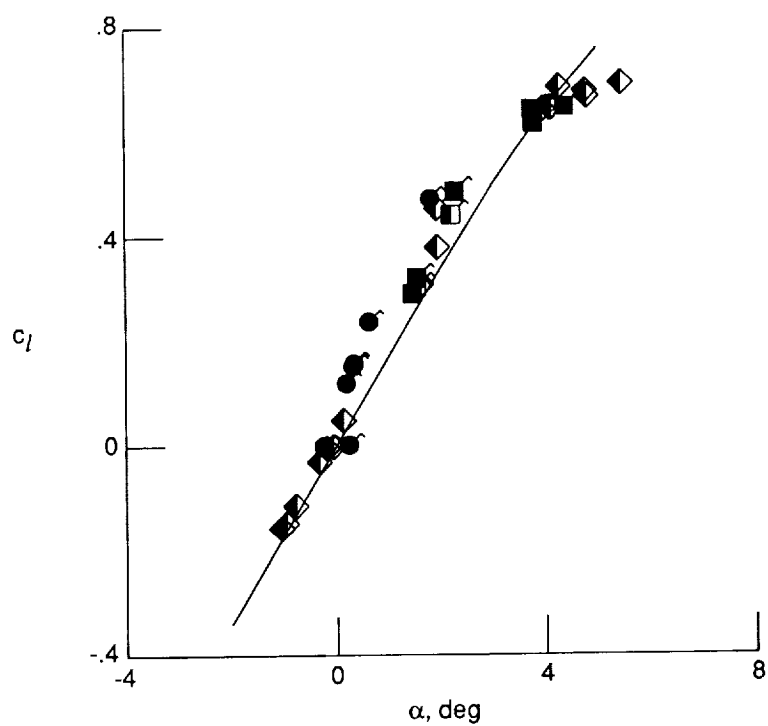


(b) TWNTN4A-corrected, fully adapted data.

Figure 8. Lift-curve data for NACA 0012 airfoil at $R_c \approx 9 \times 10^6$ and $M_T \approx 0.7$. See table I for symbol key.

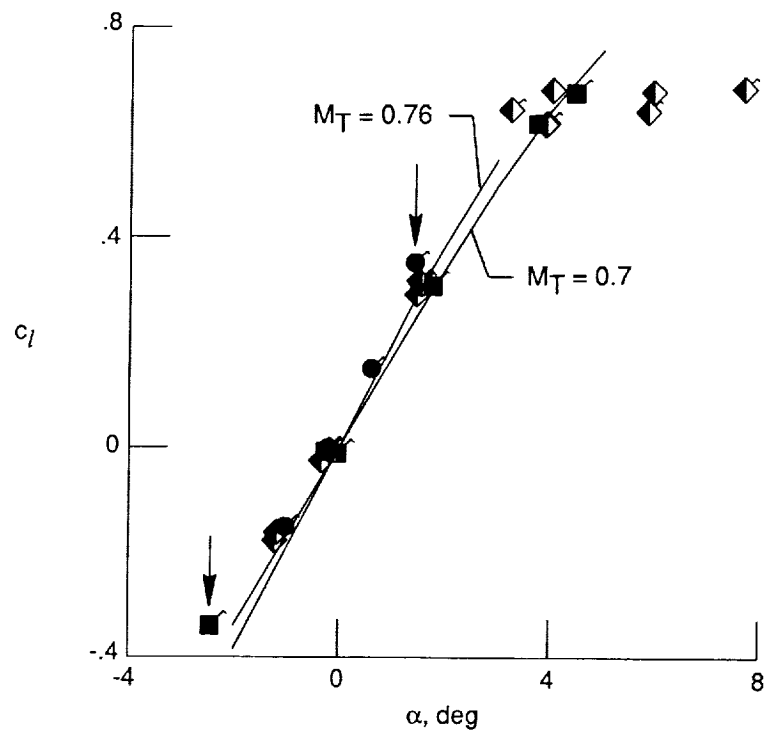


(c) Uncorrected, unadapted, or partially adapted data.

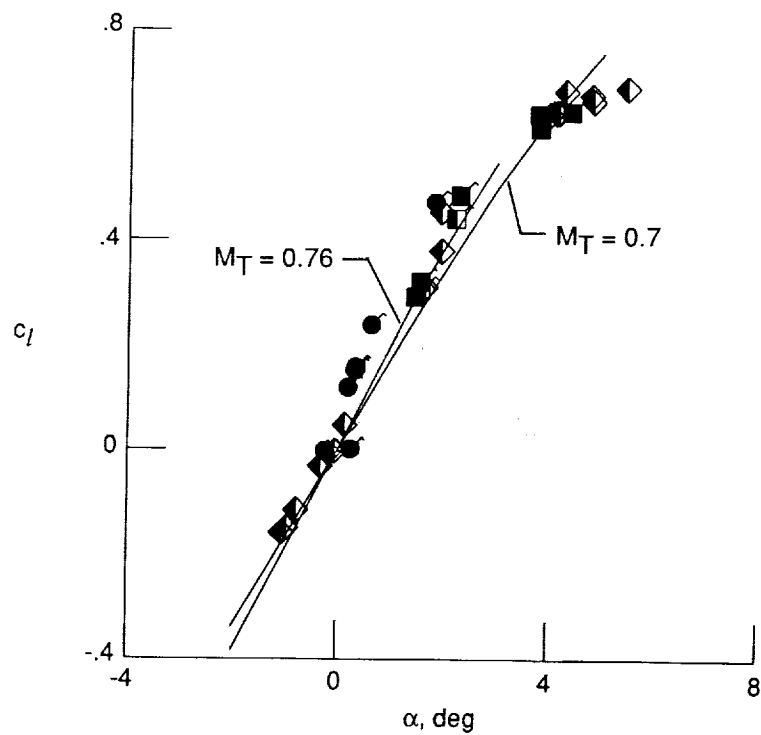


(d) TWNTN4A-corrected, unadapted, or partially adapted data.

Figure 8. Continued.

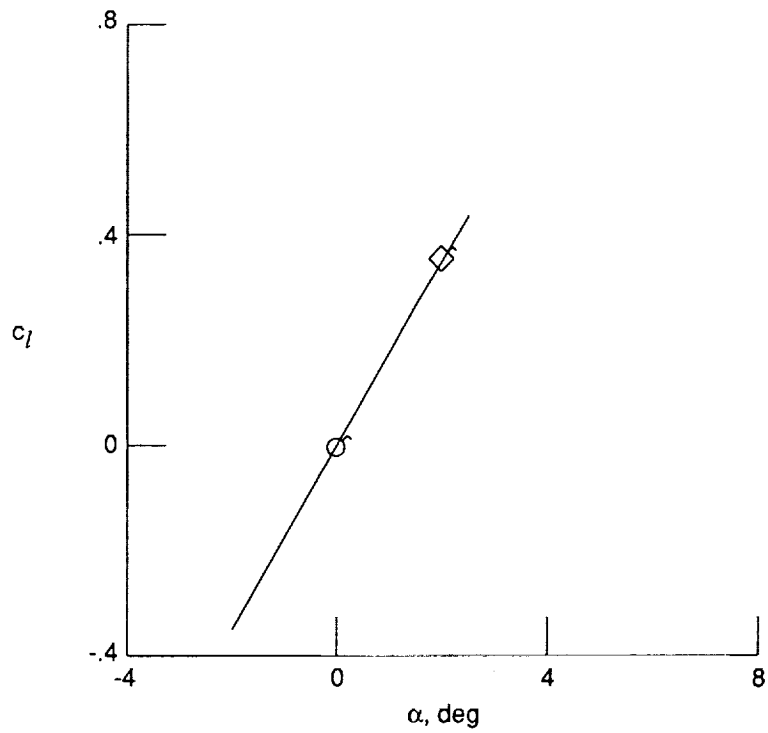


(e) TWNTN4A-corrected, fully adapted data with two N-S curves.

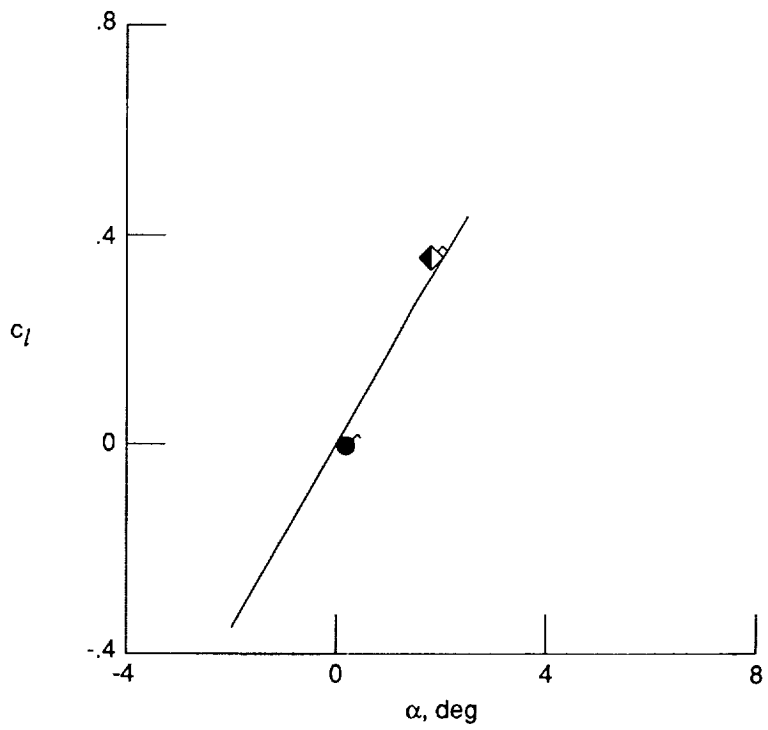


(f) TWNTN4A-corrected, unadapted, or partially adapted data with two N-S curves.

Figure 8. Concluded.

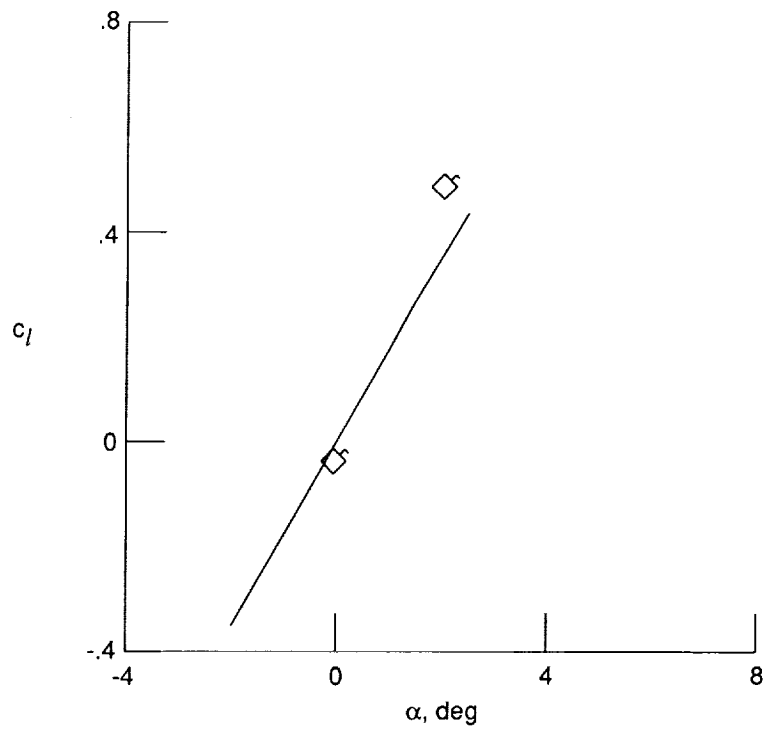


(a) Uncorrected, fully adapted data.

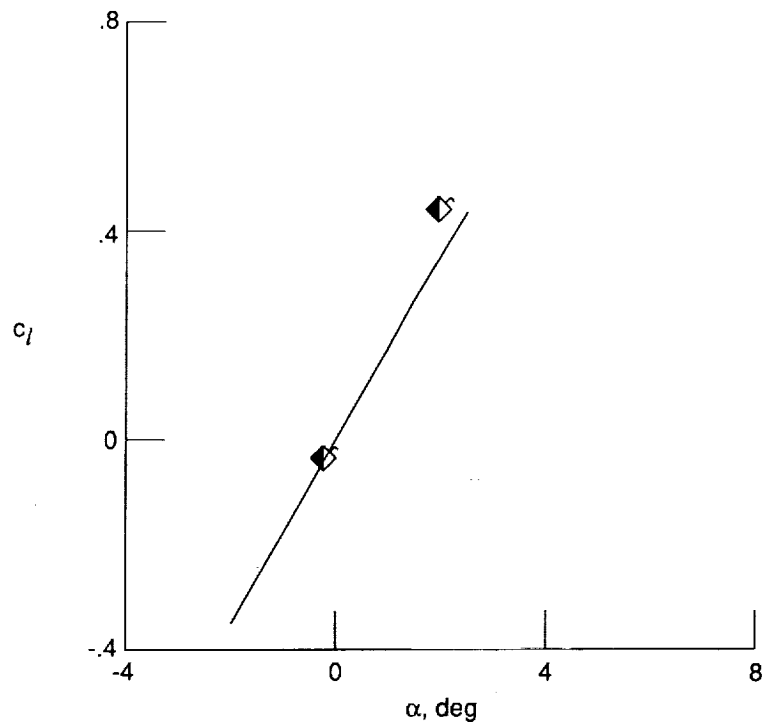


(b) TWNTN4A-corrected, fully adapted data.

Figure 9. Lift-curve data for NACA 0012 airfoil at $R_c \approx 9 \times 10^6$ and $M_T \approx 0.72$. See table I for symbol key.

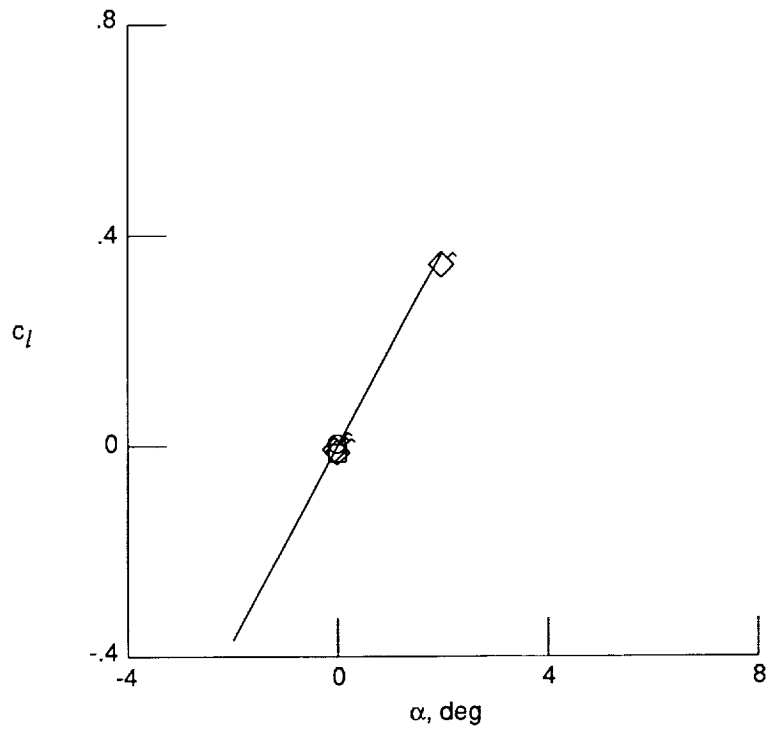


(c) Uncorrected, unadapted, or partially adapted data.

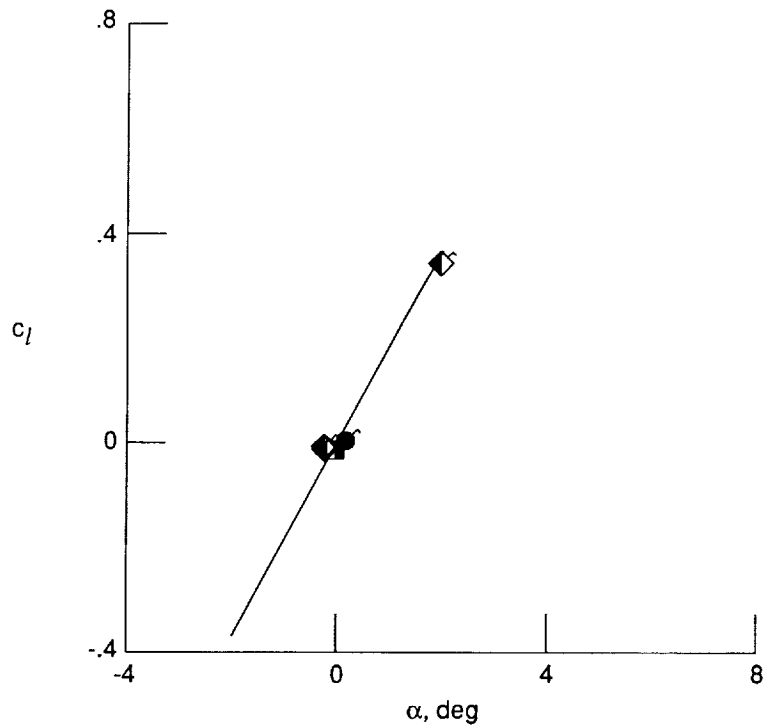


(d) TWNTN4A-corrected, unadapted, or partially adapted data.

Figure 9. Concluded.

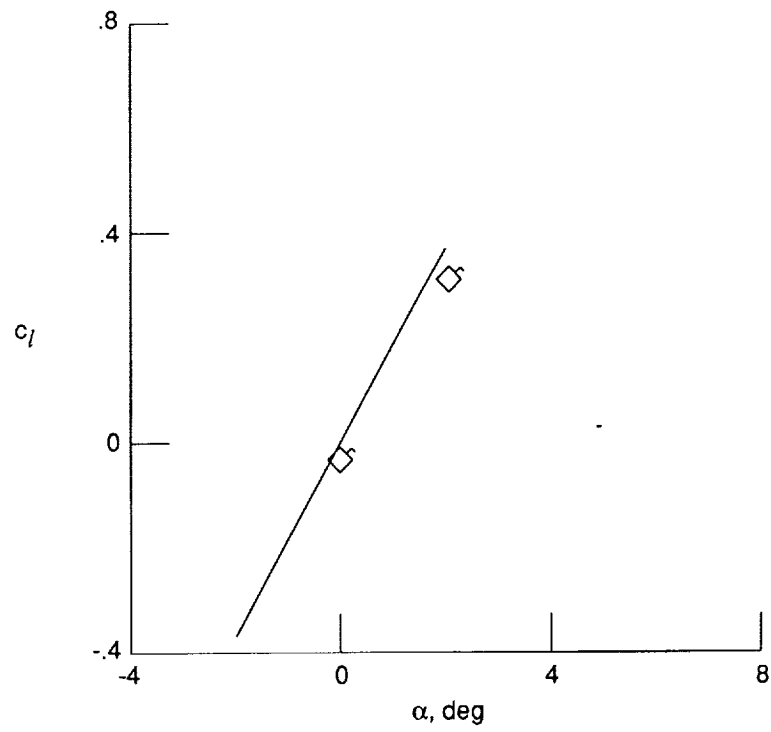


(a) Uncorrected, fully adapted data.

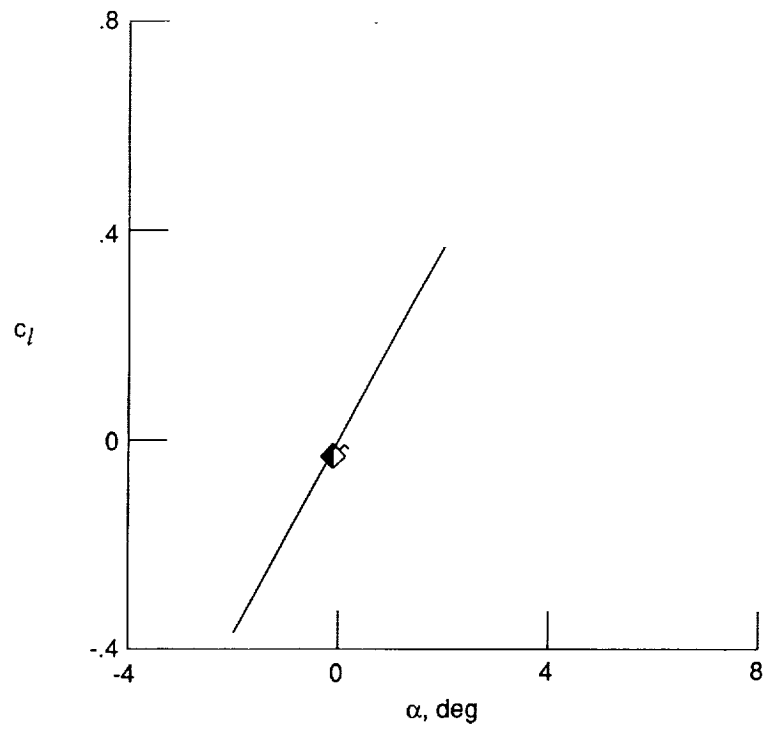


(b) TWNTN4A-corrected, fully adapted data.

Figure 10. Lift-curve data for NACA 0012 airfoil at $R_c \approx 9 \times 10^6$ and $M_T \approx 0.74$. See table I for symbol key.

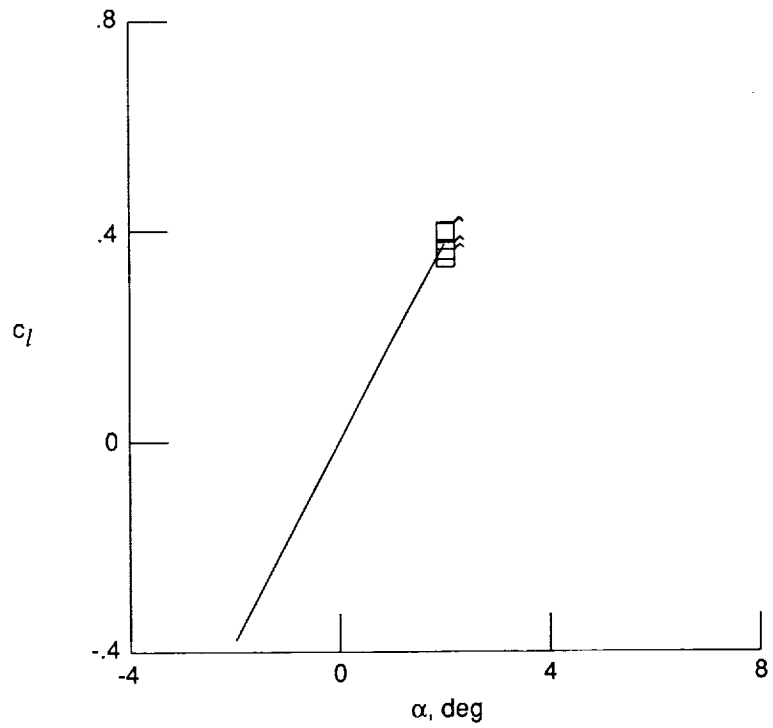


(c) Uncorrected, unadapted, or partially adapted data.

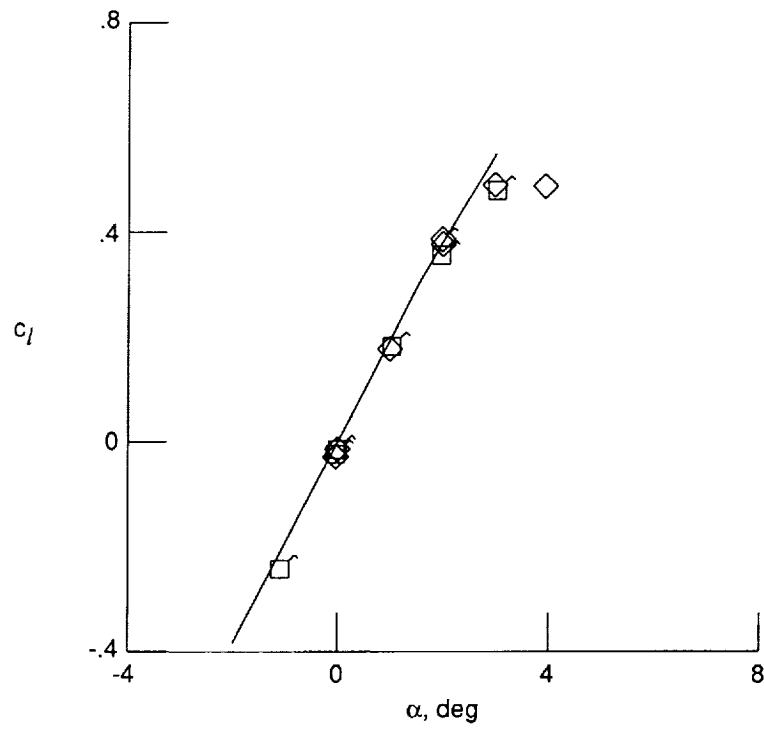


(d) TWNTN4A-corrected, unadapted, or partially adapted data.

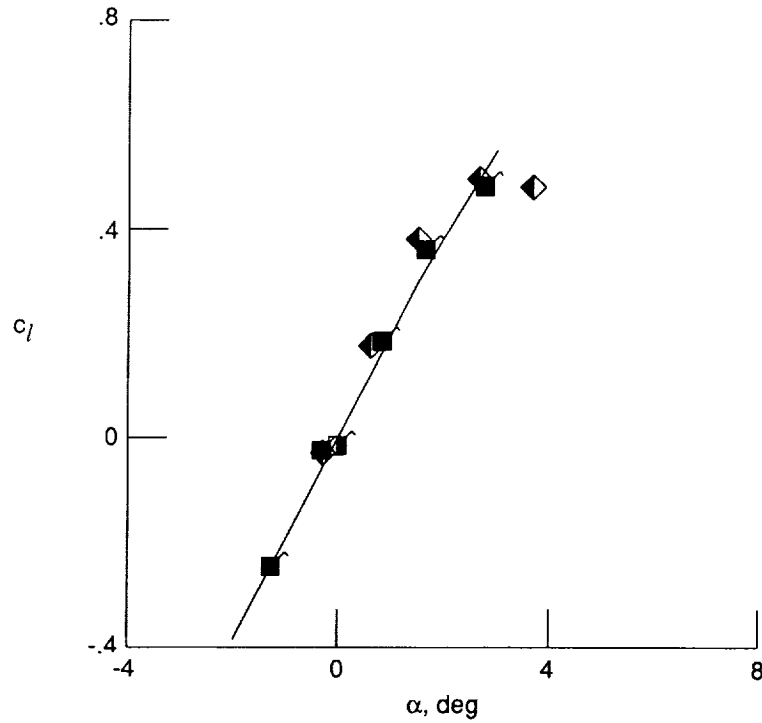
Figure 10. Concluded.



(a) Uncorrected, unadapted, or partially adapted data.

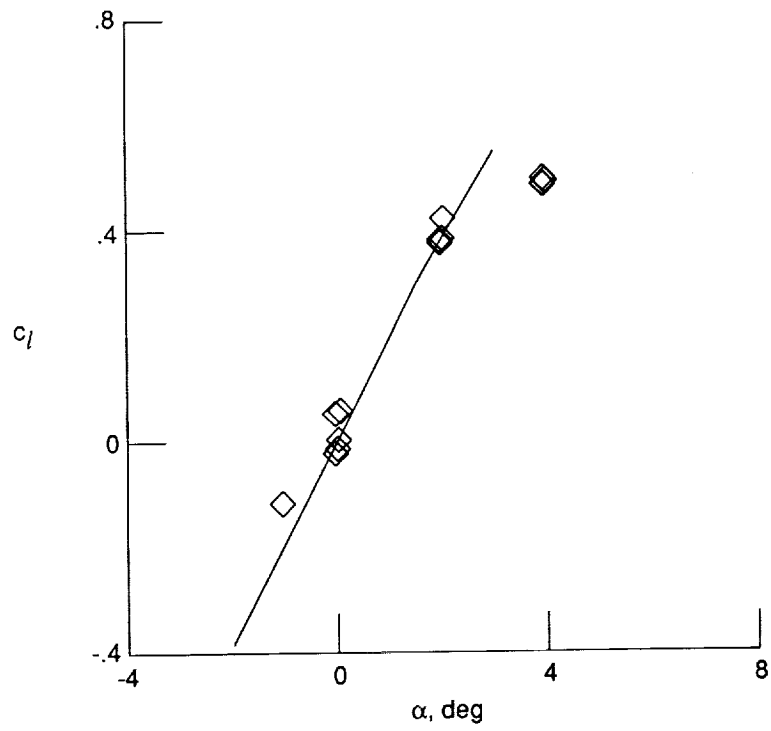


(a) Uncorrected, fully adapted data.

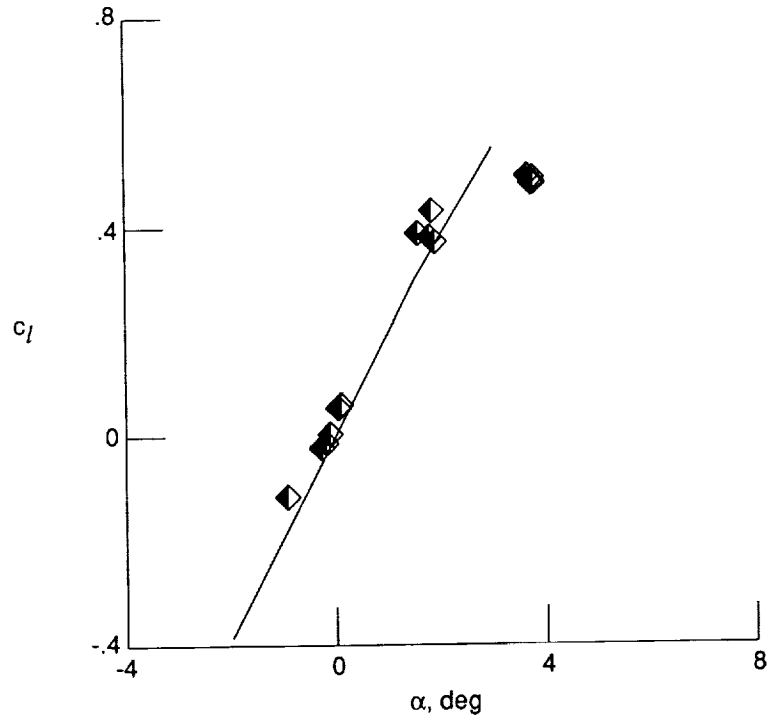


(b) TWNTN4A-corrected, fully adapted data.

Figure 12. Lift-curve data for NACA 0012 airfoil at $R_c \approx 9 \times 10^6$ and $M_T \approx 0.76$. See table I for symbol key.

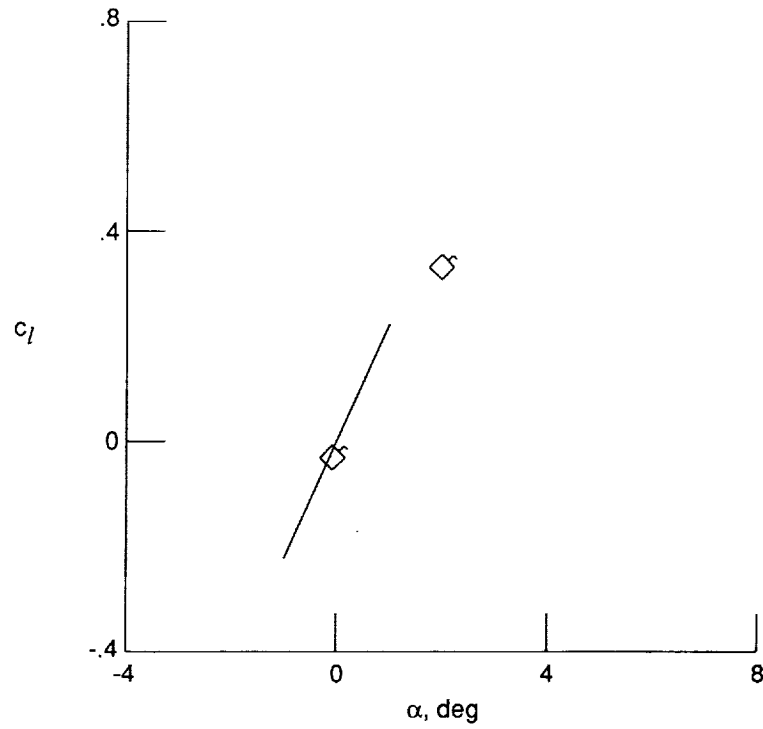


(c) Uncorrected, unadapted, or partially adapted data.

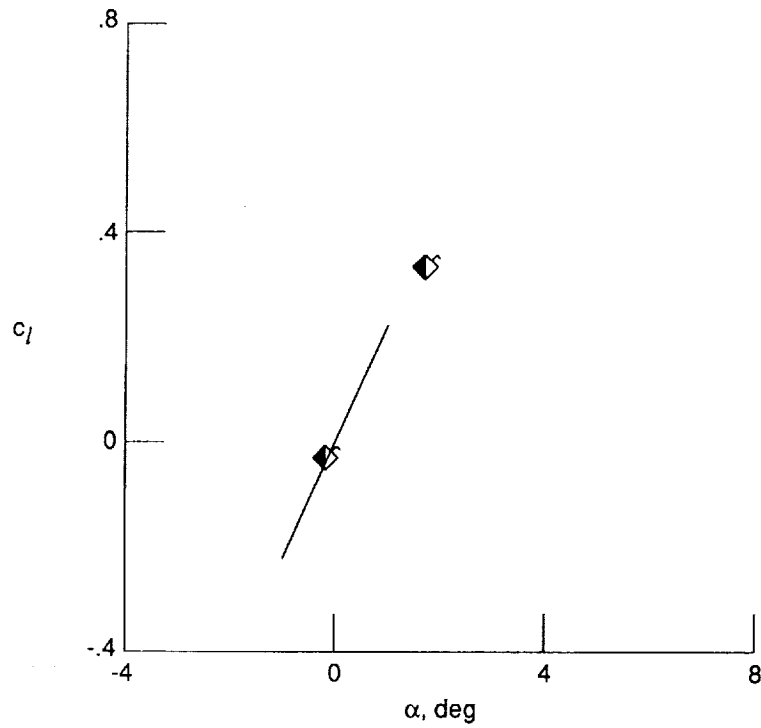


(d) TWNTN4A-corrected, unadapted, or partially adapted data.

Figure 12. Concluded.

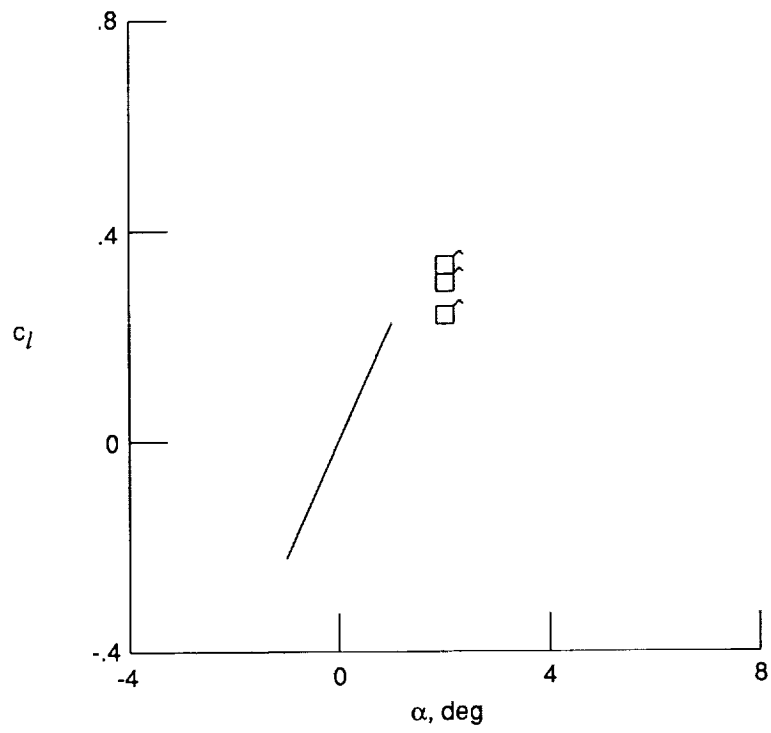


(a) Uncorrected, fully adapted data.

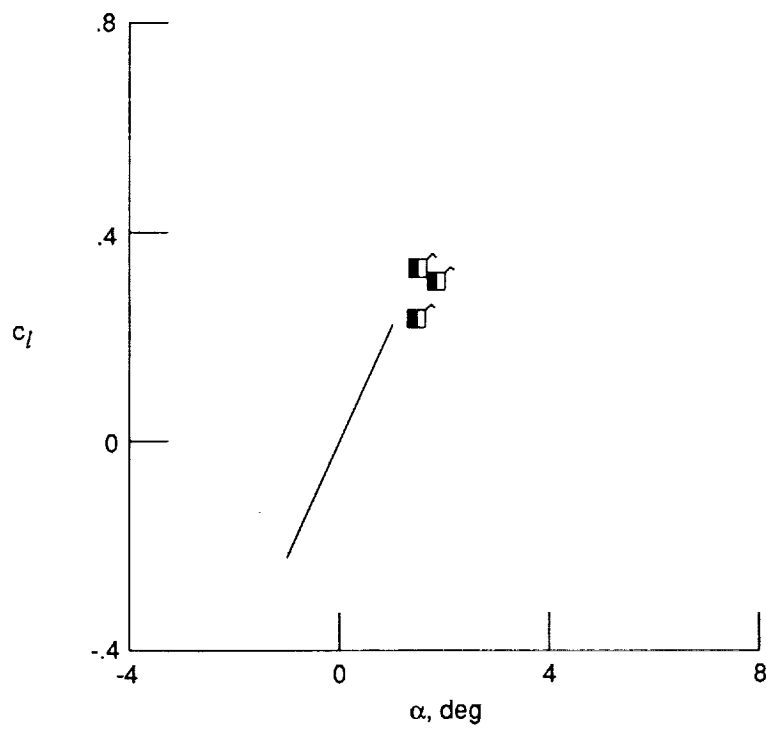


(b) TWNTN4A-corrected, fully adapted data.

Figure 13. Lift-curve data for NACA 0012 airfoil at $R_c \approx 9 \times 10^6$ and $M_T \approx 0.8$. See table I for symbol key.

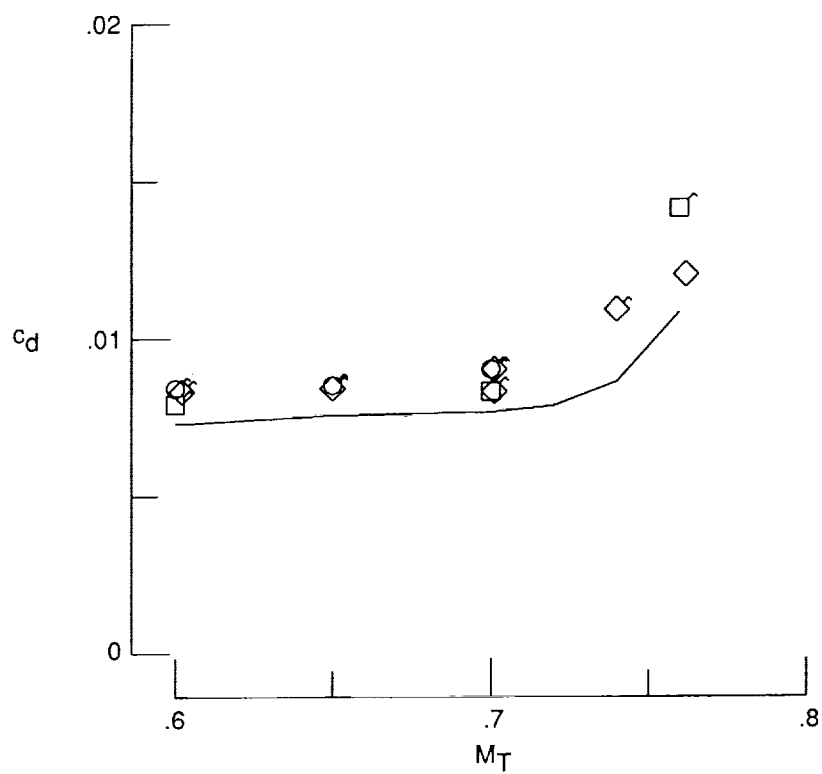


(c) Uncorrected, unadapted, or partially adapted data.

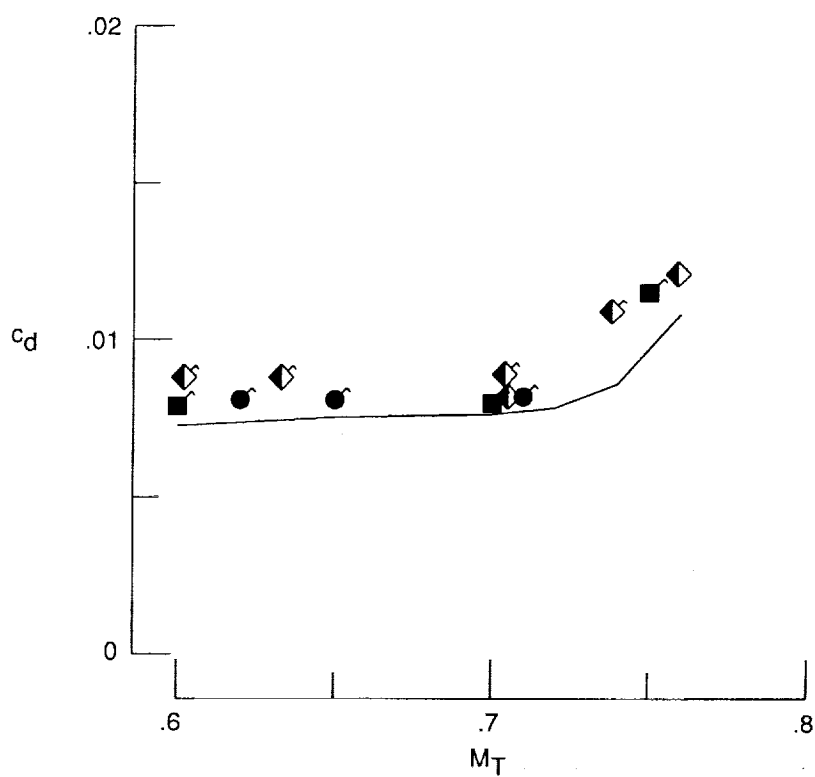


(d) TWNTN4A-corrected, unadapted, or partially adapted data.

Figure 13. Concluded.

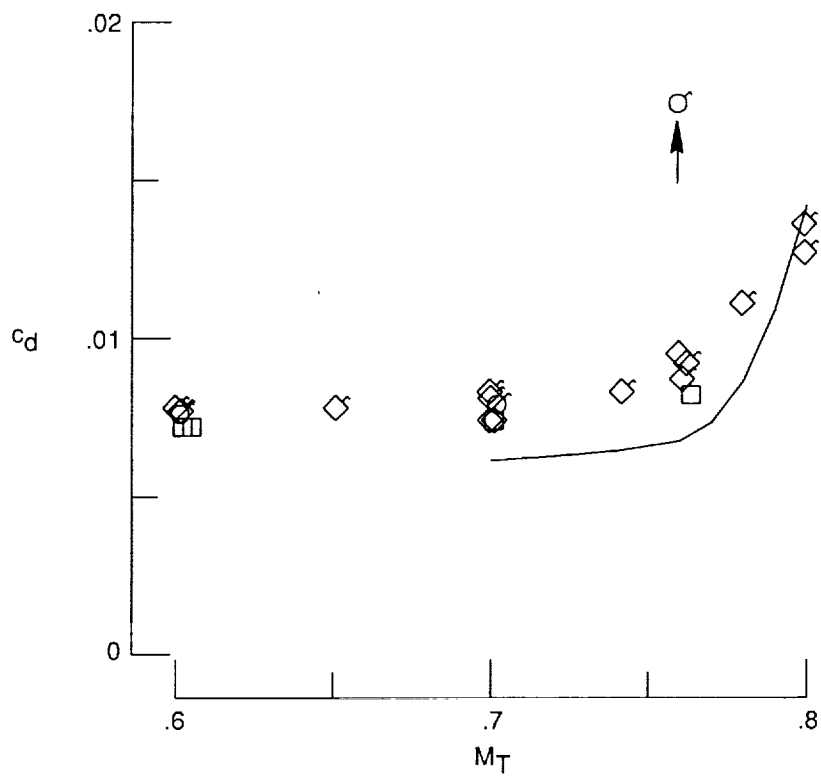


(a) Uncorrected, fully adapted data.

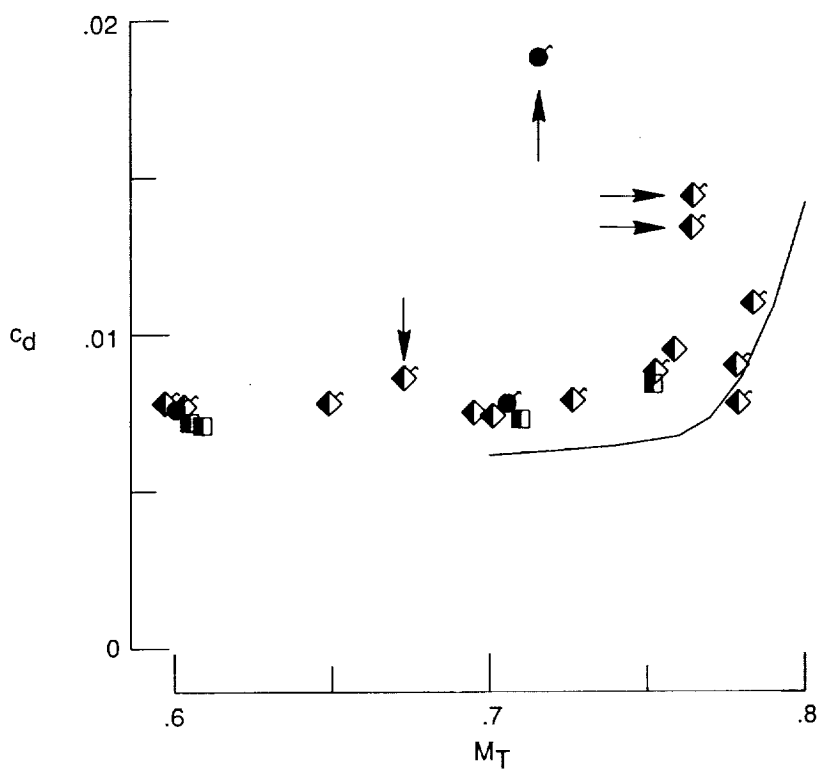


(b) TWNTN4A-corrected, fully adapted data.

Figure 14. Drag curves for NACA 0012 airfoil at $R_c \approx 9 \times 10^6$ and $c_l \approx 0.2$. See table I for symbol key.

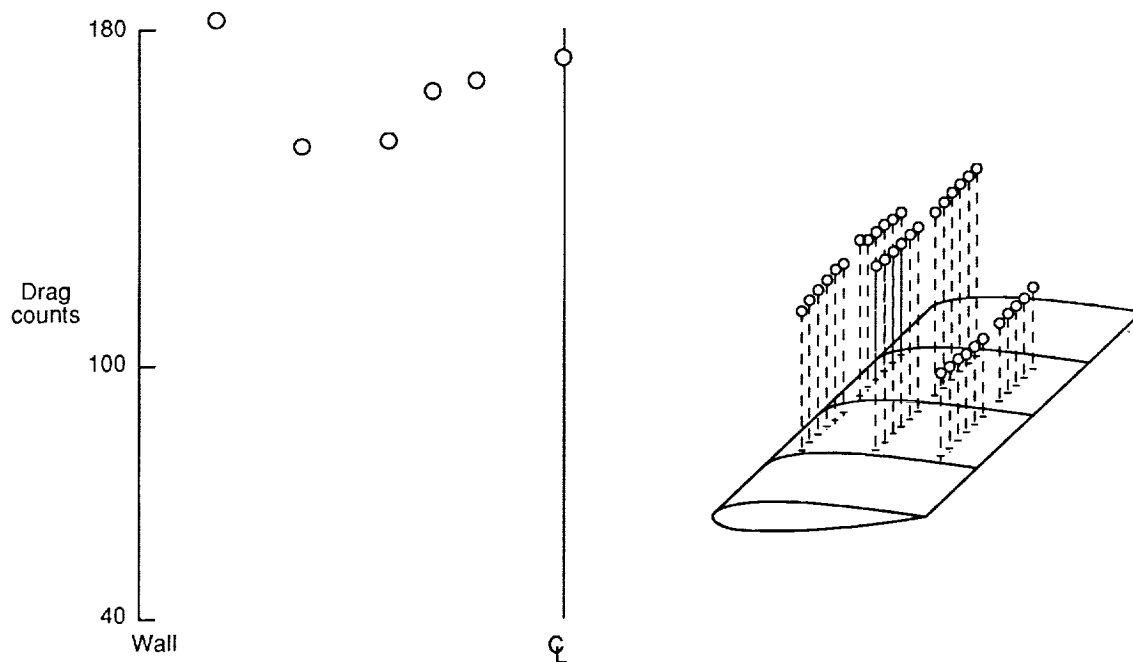


(a) Uncorrected, fully adapted data.

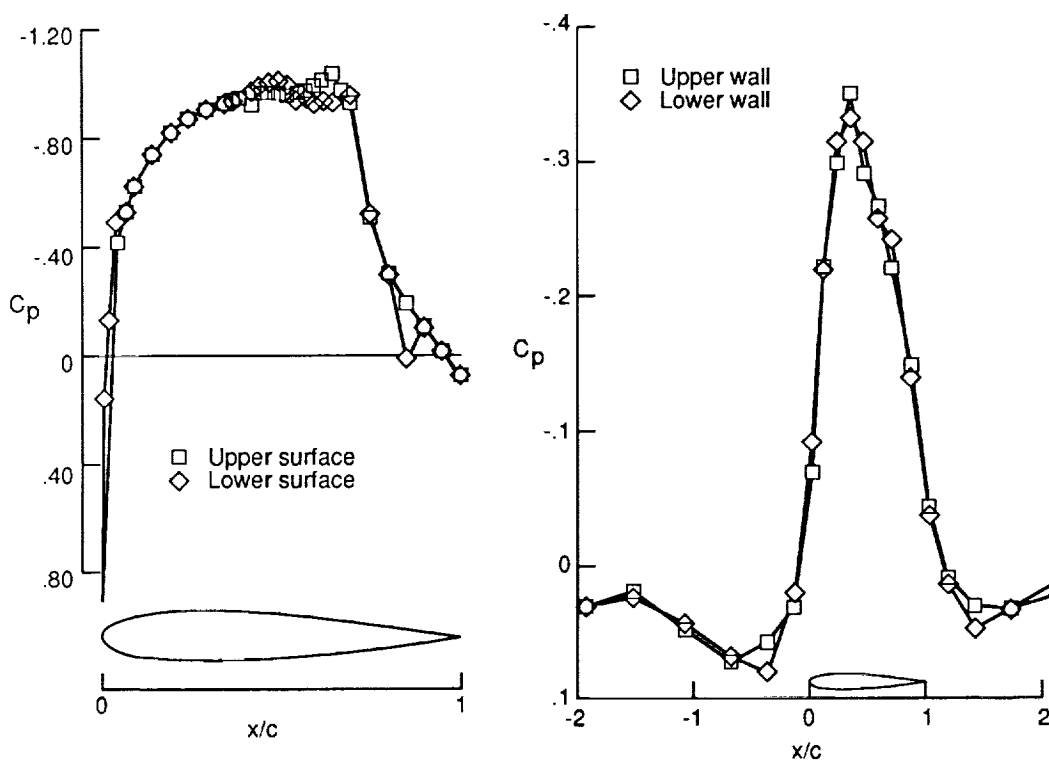


(b) TWNTN4A-corrected, fully adapted data.

Figure 15. Drag curves for NACA 0012 airfoil at $R_c \approx 15 \times 10^6$ and $c_l \approx 0$. See table I for symbol key.

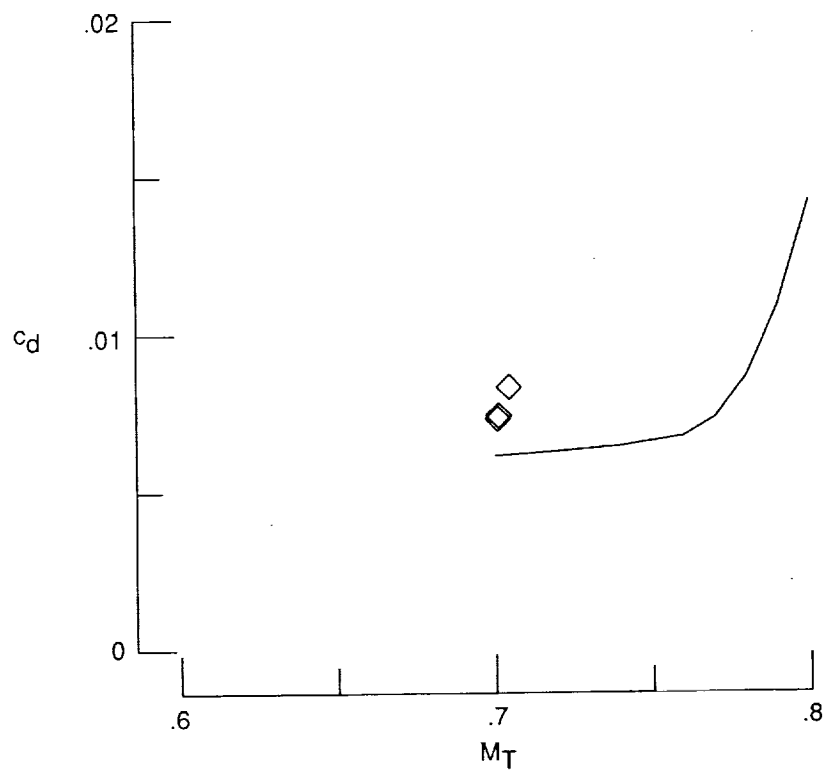


(a) Spanwise drag-rake survey and model pressure coefficient distribution.

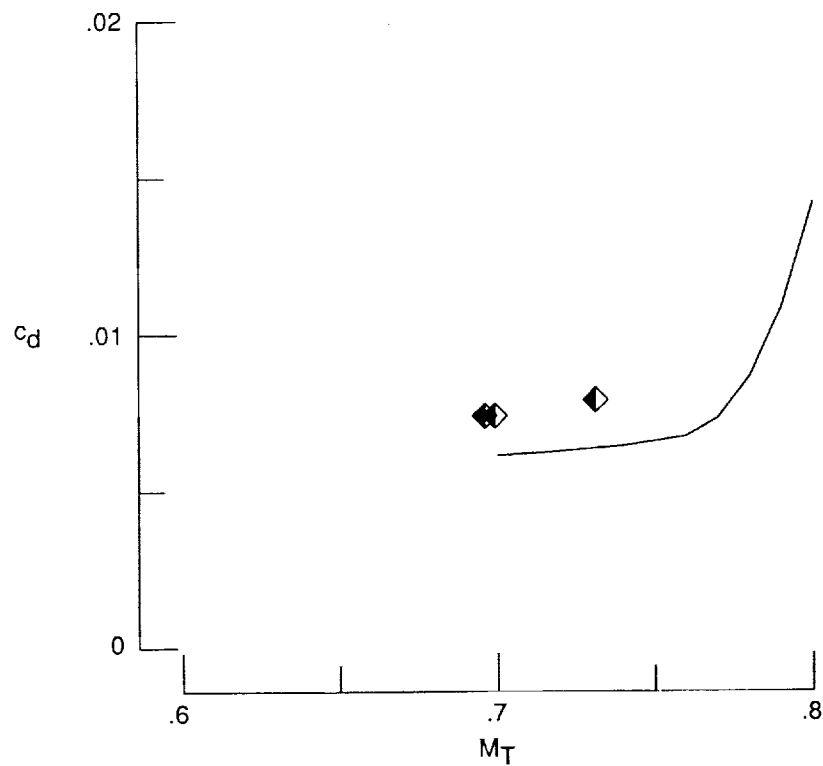


(b) Model and wall pressure coefficient distributions.

Figure 16. Preprocessor plots for NACA 0012 airfoil at $R_c \approx 15 \times 10^6$, $M_T \approx 0.76$, and $\alpha_T \approx 0^\circ$.

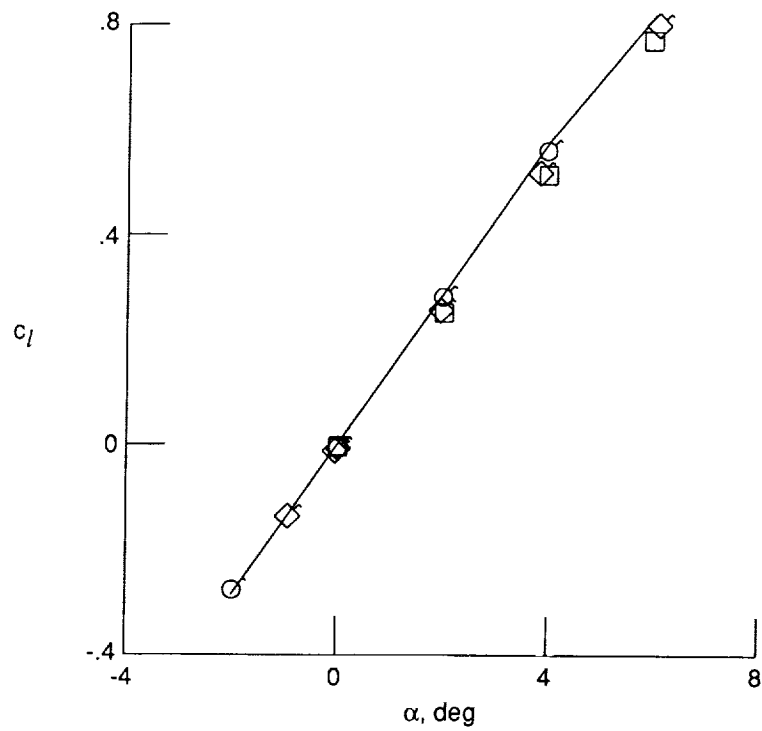


(a) Uncorrected, unadapted, or partially adapted data.

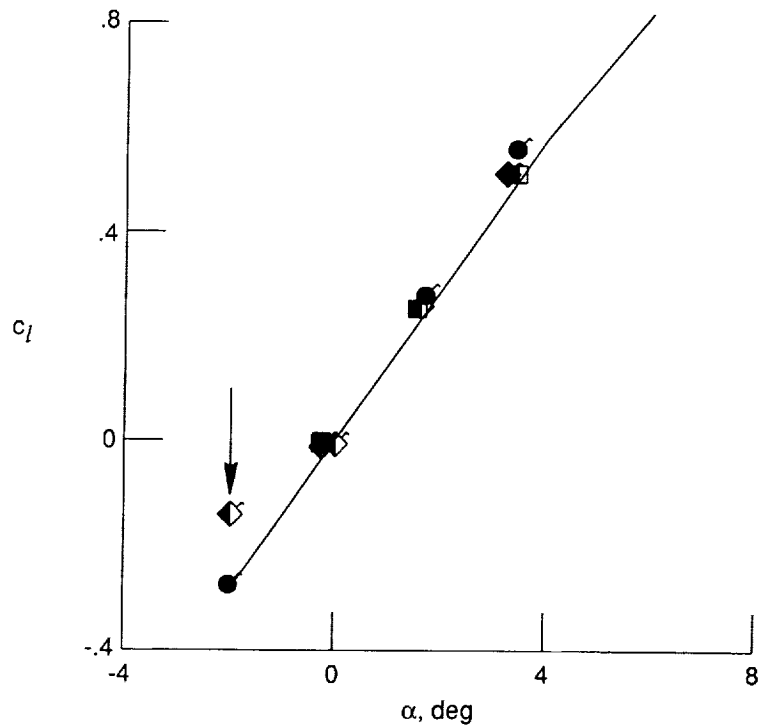


(b) TWNTN4A-corrected, unadapted, or partially adapted data.

Figure 17. Drag curves for NACA 0012 airfoil at $R_c \approx 15 \times 10^6$ and $c_l \approx 0$. See table I for symbol key.

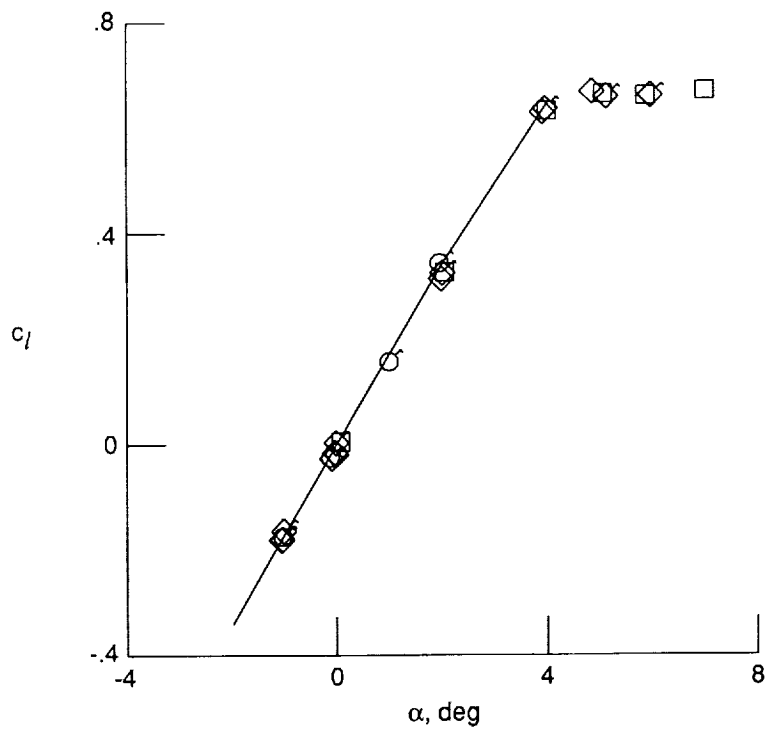


(a) Uncorrected, fully adapted data.

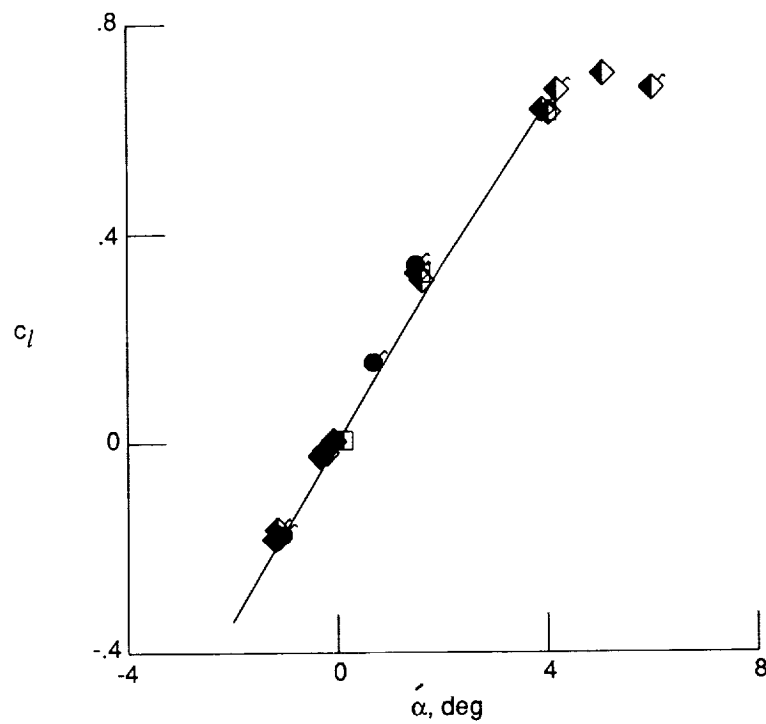


(b) TWNTN4A-corrected, fully adapted data.

Figure 18. Lift-curve data for NACA 0012 airfoil at $R_c \approx 15 \times 10^6$ and $M_T \approx 0.6$. See table I for symbol key.

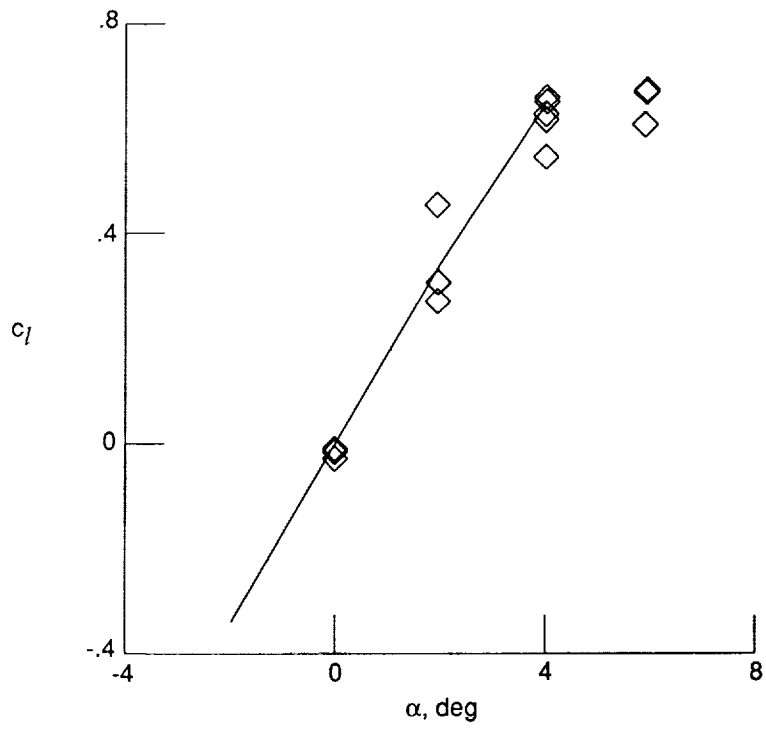


(a) Uncorrected, fully adapted data.

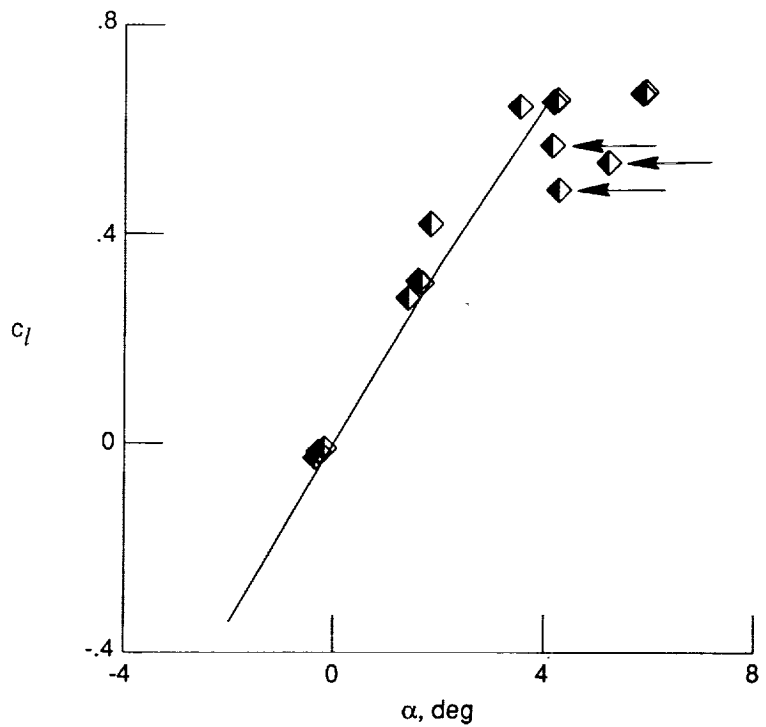


(b) TWNTN4A-corrected, fully adapted data.

Figure 19. Lift-curve data for NACA 0012 airfoil at $R_c \approx 15 \times 10^6$ and $M_T \approx 0.7$. See table I for symbol key.

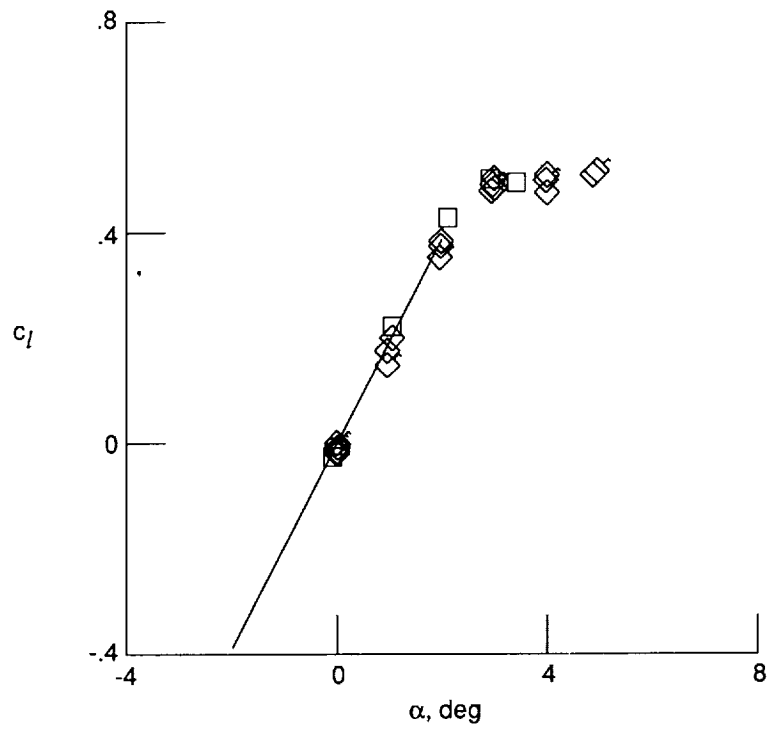


(c) Uncorrected, unadapted, or partially adapted data.

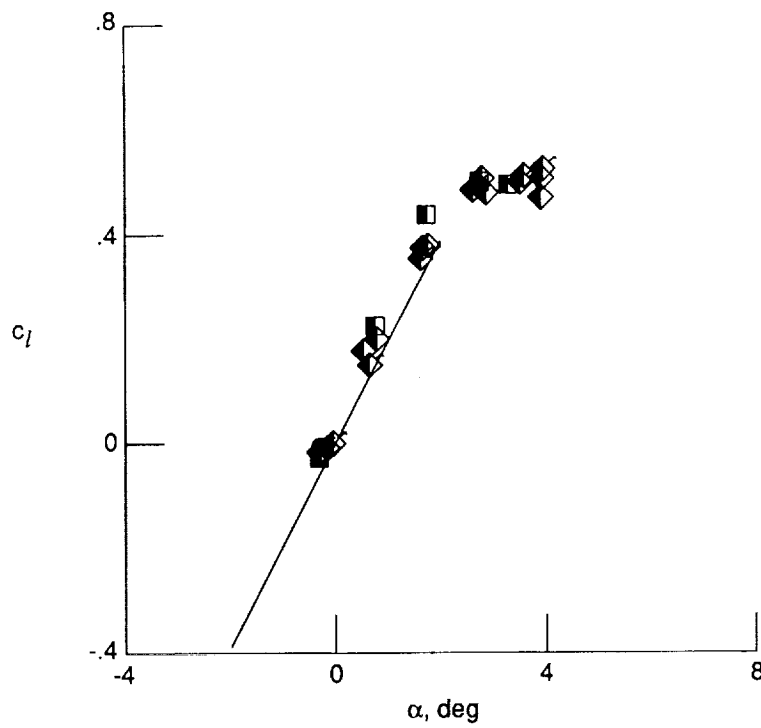


(d) TWNTN4A-corrected, unadapted, or partially adapted data.

Figure 19. Concluded.

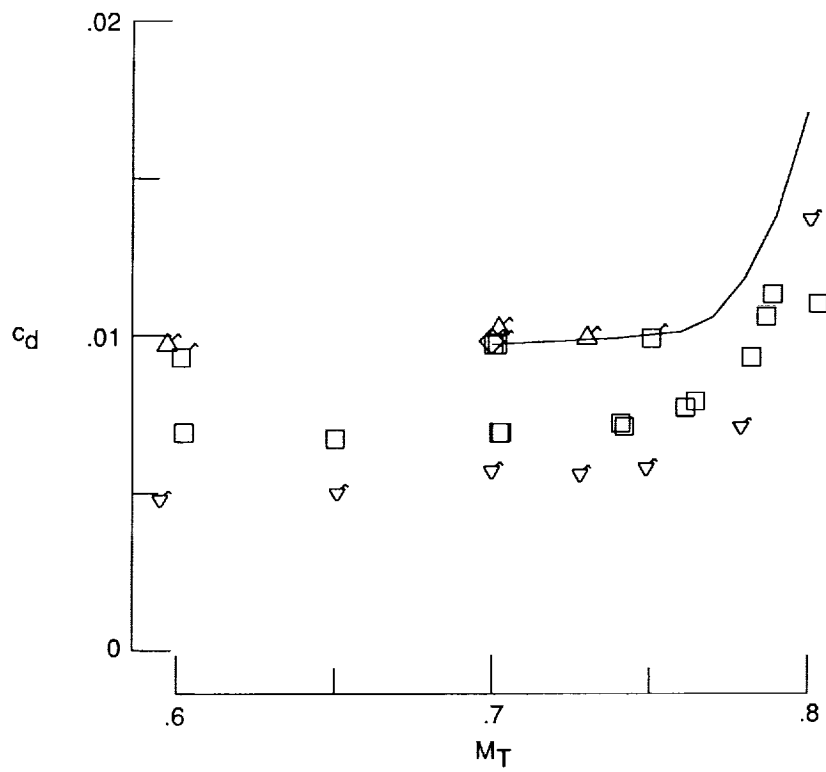


(a) Uncorrected, fully adapted data.

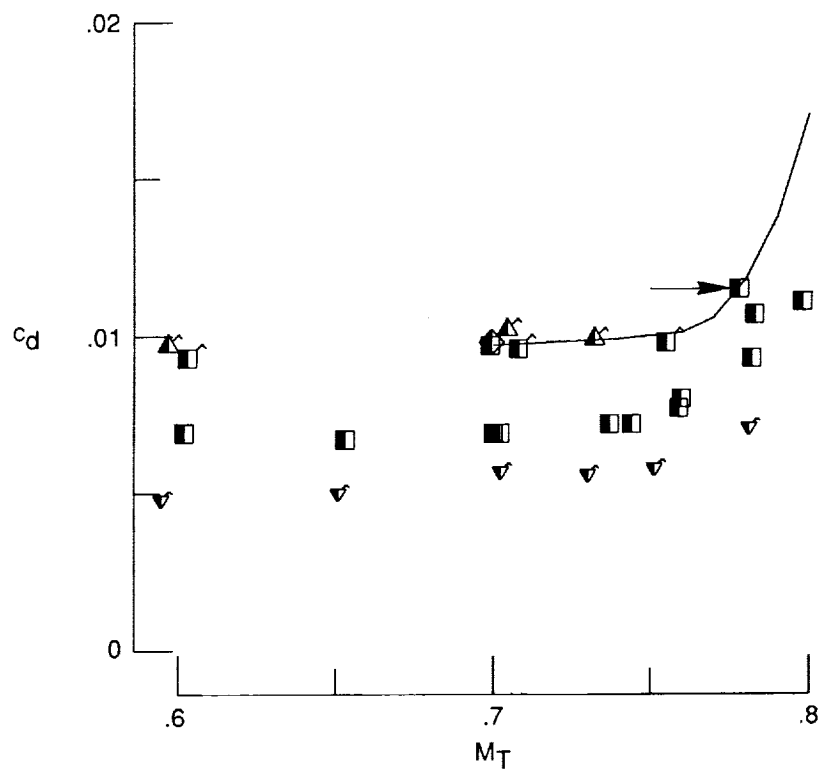


(b) TWNTN4A-corrected, fully adapted data.

Figure 20. Lift-curve data for NACA 0012 airfoil at $R_c \approx 15 \times 10^6$ and $M_T \approx 0.76$. See table I for symbol key.

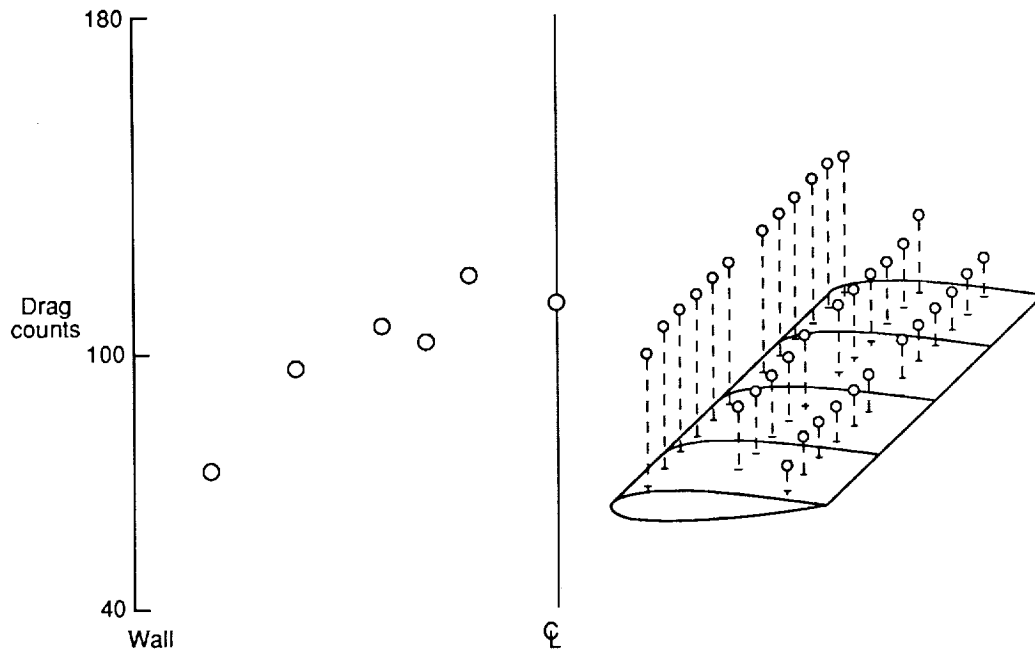


(a) Uncorrected, fully adapted data.

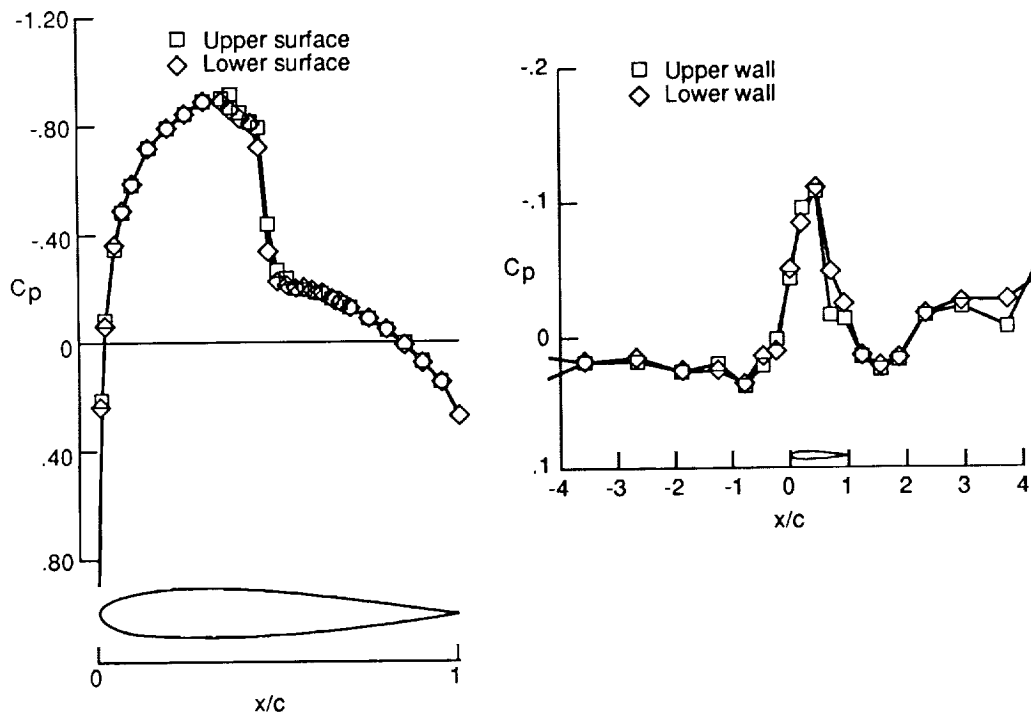


(b) TWNTN4A-corrected, fully adapted data.

Figure 21. Drag curves for NACA 0012 airfoil at $R_c \approx 3 \times 10^6$ and $c_l \approx 0$. See table I for symbol key.

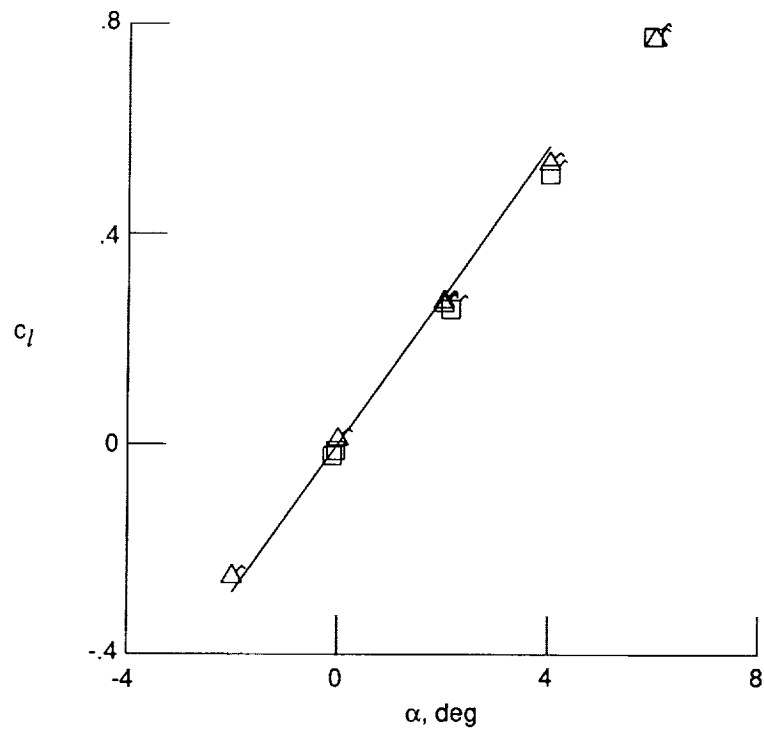


(a) Spanwise drag-rake survey and model pressure coefficient distribution.

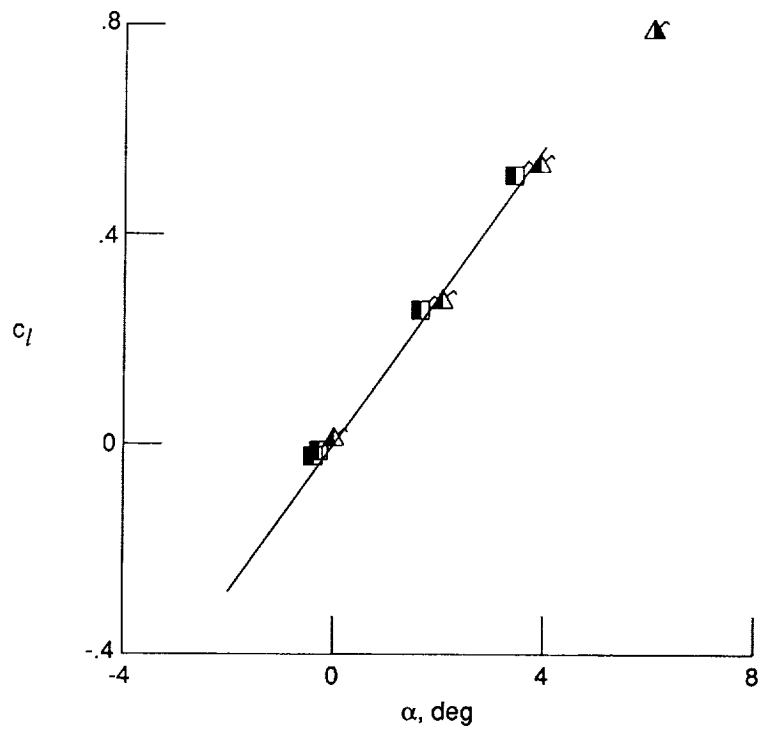


(b) Model and wall pressure coefficient distributions.

Figure 22. Preprocessor plots for NACA 0012 airfoil at $R_c \approx 3 \times 10^6$, $M_T \approx 0.79$ and $\alpha_T \approx 0^\circ$.

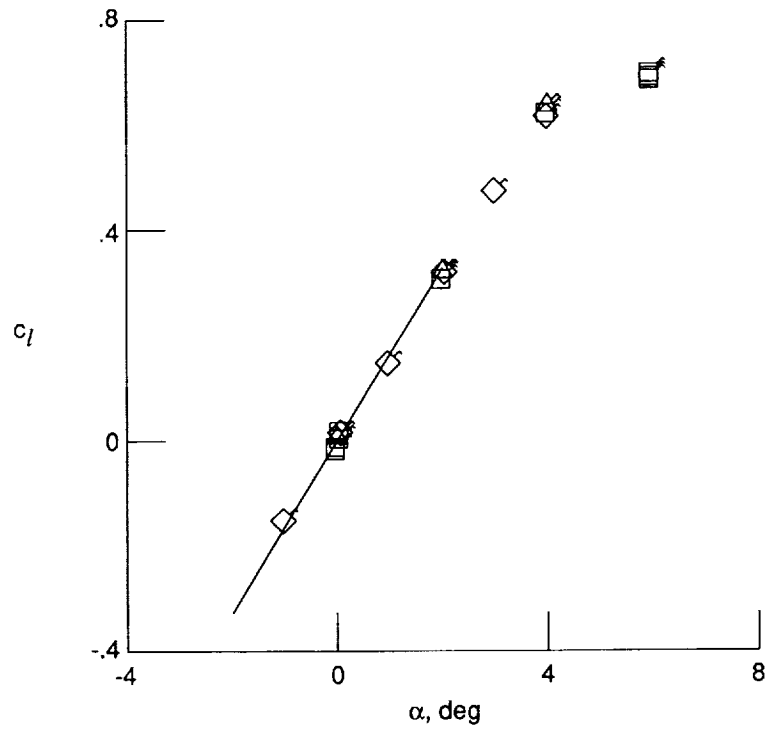


(a) Uncorrected, fully adapted data.

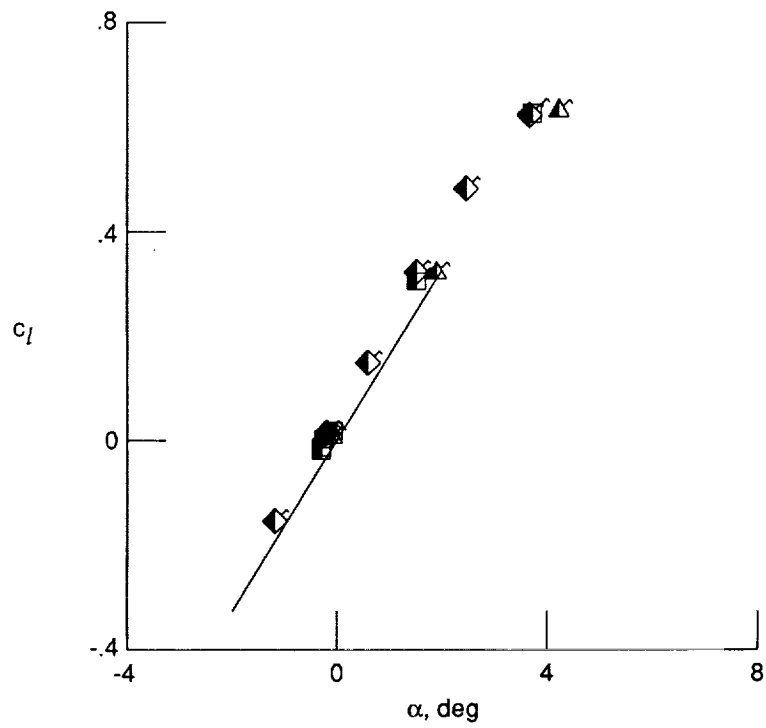


(b) TWNTN4A-corrected, fully adapted data.

Figure 23. Lift-curve data for NACA 0012 airfoil at $R_c \approx 3 \times 10^6$ and $M_T \approx 0.6$. See table I for symbol key.

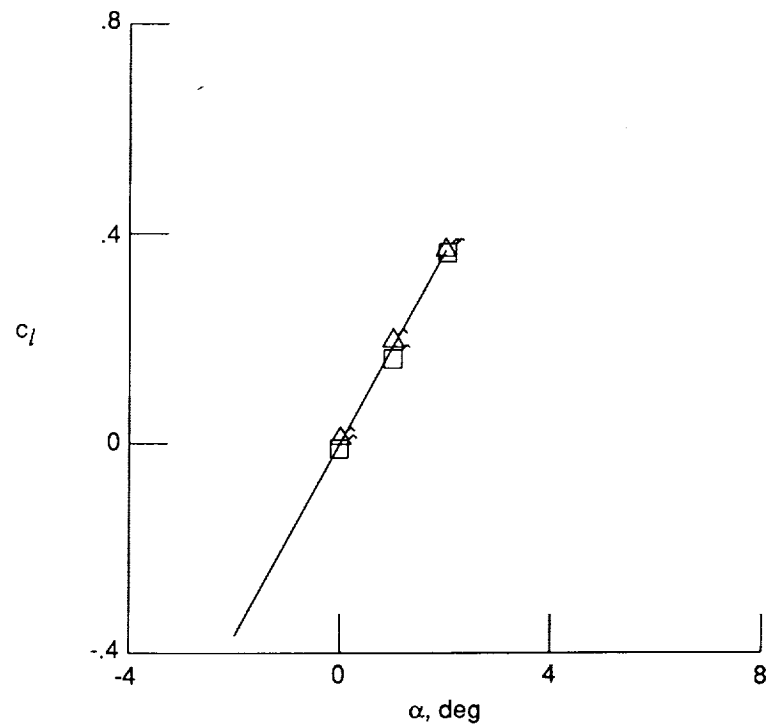


(a) Uncorrected, fully adapted data.

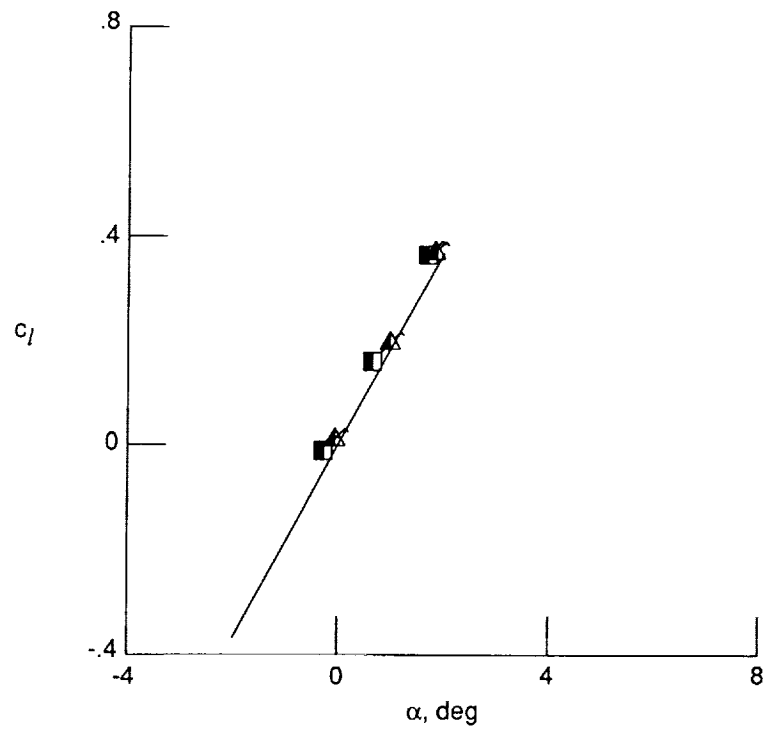


(b) TWNTN4A-corrected, fully adapted data.

Figure 24. Lift-curve data for NACA 0012 airfoil at $R_c \approx 3 \times 10^6$ and $M_T \approx 0.7$. See table I for symbol key.

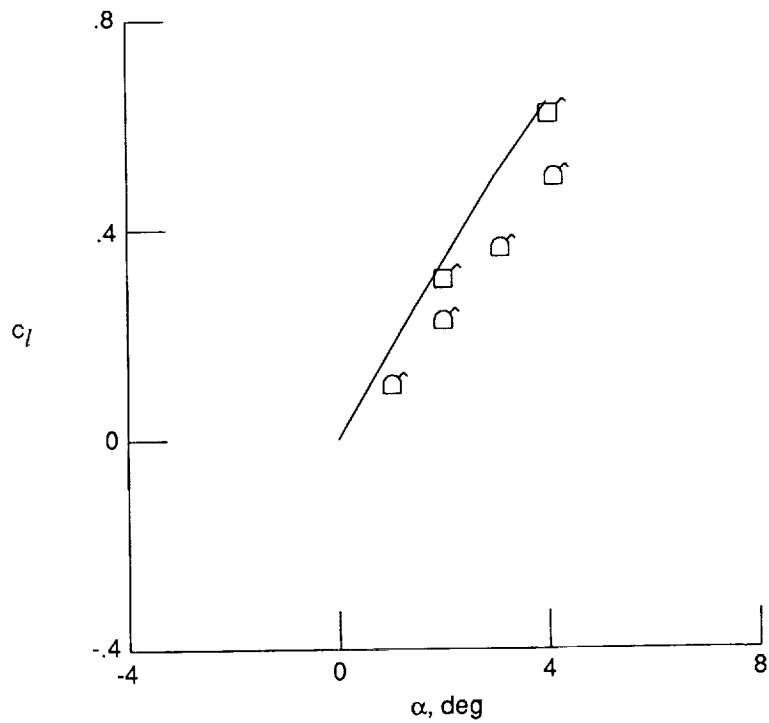


(a) Uncorrected, fully adapted data.

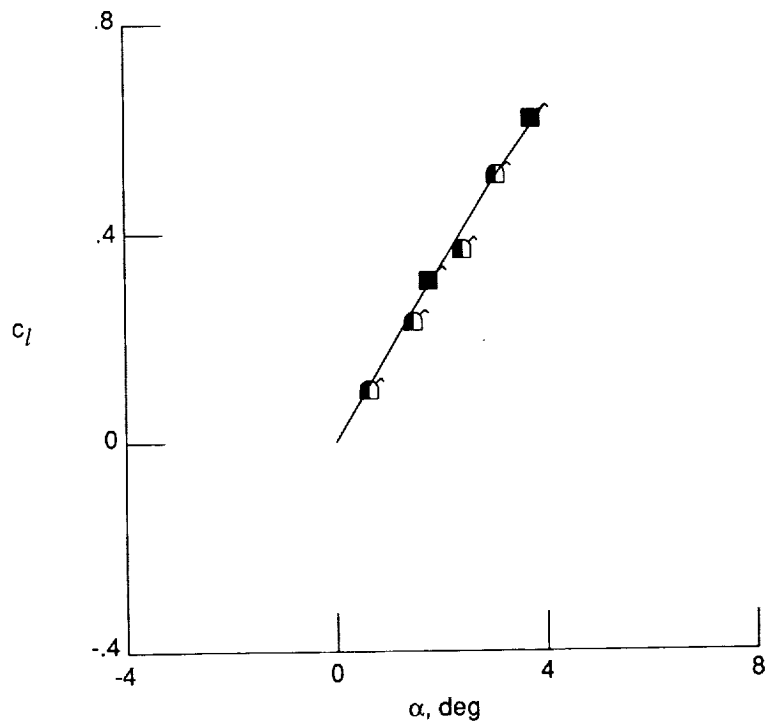


(b) TWNTN4A-corrected, fully adapted data.

Figure 25. Lift-curve data for NACA 0012 airfoil at $R_c \approx 3 \times 10^6$ and $M_T \approx 0.75$. See table I for symbol key.

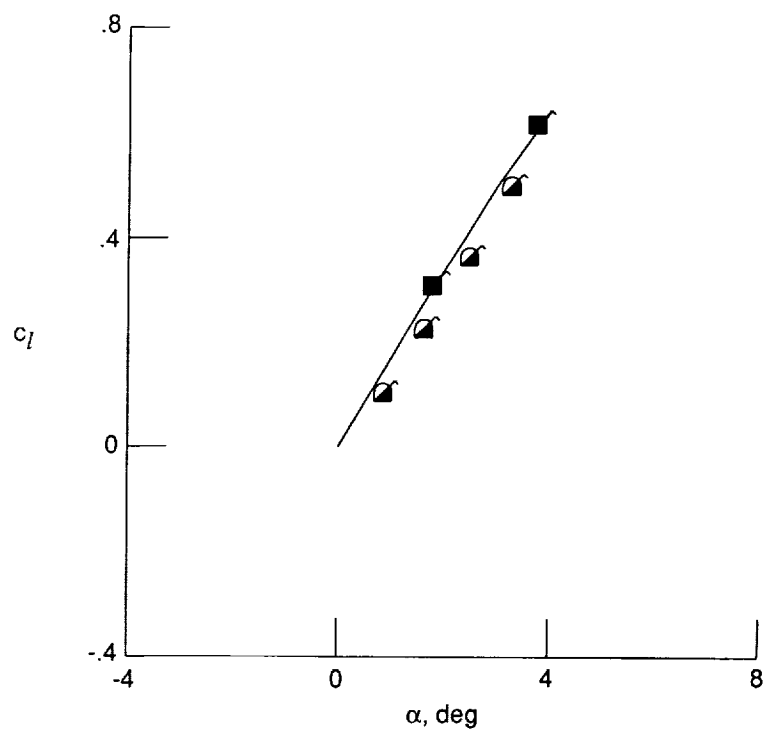


(a) Uncorrected, fully adapted data and slotted-wall data.



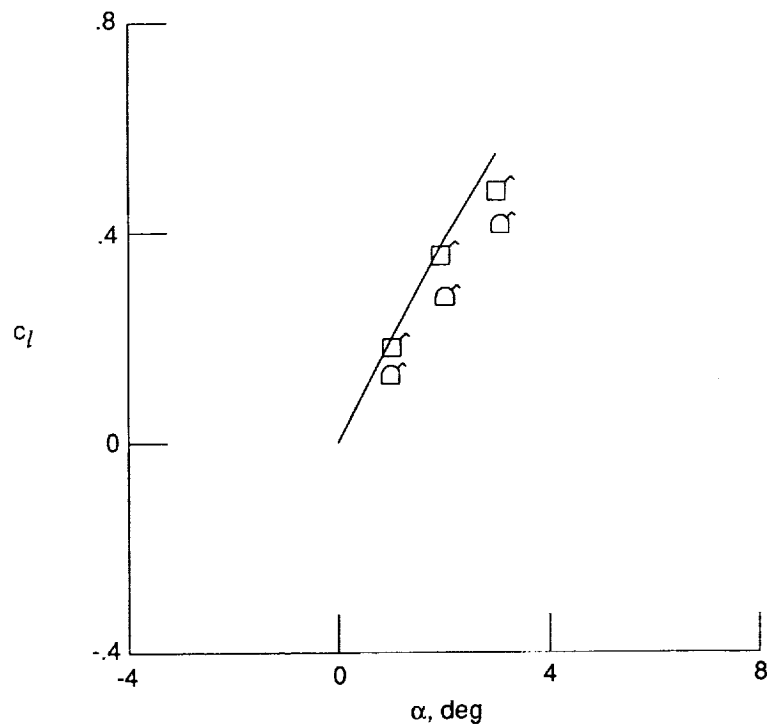
(b) TWNTN4A-corrected, fully adapted data and TWINTN4-corrected slotted-wall data.

Figure 26. Lift-curve data for NACA 0012 airfoil at $R_c \approx 9 \times 10^6$ and $M_T \approx 0.7$. See table I for symbol key.

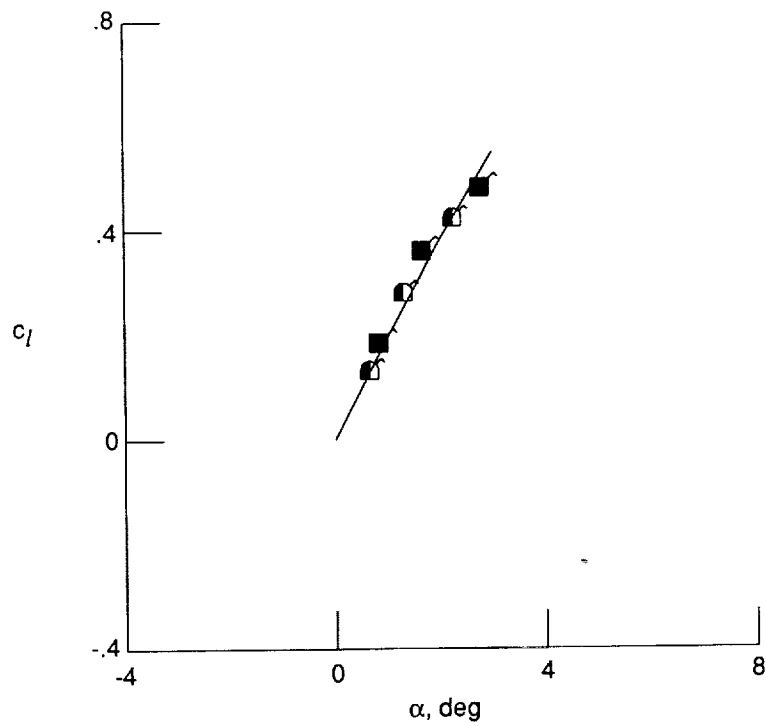


(c) TWNTN4A-corrected, fully adapted data and EDM-corrected slotted-wall data.

Figure 26. Concluded.

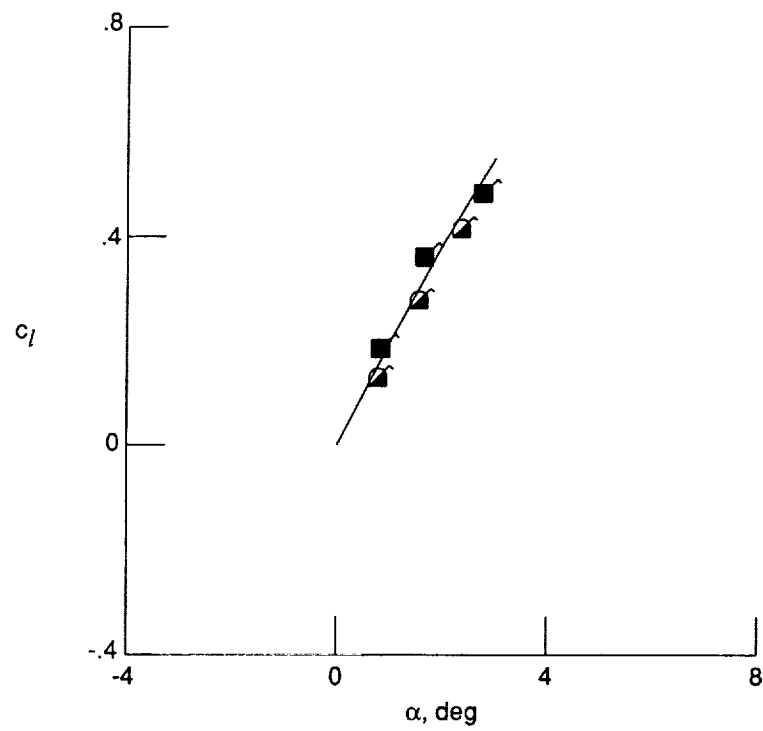


(a) Uncorrected, fully adapted data and slotted-wall data.



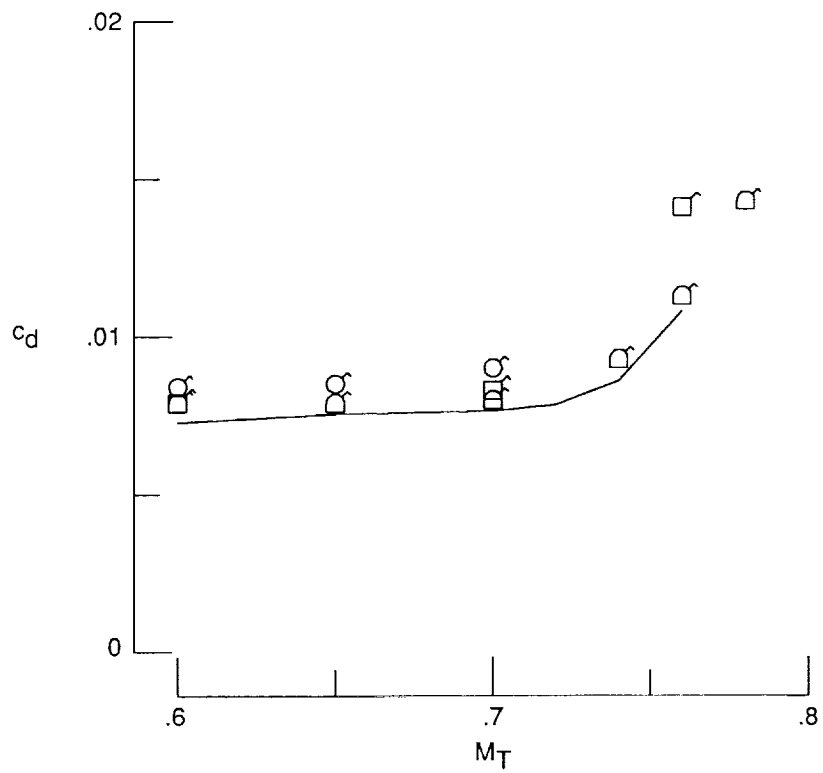
(b) TWNTN4A-corrected, fully adapted data and TWINTN4-corrected slotted-wall data.

Figure 27. Lift-curve data for NACA 0012 airfoil at $R_c \approx 9 \times 10^6$ and $M_T \approx 0.76$. See table I for symbol key.

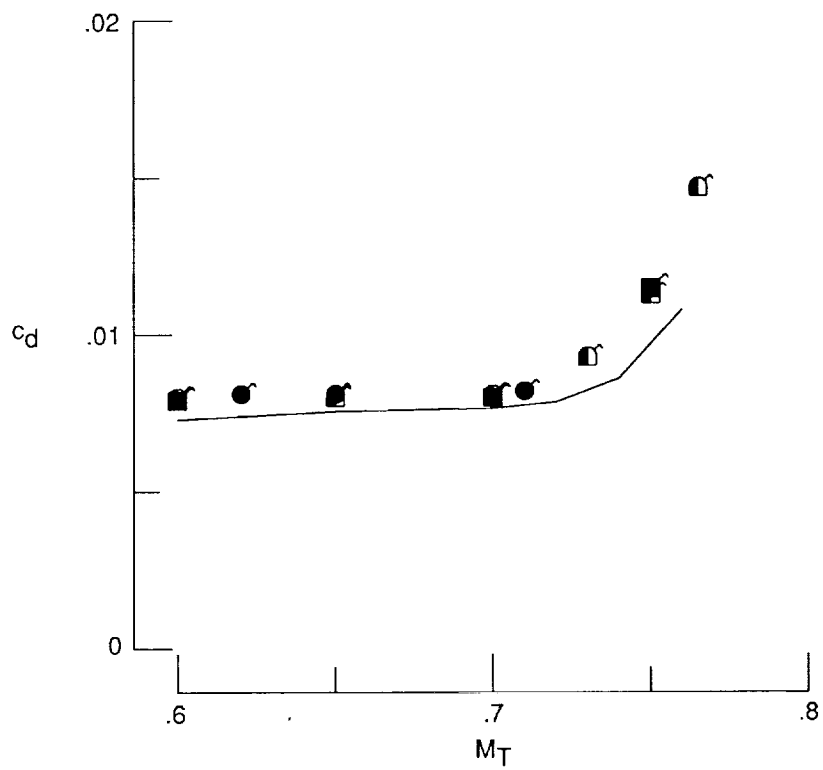


(c) TWNTN4A-corrected, fully adapted data and EDM-corrected slotted-wall data.

Figure 27. Concluded.

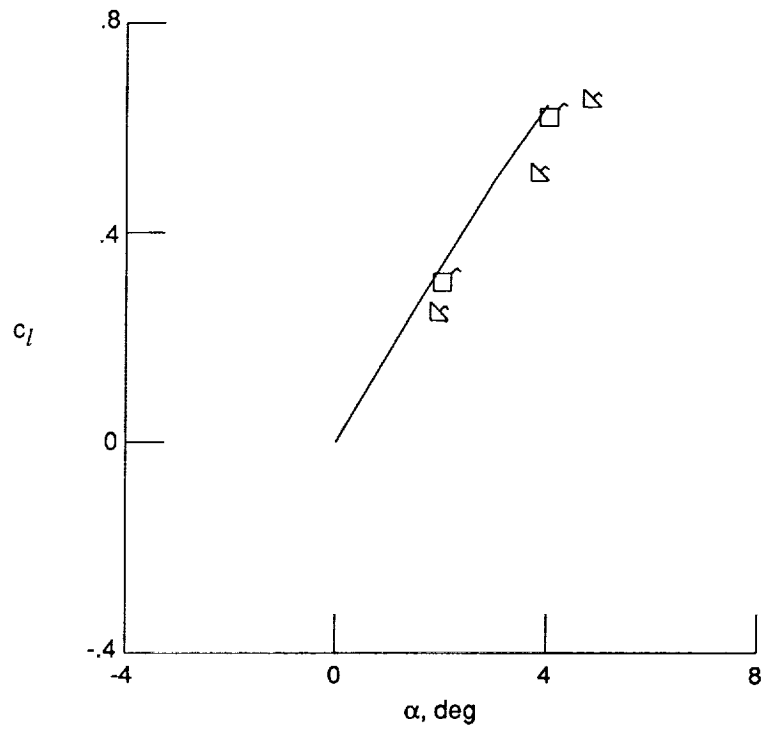


(a) Uncorrected, fully adapted data and slotted-wall data.

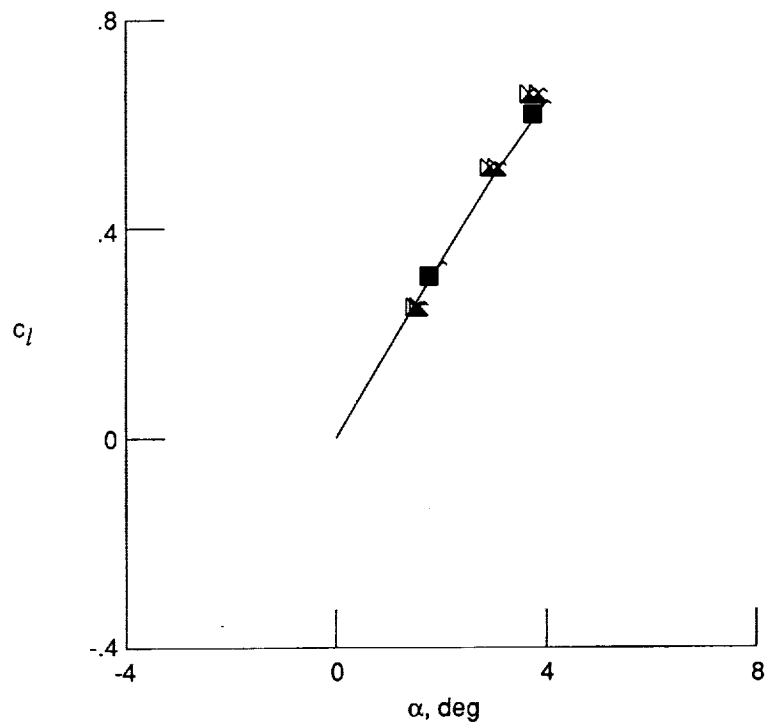


(b) TWNTN4A-corrected, fully adapted data and TWINTN4-corrected slotted-wall data.

Figure 28. Drag curves for NACA 0012 airfoil at $R_e \approx 9 \times 10^6$ and $c_l \approx 0.2$. See table I for symbol key.

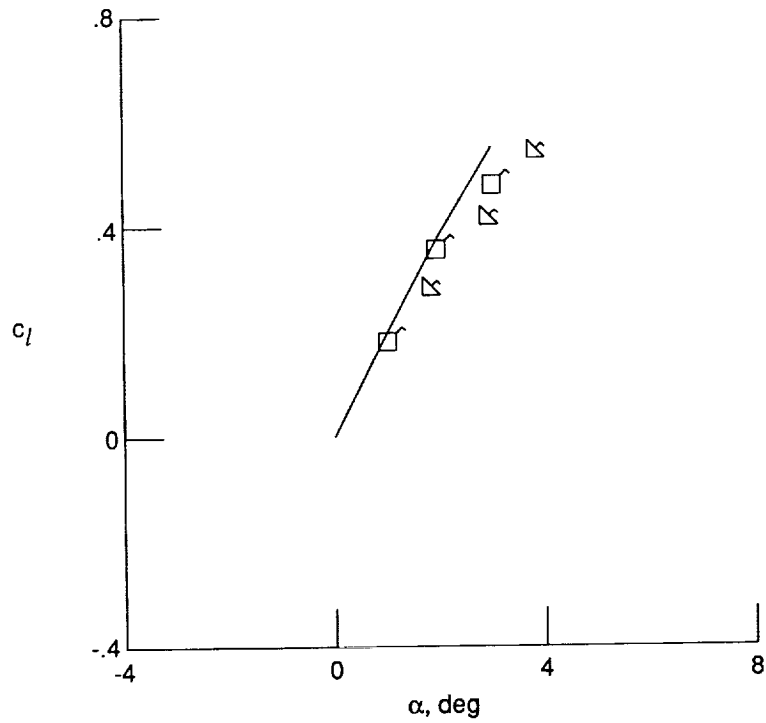


(a) Uncorrected, fully adapted data and slotted-wall data.

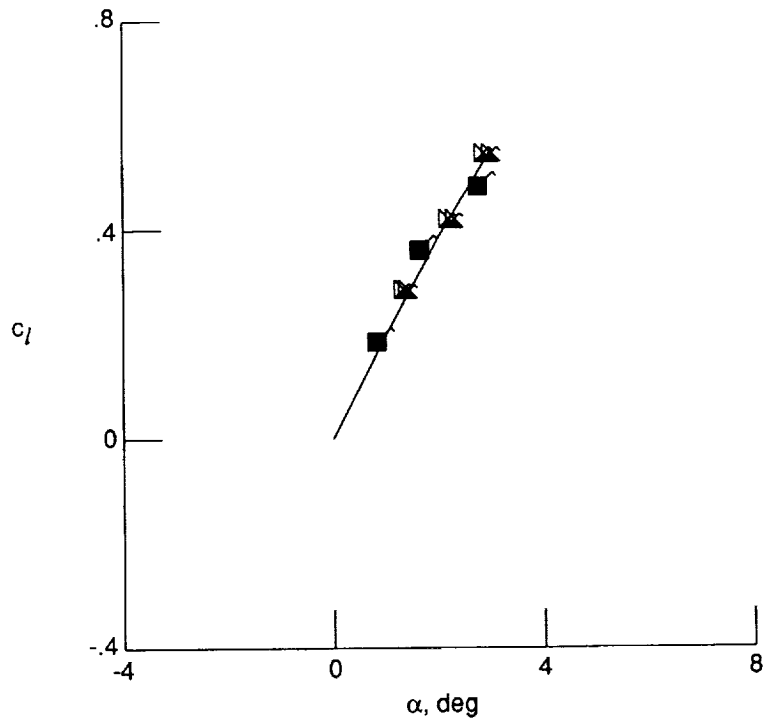


(b) TWNTN4A-corrected, fully adapted data and EDM-corrected slotted-wall data.

Figure 29. Lift-curve data for NACA 0012 airfoil at $R_c \approx 9 \times 10^6$ and $M_T \approx 0.7$. See table I for symbol key.

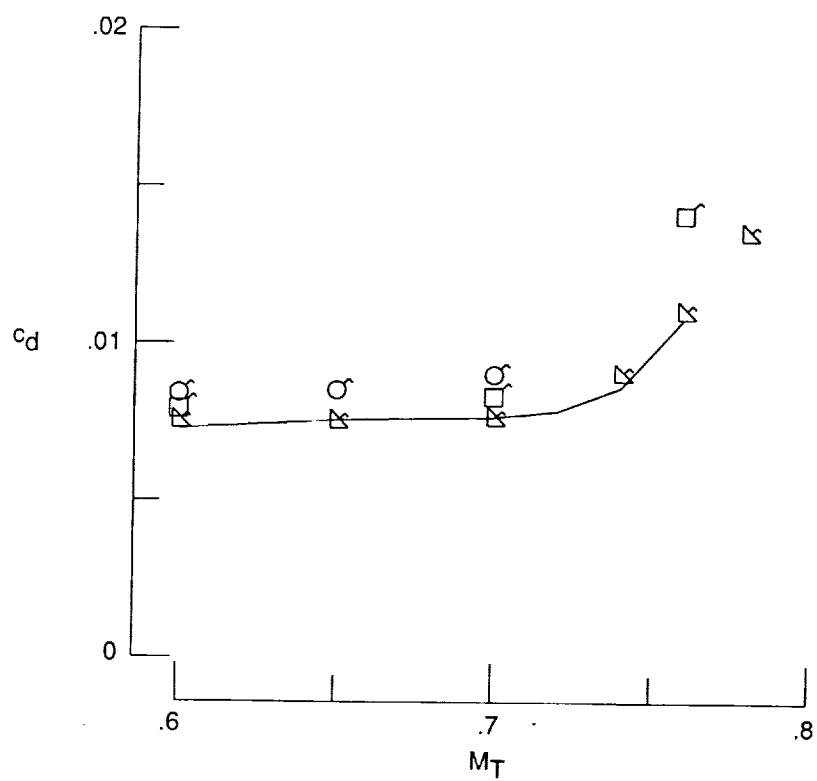


(a) Uncorrected, fully adapted data and slotted-wall data.

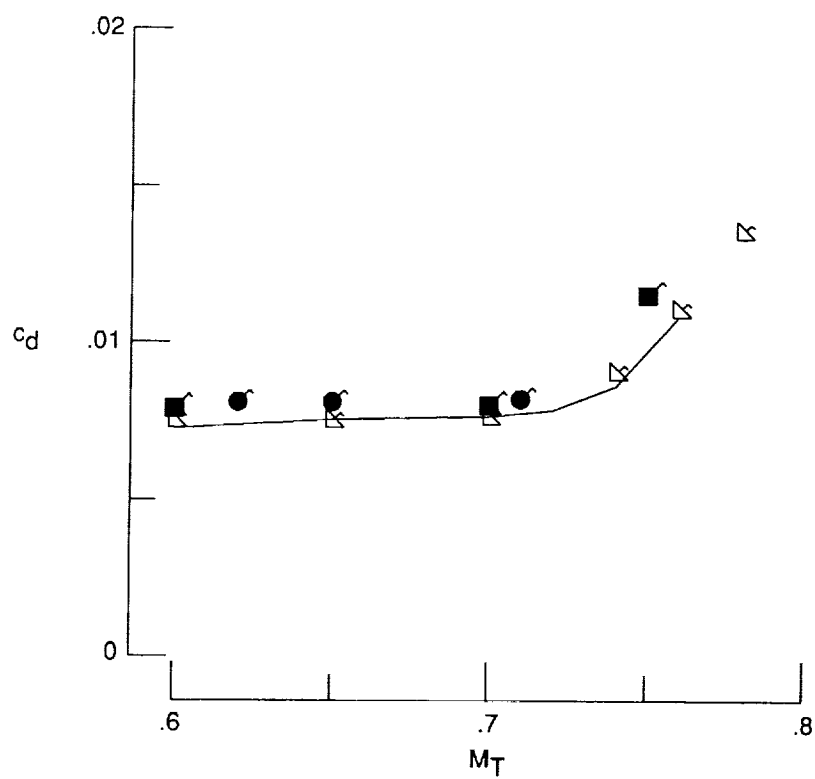


(b) TWNTN4A-corrected, fully adapted data and EDM-corrected slotted-wall data.

Figure 30. Lift-curve data for NACA 0012 airfoil at $R_c \approx 9 \times 10^6$ and $M_T \approx 0.76$. See table I for symbol key.



(a) Uncorrected, fully adapted data and slotted-wall data.



(b) TWNTN4A-corrected, fully adapted data and uncorrected slotted-wall data.

Figure 31. Drag curves for NACA 0012 airfoil at $R_c \approx 9 \times 10^6$ and $c_l \approx 0.2$. See table I for symbol key.

1. Report No. NASA TP-3070		2. Government Accession No.		3. Recipient's Catalog No.	
4. Title and Subtitle Wall-Interference Assessment and Corrections for Transonic NACA 0012 Airfoil Data From Various Wind Tunnels				5. Report Date April 1991	
				6. Performing Organization Code	
7. Author(s) Lawrence L. Green and Perry A. Newman				8. Performing Organization Report No. L-16721	
				10. Work Unit No. 505-61-01-04	
9. Performing Organization Name and Address NASA Langley Research Center Hampton, VA 23665-5225				11. Contract or Grant No.	
				13. Type of Report and Period Covered Technical Paper	
12. Sponsoring Agency Name and Address National Aeronautics and Space Administration Washington, DC 20546-0001				14. Sponsoring Agency Code	
15. Supplementary Notes Presented in part as AIAA 87-1431, June 8-10, 1987, in Honolulu, Hawaii; condensed from thesis given in partial fulfillment of the requirements for the Degree of Master of Science, George Washington University, Washington, D.C., April 1988.					
16. Abstract A nonlinear, four-wall, post-test wall-interference assessment/correction (WIAC) code has been developed for transonic airfoil data from solid-wall wind tunnels with flexibly adaptive top and bottom walls. The WIAC code has been applied over a broad range of test conditions to four sets of NACA 0012 data from two different adaptive-wall wind tunnels. The data include many test points for fully adapted walls as well as numerous partially adapted and unadapted test points, which together represent many different model/tunnel configurations and possible wall-interference effects. Small corrections to the measured Mach numbers and angles of attack are obtained from the WIAC code even for the fully adapted data; these corrections generally improve the correlation among the various sets of airfoil data and simultaneously improve the correlation of the data with calculations from a two-dimensional, free-air Navier-Stokes code. The WIAC corrections for airfoil data taken in test sections with fully adapted walls are shown to be significantly smaller than those for comparable airfoil data from test sections with straight, slotted walls. This indicates, as expected, a lesser degree of wall interference in the adaptive-wall tunnels relative to the slotted-wall tunnels. Application of the WIAC code to these data has, however, been somewhat more difficult and time-consuming than initially expected from similar previous experience with WIAC applications to slotted-wall data.					
17. Key Words (Suggested by Author(s)) Wall-interference assessment/correction (WIAC) Transonic flow Adaptive-wall tunnel Sidewall boundary-layer (SWBL) effects				18. Distribution Statement Unclassified—Unlimited	
				Subject Category 02	
19. Security Classif. (of this report) Unclassified		20. Security Classif. (of this page) Unclassified		21. No. of Pages 61	22. Price A04

